EFFECT OF HEAT TREATMENT PARAMETERS ON MECHANICAL AND METALLURGICAL PROPERTIES OF HOT FORGED REBAR

Lappeenranta-Lahti Univeristy of Technology LUT

LUT School of Energy Systems

Mechanical Engineering

2024

Taneli Salonen

Examiners: Associate Professor, Tuomas Skriko

M.Sc. (Tech.), Esa Hiltunen

ABSTRACT

Lappeenranta-Lahti Univeristy of Technology LUT

LUT School of Energy Systems

Mechanical Engineering

Taneli Salonen

Effect of heat treatment parameters on mechanical and metallurgical properties of hot forged rebar

Master's thesis

2024

91 pages, 54 figures and 10 tables 1 appendices

Examiners: Associate Professor, Tuomas Skriko
M.Sc. (Tech.), Esa Hiltunen

Keywords: Rebar, Hot upset forging, Induction heating, Heat-treatment, Quenching, Self-tempering

Mechanical properties of iron alloys, such as strength, hardness, and toughness, can be modified with a controlled process of heating and cooling, known as heat treatment. This thesis proposes the effect of different heat-treatment parameters on the mechanical and metallurgical characteristics of headed rebars during the hot forging process.

According to the literature review, heating and cooling parameters for different-sized rebars are determined with the help of simulation software. By making experimental tests such as tensile tests, hardness measurements, and metallography for the rebars, the theory-based simulation results can be verified and adjusted.

TIIVISTELMA

Lappeenrannan–Lahden teknillinen yliopisto LUT

LUTin energiajärjestelmien tiedekunta

Konetekniikka

Taneli Salonen

Lämpökäsittelyparametrien vaikutus kuumataotun harjateräksen mekaanisiin ja metallurgisiin ominaisuuksiin

Diplomityö

2024

91 sivua, 54 kuvaa ja 10 taulukkoa 1 liitettä

Tarkastajat: Apulaisprofessori, Tuomas Skriko
DI, Esa Hiltunen

Avainsanat: Harjateräs, tyssäys, induktiokuumennus, lämpökäsittely, karkaisu, päästö

Teräksen mekaanisia ominaisuuksia, kuten lujuutta, sitkeyttä, ja kovuutta voidaan muokata kontrolloidulla lämmitys- ja lämpökäsittelyprosessilla. Tämän työn tavoitteena on löytää harjateräksen mekaanisiin- ja metallurgisiin ominaisuuksiin sekä laatuun vaikuttavat parametrit tyssäysprosessin aikana tapahtuvassa lämmityksessä ja lämpökäsittelyssä sekä määrittää nämä niin että tyssätyn tuotteen lujuusominaisuudet ovat hyvät.

Teoriaan, simulaatioihin sekä kokeellisiin tutkimuksiin pohjautuen erikokoisille harjateräksille määritetään lämmitys- ja jäähdytysparametrit. Lämpökäsiteltyjen harjaterästen mikrorakennetta tarkastellaan metallografisesti.

ACKNOWLEDGMENTS

I want to thank all the personnel from the target company for offering this interesting subject and providing support and guidance during the study. Thanks to Professor Tuomas Skriko and Laboratory engineer Esa Hiltunen from LUT University for supervising this work. I would also like to thank Antti Heikkinen and Shahriar Afkhami from the university staff for their help. I appreciate the time and effort you all gave to this study.

I am grateful for all the friends, experiences, and memories I gained during my time in Lappeenranta and Antwerp while studying. Special thanks to Koneenrakennuskilta and PoWi for offering a good balance for studying.

Lastly, thanks to my family and Pia for all the support during my studies and writing of this thesis.

Taneli Salonen

Lahti 3.1.2024

SYMBOLS AND ABBREVIATIONS

Roman characters

A	surface area of the workpiece	[mm^2]
A_1	lower critical temperature	[°C]
A_3	upper critical temperature	[°C]
A_{qt}	total elongation	[%]
c	specific heat	[J/kg·°C]
d	rebar diameter	[mm]
k	thermal conductivity	[W/m·k]
L_b	heating lenght	[mm]
M_f	martensite finish temperature	[°C]
M_s	martensite start temperature	[°C]
M_{50}	50% martensite composition temperature	[°C]
m_w	mass of heated workpiece	[kg]
P_w	heating power	[W]
q	heat flux	[W/m^2]
R	workpiece radius	[mm]
R_b	bar radius	[mm]
R_{eH}	upper yield strength	[MPa]
R_i	coil inner radius	[mm]
R_m	tensile strenght	[MPa]
$R_{p0,2}$	0,2% offset yield strenght	[MPa]

T	temperature	[K]
T_a	ambient temperature	[K]
T_c	cooling rate	[K]
T_f	final temperature	[K]
T_{in}	start temperature	[K]
T_s	surface temperature	[K]
t	heating time	[s]
V	workpiece volume	[mm^3]
x	direction of heat flow	

Greek characters

α	convection heat-transfer coefficient	[$W/m^2 \cdot K$]
β	rib inclination	[°C]
δ	penetration depth	[m]
ϵ	emissivity coefficient	
μ_r	magnetic permeability	
ρ	density	[kg/m^3]
ρ_e	electrical resistivity	[Ω·m]
σ	electrical conductivity	[S/m]
σ_c	coil overhang	[mm]

Constants

σ_s	Stefan-boltzman constant	$5.67 \cdot 10^{-8}$ W/m^2K^4

Abbreviations

α-Fe Ferrite

γ-Fe Austenite

AC Alternating current

As Arsenic

Bcc body-centered cubic

C Carbon

CCT-diagram Continuous Cooling Transformation diagram

CE Carbon equivalent

Cr Chromium

Cu Copper

EAD European Assestment Document

EOTA European Organisation of Technical Assestment

Fcc face-centered cubic

Fe Iron

Fe_3C Cementite

IH Induction Heating

Mn Manganese

Mo Molybdenum

N Nitrogen

Ni Nickel

P Phosphorus

Q&T Quenching and tempering

QST Quenching and self-tempering

S Sulfur

Si Silicon

STT Self-tempering temperature

TT Tempering temperature

TTT-diagram Time Temperature Transformation diagram

V Vanadium

wt%C Carbon content by weight

TABLE OF CONTENTS

1 INTRODUCTION

Concrete withstands compression well but has poor tensile strength. By reinforcing the concrete with steel, the necessary tensile strength can be achieved. A reinforced steel bar, shorted as rebar, is a common reinforcement material used. Adequate steel anchoring into concrete is needed to ensure proper reinforcing, which can be achieved by having a mechanical deformation at the end of the rebar. Plenty of anchoring methods have been used and developed over time, but the use of headed anchoring over hooks and bends has gained popularity due to easy installation and less congestion while reinforcing.

The head can be attached to one or both ends of the rebar using threading, welding, or forging. This thesis focuses on headed rebar manufacturing with a hot upset forging process. The goal is to analyze how different parameters during the heating and heat treatment processes affect the metallurgical and mechanical properties of the headed rebar and how the best mechanical properties can be achieved by adjusting these parameters. In Figure 1, a hot upset forged rebar after the forging process can be seen. The headed rebar in the picture is only illustrative and unrelated to the company commissioning this work.

Figure 1: Hot upset forged headed rebar (LinkStudPSR 2023).

1.1 Background and motivation

So far, the company commissioning this work has found good strength and metallurgical properties for the headed rebars by testing out different process parameters over time. The company has upset forging lines in many countries, and the heating- and cooling parameters

during the manufacturing vary between the factories. By commissioning this work, the company aims to gain a deeper understanding of how the heat treatment affects the properties of the rebar, and what are the best parameters in practice to use in every production unit, based on theory.

1.2 Objectives and conceptual framework

This research aims to find out how different heating- and heat treatment parameters during the forging process affect the mechanical and metallurgical properties of the forged rebar. The objectives and research questions can be divided into two sections:

1. Heating: How should the rebar be heated before the upset forging? What factors affect the heating process? E.g., finding proper heating length and time. Induction heating machinery is used for heating.

2. Heat treatment: How should the rebar be heat treated after forging to gain good mechanical properties? Analysis of using Quenching and self-tempering (QST) as a heat treatment method.

Simulations for both heating and heat treatment will be provided based on the literature review. The best possible parameters for heating and cooling are proposed with a combination of previous knowledge inside the company, literature review, simulations, tensile test, metallography, and hardness measurements. In Figure 2, the conceptual framework of the thesis is provided.

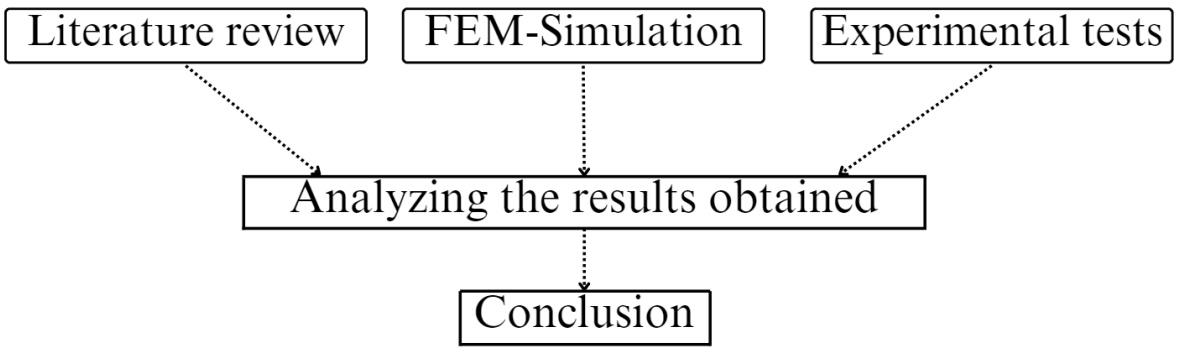

Figure 2: Conceptual framework of the study.

1.3 Scope

One of the important aspects of the upset forging process is the input parameters for the forging process. The company has already defined these parameters, so the focus is on defining the heating and heat treatment parameters for the process. The material analyzed in this study

is a reinforced steel bar, a commonly forged material in the company. Other materials are also forged, but to limit the scope of this work, only reinforced steel is analyzed. The knowledge and expertise gathered in this work can be used in further studies for other materials.

In this study, three different rebar diameters, 10mm, 20mm, and 32mm, are analyzed. Many more rebar sizes are forged in production, but analyzing each of them in this work would make it long and hard to follow. The sizes chosen for this work are taken evenly from the sizes produced, so the results can possibly be used to define heating and heat treatment parameters to other rebar diameters. The experimental tests are done for 10mm and 20mm rebars. 32mm is left out as forging it with the machinery used to make the test samples is not possible. Even though 32mm is not used in experimental tests, making the induction heating and heat treatment simulations for it helps to understand the effect of the workpiece size on the hot working process.

1.4 Research methods

A literature review is done by utilizing academic publications, industrial handbooks, and manuals. Online databases and university libraries are used as the primary source of literature. More information about the topic is gained by having interviews and discussions with people with knowledge related to the work, for example, with the target company's staff and university.

Both heating and heat treatment are simulated. For heating, the simulation is done with Cenos induction heating software, as the heating is done with induction heating. For cooling, Comsol multiphysics is used. The experimental tests made for 10 and 20-mm rebars consist of a tensile test, hardness measurements, and metallography. The tensile test is done on the company's premises, and metallography for chosen bars is done on the university's premises.

2 REINFORCED STEEL BAR

A reinforced steel bar, often referred to as rebar, is used to reinforce concrete. Because the tensile strength of concrete is usually around 10% of the compression strength, it often requires reinforcement with steel to achieve the necessary tension strength. This combination of materials creates reinforced concrete, which can withstand various forces over large spans, including wind, earthquakes, and vibration. (Bustillo Revuelta 2021, p. 221.)

This chapter introduces properties that are needed for rebar steel according to standards. The properties and design of rebar are specified by standards that might differ depending on the area or country. Standards are used to ensure that the material possesses the necessary mechanical properties and characteristics for the intended application. In this work, European EN, Finnish SFS, German DIN, and British BS standards are used to specify the properties and design of the rebar.

The properties specified in the standards are compared to the inspection certificates from steel mills for the three batches used for testing later in this study. Batch 1 is for 10 mm, Batch 2 is for 20mm, and Batch 3 is for 32mm diameter rebar steel. The purpose of an inspection certificate is to verify that the material inspected conforms with the material properties agreed upon between the steel mill and the buyer.

2.1 Grading and naming

Rebar grades are set by standards, and the naming structure can differ regarding standardization organization. In Europe, a common grading system follows the structure shown in Figure 3 below.

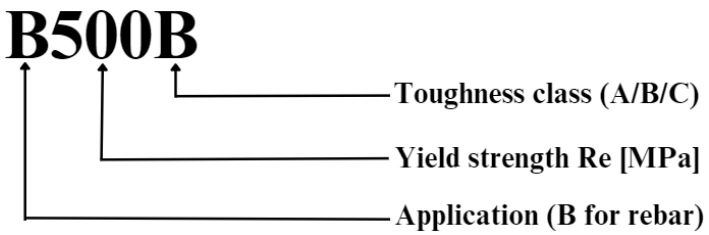

Figure 3: Typical naming structure of rebars in Europe.

The first single letter in the naming refers to the application, which is always the letter B for rebars. The numbering in the center represents the minimum yield strength of the rebar,

and the last single letter is the toughness class. (Heaton Manufacturing 2020) In this work, reinforced bars tested and analyzed are all class B500B rebar steels.

2.2 Mechanical properties

Typically, minimum mechanical properties of rebars are specified with the following parameters (EN-10080 2005):

- Upper Yield strength R_{eH} (MPa)
- Ratio of tensile- and yield strength R_m/R_{eH}
- Total elongation A_{qt} (%)

Yield strength is the magnitude of the tensile stress when a permanent deformation occurs in a material. Plastic deformations will occur when stress higher than the yield strength is applied. Tensile strength describes the maximum stress that the material can tolerate before breaking. Total elongation is the elongation of the material until it breaks. It is determined as a percentage of the original length of the metal.

The values presented above can be determined by making a tensile test. During the test, an increasing load is applied to the test piece while the strain is being measured. As a result, a stress-strain curve is achieved, where the values for the material properties mentioned above can be measured. Typically, an engineering stress-strain curve is used in which the changes in the cross-sectional area of the material during the deformation are not taken into account, which makes the curve differ from the real stress-strain curve in which the changes are considered. An engineering stress-strain curve is often used instead of a true stress-strain curve as it is easier to obtain the data than through true stress-strain curves, and it is adequate enough for engineering calculations. (Capar 2023)

A typical engineering stress-strain curve is shown in Figure 4 below. For some materials, often also in tensile tests for reinforced bar, the yield point is not easily detectable, so instead of using R_{eH} offset yield strength $R_{P0,2}$ is determined. $R_{P0,2}$ approximates the material elastic limit and is the stress value corresponding to the 0.2% plastic strain.

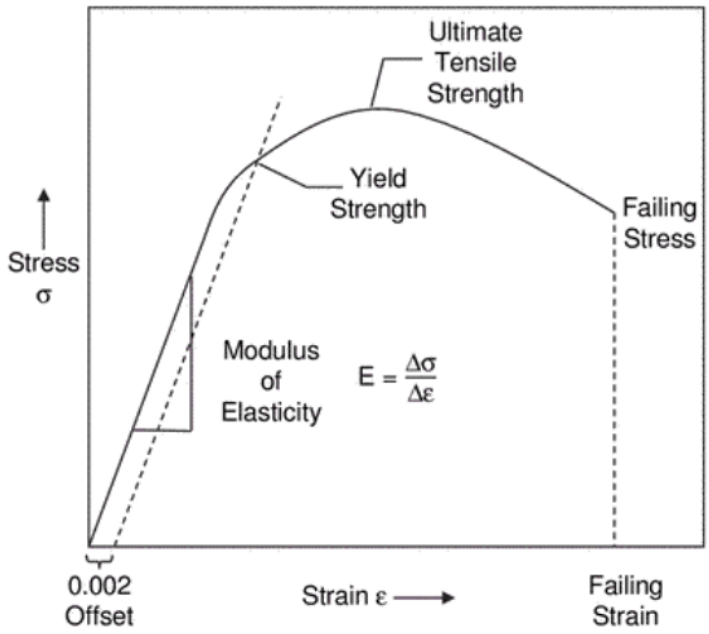

Figure 4: Engineering stress-strain curve (Campbell 2008, p. 203).

Reinforced steel bars are graded in three classes, A, B, and C, according to their tensile properties and flexibility. Class A has the lowest tensile- and ductility properties, and class C has the highest. For rebars, class B is the most commonly used. Table 1 below lists the minimum requirements for each class according to the SFS-1300 standard.

Table 1: Minimum tensile properties for rebar grades (SFS-1300).

Class	R_{eH} (MPa)	R_m/R_{eH}	A_{qt} (%)
A	400-700	1.05	2.5
B	400-700	1.08	5
C	400-700	min 1.15 max 1.35	7.5

Table 2 shows the tensile properties of the batches used in tests later on. The main goal of the hot working process is to maintain these values.

Table 2: Test batch tensile properties.

Batch	R_{eH} (MPa)	R_m/R_{eH}	A_{qt} (%)
1 (d = 10mm)	536	1.15	7.5
2 (d = 20mm)	545	1.22	10.1
3 (d = 32mm)	552	1.2	10.4

2.3 Chemical composition

The main alloying elements of steel are Iron (Fe) and Carbon (C). The carbon composition in steels is under 2.1 %, and iron-carbon alloys with higher carbon amounts are called cast irons. Rebar steel is alloy steel because it contains other alloying elements beyond carbon. The raw material used to manufacture carbon steel rebars is typically recycled steel, refined to remove some of the impurities it may contain (Hongteng 2023). Table 3 below lists common alloying elements and impurities seen in rebar steels and their effect on rebar's properties. (American Welding Society (AWS) 2015, p. 37-43), (Djavanroodi and Salman 2017, p.3), (Leong, n.d.)

Table 3: Influence of alloying elements and impurities commonly contained in rebar steels.

Element	Property
Carbon (C)	Main alloying element.% by mass affects hardness, strength, weldability, and brittleness; excess carbon is considered as impurity
Sulfur (S)	Impurity, In steels, sulfur forms iron sulfate FeS which causes hot shortness
Phosphorus (P)	Impurity, increases brittleness and decreases toughness
Nitrogen (N)	Impurity, increases brittleness over time in low alloy steels known as strain ageing.
Copper (Cu)	Alloy, used to increase resistance to corrosion, too high Cu-% affects weldability
Manganese (Mn)	Alloy, Increases tensile strength and responsiveness to heat treatment, counters the brittleness from sulfur
Chromium (Cr)	Impurity, Increases corrosion resistance, affects the carbon equivalent
Nickel (Ni)	Alloy Increases strength, ductility, and hardness.
Molybdenum (Mo)	Alloy, Enhances hardenability, Increases toughness, and improves strength at higher temperatures. reduces temper embrittlement
Silicon (Si)	Impurity, improves hardness and strength properties. decreases toughness
Arsenic (As)	Impurity, causes embrittlement during heat treatment
Vanadium (V)	Alloy, used to achieve finer grain size

The maximum amount of some individual elements and the maximum carbon equivalent are set by standards. Maximum values for individual elements for cast analysis according to EN-10080 are shown in Table 5 together with the chemical composition of the batches used later in an experimental test. The chemical composition can be measured with cast- or product analysis; typically, both values are specified in standards. The production batches tested in this study have used cast analysis as a measurement method.

Carbon equivalent (CE) is a factor used mainly to predict the weldability of the material but also to predict the heat treating and casting properties of the material. In *CE*, the alloying elements of the metal are converted to the equivalent carbon percentage. This is done because the phase transformations happening in iron-carbon are better understood than in iron alloys, making it easier to estimate the phase transformations happening and, therefore, to predict the material's properties. A large CE number reflects poor weldability and a higher probability of having brittle failures while heat-treating the material.(Molderings 2020) The equation below is commonly used for carbon and low alloy steels to achieve the value of carbon equivalent:

$$CE = C + \frac{Mn}{6} + \frac{Cr + Mo + V}{5} + \frac{Ni + Cu}{15} \tag{2.1}$$

Where the symbols of the chemical elements indicate their content in % by mass. (EN-10080 2005, p. 14.) Different formulas to calculate CE have been developed for different analyses, and the values achieved from them can differ. The formula above is used in most standards for rebar steels, such as in European EN-, German DIN-, and Finnish SFS standards. When utilizing the Equation 2.1 to calculate the CE value, the weldability of the material is defined according to the Table 4 below. According to the table, rebar steel is often referred to as a material with good to fair weldability and, therefore, suitable for hot working and heat treatment. (Herring 2015)

Table 4: Weldability of material based on the CE value (Herring 2015).

Carbon equivalent	Weldability
Over 0.5	Poor
Between 0.46 to 0.5	Decent
Between 0.41 to 0.45	Good
Between 0.36 to 0.40	Very good
Under 0.35	Excellent

The inspection certificates and information provided on them differ between steel mills. Some manufacturers only provide necessary information about the metal, i.e., only the values specified in the standards or needed to calculate CE. At the same time, some inspection certificates include a more precise chemical composition list. As the Table 5 shows, variations in chemical composition in rebar production are seen.

Table 5: Max. values of individual elements (% by mass) and test batch values.

	C	S	P	N	CU	CE
EN-10080	0.22	0.05	0.05	0.012	0.8	0.5
Batch 1	0.18	0.022	0.019	0.011	0.21	0.43
Batch 2	0.21	0.023	0.023	0.008	0.41	0.37
Batch 3	0.20	0.020	0.021	0.009	0.32	0.43

3 PHYSICAL METALLURGY OF STEELS

Physical metallurgy deals with the relationship between the material's physical properties and microstructure. In the case of steel, physical metallurgy plays a crucial role in determining the properties and behavior of the material. The physical properties of steels, such as strength, toughness, and ductility, are strongly influenced by their microstructure.

The final product's physical properties can be modified in the desired direction by adjusting the heating and cooling processes. To succeed in this, studying different equilibrium and metastable phases of steel and their formation methods is important. Ferrite, austenite, graphite, and, to some extent, Cementite (a very stable iron carbide) are the equilibrium phases of steel, whereas pearlite, martensite, and bainite are known as the metastable phases of steel. In this chapter, these phases are analyzed more precisely.

3.1 Allotropes of iron

Most metals, including steel, have a crystalline structure when they are in solid state. During the solidification process (molten material solidifies), the atoms will arrange repeatedly in a certain three-dimensional pattern where the energy bound of the atoms is at its lowest. The smallest particle of the crystal lattice, called a unit cell, determines the whole symmetry and structure of the crystal. (Kauppi 2020)

More than 95% of the composition of steel is iron, which makes it essential to study the different crystalline structures possible for iron. When steels are solid, they rely on two allotropes: ferrite and austenite.

Ferrite (α-Fe) is the unit cell of iron under the temperature of 912°C. In ferrite, there are overall 2 iron atoms inside the cubic: 1/8 in each corner and one in the center. This crystal structure is also known as body-centered cubic (Bcc) structure. (Verhoeven 2007, p. 200.) In Figure 5 the structure of α-Fe is shown.

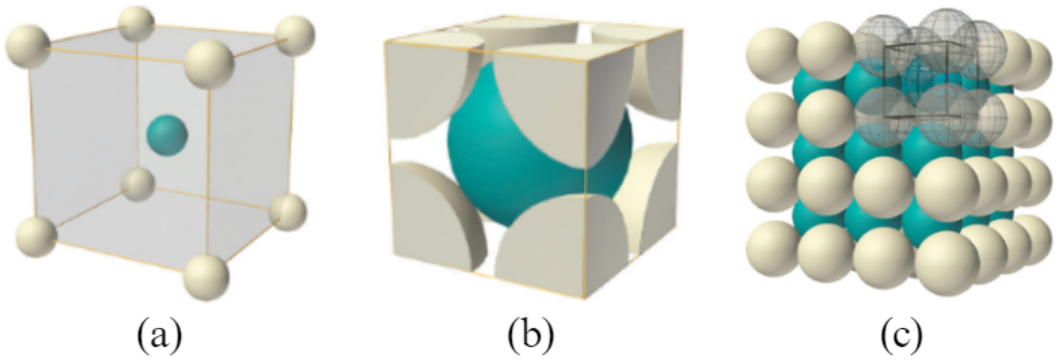

Figure 5: Bcc crystal structure: (a) unit cell, (b) unit cell with closely packed atoms, (c) repeated bcc-structure pattern (Chemistry LibreTexts 2013).

When iron is heated over 912 °C, the crystal structure changes from ferrite to Austenite (γ-Fe). In austenite, there are 4 atoms inside the cube: 1/8 in each corner and ½ on each side of the cube. This crystal structure is also known as face-centered cubic (Fcc) structure (Verhoeven 2007). Fcc-structure is illustrated in Figure 6 below.

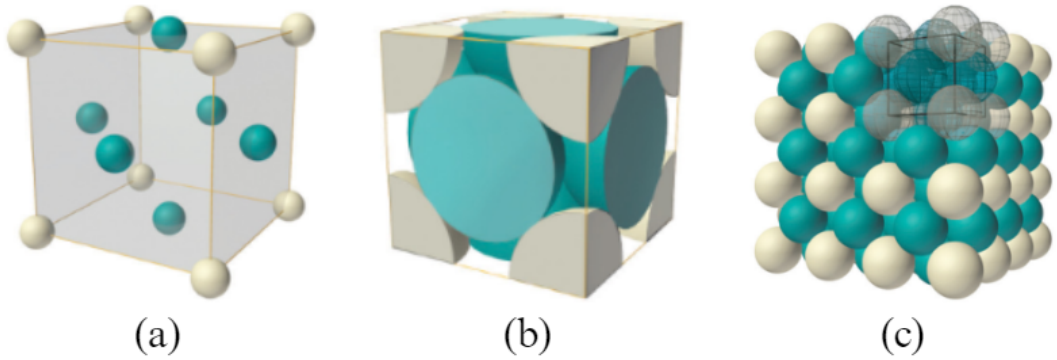

Figure 6: Fcc crystal structure: (a) unit cell, (b) unit cell with closely packed atoms, (c) repeated fcc-structure pattern (Chemistry LibreTexts 2013).

Carbon is the other main element of steel, and differences in the solubility of carbon between ferrite and austenite, together with allotropy, are the basis for the wide range of steel properties. Therefore, in steel, Carbon content by weight (wt%C) is essential to consider in physical metallurgy.

The size of the carbon atom is 1/30 of the size of the iron atom, meaning that carbon is small enough to fit between the gaps of the iron atoms. An interstitial solid solution is one in which tiny atoms occupy the interstices between larger solvent atoms. The interstitial sites are larger in austenite than in ferrite, meaning carbon is more soluble in austenite than in ferrite. For pure austenite, 2,11% by weight at 1150°C is the maximum carbon content (2,11 $wt\%C$),

and for ferrite, the maximum is 0.02 $wt\%C$ in temperature of 727°C (Dossett 2020, p. 29). Ferrite is a relatively pure form of iron because of its low carbon content.

When the solubility of carbon is exceeded in either austenite or ferrite, the excess carbon atoms that cannot anymore be placed between the iron atoms will combine iron-carbide compound known as Cementite (Fe_3C). In Cementite, there are three iron atoms for each iron atom, giving it a 6.7 $wt\%C$. Cementite is harder but more brittle than ferrite or austenite, and the amount, shape, and distribution of cementite in the microstructure change the physical properties of steel. (p. 30-31.) Cementite is a metastable phase relative to the equilibrium between iron and graphite, but achieving the equilibrium in low-carbon steels is hard without long-time annealing. Cementite is considered sufficiently stable to be used as a near-equilibrium phase, so its use when analyzing most steels' behavior should be considered instead of graphite. (Bhadeshia and Honeycombe 2017, p. 59.)

3.2 Iron-carbon phase diagram

A phase transformation happens when any material changes its atomic arrangement from one to another when it is heated or cooled. Phase diagrams identify the conditions at which a substance transitions to different phases.

The iron-carbon phase diagram represents the phases and phase transformations at different temperatures and carbon concentrations for iron-carbon alloys. Fe-C-diagram can only be used to predict equilibrium transformations, which means that the phase change is very slow (near equilibrium) heating or cooling, where the temperature stays constant, and enough energy (heat) is added or released to complete the phase transformation. Often, steels contain other additive elements or impurities that change the boundaries of the phases in the Fe-C diagram. For example, nickel and manganese extend the temperature area where austenite is stable, and chromium and molybdenum, on the other hand, restrict the austenite stability. As a result, using the Fe-C diagram directly for commercial materials and in practice is difficult. However, it is still important to understand the relationship between heat treatment and the microstructure of steel. (Dossett 2020, p. 33-38.) In Figure 7 below a iron-carbon phase diagram is shown. The area of interest regarding this study is marked with a red color.

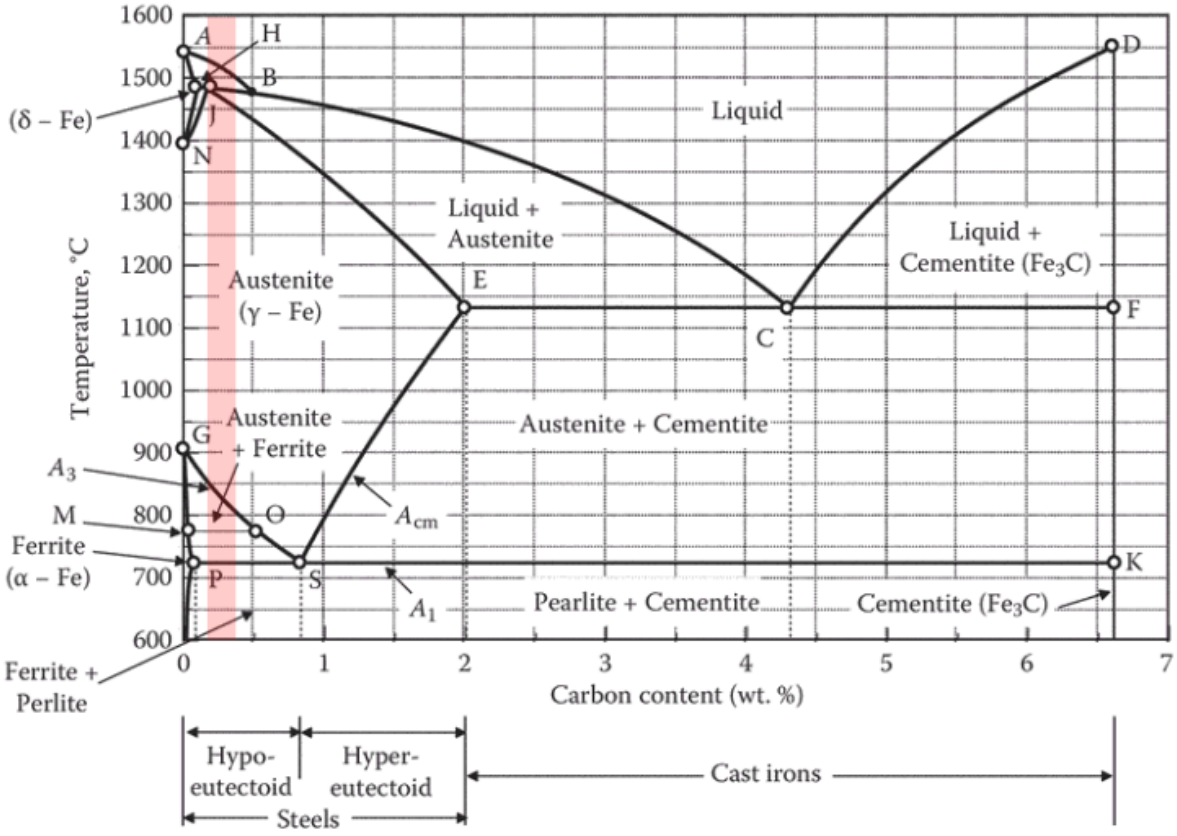

Figure 7: Iron-carbon phase diagram with area of interest marked with red (Rudnev 2017, p. 146).

3.2.1 Critical transformation temperatures

As shown in the FE-C diagram above, low carbon steel with 0.2 $wt\%C$ is liquid above temperatures over 1470 °C. The melting temperature depends on the $wt\%C$ of the steel: for reinforced steel, it is typically around 1450 °C to 1500 °C. Iron will start to transform into austenite when the temperature drops below this.

Pure iron starts to transfer from austenite to ferrite when the temperature drops below 912°C. This transition temperature is called upper critical temperature and is marked as A_3. When carbon is added to iron, the temperature in which this transformation occurs gets lower until 0.77 $wt\%C$, which then increases again. For example, for steel with a carbon content of 0.2 $wt\%C$, the transformation temperature from γ-Fe to α-Fe is around 830°C. Maximum lowering in the transformation temperature can be seen in the carbon content of 0.77 $wt\%C$. This is also known as the eutectoid point, often rounded up to be 0,8 $wt\%C$. Suppose steels contain less carbon than 0.8 $wt\%C$ (hypoeutectoid steels) or more carbon (hypereutectoid steels). In that case, the transition from austenite to ferrite goes through a heterogeneous two-phase field before the lower critical temperature of 727 °C is reached (A_1-temperature). At the A_1-temperature, all the austenite has changed into ferrite and cementite without depending

on the $wt\%C$ of the alloy. (Dossett 2020, p. 43.) In temperatures below the lower critical temperature (A_1), the micro-structure of the steel depends on the $wt\%C$ that the alloy has.

For ferritic iron, the maximum carbon percent that dissolves in the interstices is around 0.02%. The excess carbon that the iron has inside its interstices while being in the austenite phase will transform into cementite when the iron moves into the ferritic phase area. This will result in the formation of a mixture of cementite and ferrite grains. As the standards regarding rebar steel properties marked out, the carbon content of rebar steels is restricted to be under 0.24 $wt\%C$. This means a ferritic-pearlitic microstructure is formed when rebar steels are cooled down in equilibrium conditions.

3.2.2 Formation of pearlite

If the $wt\%C$ of the steel is 0.77 (eutectoid point) in slow cooling and near-equilibrium conditions, a two-phased, lamellar structure of cementite and ferrite layers known as pearlite forms. For hypoeutectoid steels like rebar, some of the iron will form ferrite called proeutectoid ferrite before the eutectoid temperature causing a mixed ferrite-pearlite microstructure. How much pearlite is formed depends on the carbon content and the respective microstructure fractions of ferrite and pearlite in the eutectoid temperature of 727°C for hypoeutectoid steels, which can be calculated using the lever rule. This rule states that the volume percentage of pearlite increases as the carbon content increases until it is 100% eutectoid composition. Lever rule can be seen below: (Bhadeshia and Honeycombe 2017, p. 41, 62.)

$$Ferrite\% = \frac{C\% - 0.222}{0.76 - 0.222} \tag{3.1}$$

Eutectoid steel (Pearlite) has a good combination of strength and ductility, and it is used in applications where both of these properties are important. Pearlite also has good wear- and fatigue resistance and reasonable fracture toughness. An example of a product that is made out of pearlite is high-strength wires. (Colpaert 2018, p. 117.) In Figure 8, a microstructure of both pearlite (left side) and hypoeutectoid steel (right side) are shown.

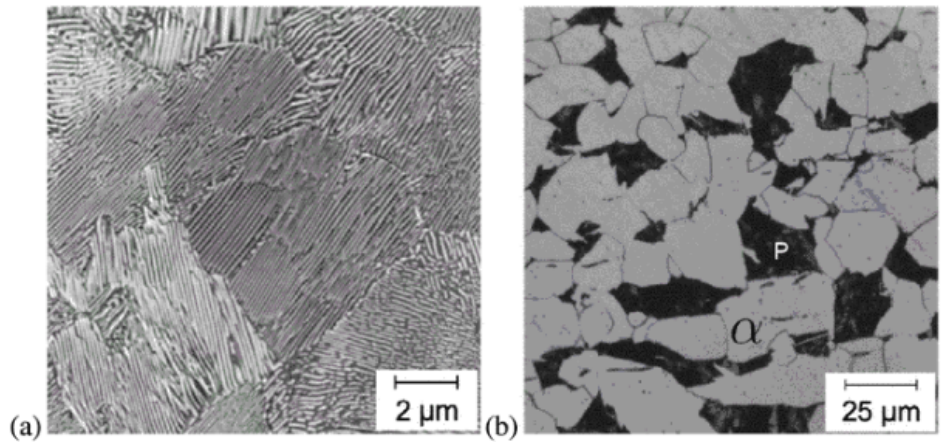

Figure 8: (a) Fully pearlitic 0.76 $wt\%C$ steel and (b) 0.2 $wt\%C$ hypoeutectoid steel (Bhadeshia and Honeycombe 2017, p. 62).

3.3 Metastable phases of steel

As marked out in previous section 3.2, the Fe-C phase diagram only shows the end products when the cooling rate of the material is relatively slow and near equilibrium. When the cooling rate is higher than that, the excess carbon atoms do not have enough time to diffuse and form pearlite. This causes carbon atoms to become trapped inside the ferrite lattice, causing the carbon composition to rise well above the maximum possible 0.02 $wt\%C$ in ferrite, forming new possible metastable phase structures depending on the cooling rate. (Dossett 2020, p. 32.) Therefore, the formed phases, their compositions, and amounts cannot be estimated using the phase diagram. The increased cooling rate makes it possible to form two new structures, bainite or martensite. (Verhoeven 2007, p. 26.)

3.3.1 Formation of martensite

When steel in the austenite region is quickly cooled to low temperatures, such as room temperature, it can lead to martensite formation. When martensite is formed, the cooling rate is sufficient for the austenite lattice to deform without any atom diffusion. Therefore, to obtain martensite, the steel must be cooled from austenite quickly enough to avoid transformation to any other solid state like pearlite. (Bhadeshia and Honeycombe 2017, p. 137.)

Martensite is a very brittle material, and its mechanical properties, such as strength and hardness, increase together with the growing carbon content. The material's brittleness can be removed while losing some hardness by heating the material a bit, known as tempering, resulting in a tempered martensite. (Verhoeven 2007, p. 27-28.)

Two types of martensite can be formed depending on the carbon content. Between 0 to 0.6 $wt\%C$, lath martensite is formed, and with carbon content above 1 $wt\%C$, plate martensite

is formed. Between 0.6 and 1 $wt\%C$, the structure is a mixture of these two. Temperature also affects the formation of lath and plate martensite. Lattice martensite forms at higher temperatures than plate martensite. Lath martensite is always formed for rebars due to its low carbon content. Lath martensite consists of lath-shaped structures parallel to each other, and the appearance can sometimes be fuzzy looking. Figure 10 (left-side) shows an optical micrograph of a lath-shaped martensite. (Verhoeven 2007, p. 27-28.)

Martensite formation in carbon steels occurs in a temperature range where the upper limit is marked as martensite-start temperature (M_s) and the lower limit with martensite finish temperature (M_f). Between M_s and M_f temperatures, some of the austenite will transform to martensite, and the rest of the structure stays in a form called retained austenite, which is retained after going under M_f-temperature. Couple elements as an exception (Co and Al), alloying substances make martensite formation more difficult, resulting in a decrease in M_s and M_f values. For low alloy steels, M_s-value can be calculated according to the chemical composition of the steel with the following equation: (Heidari Ghaleh 2011, p. 5.)

$$M_s = 561 - (474 * \%C) - (33 * \%Mn) - (17 * \%Ni) - (17 * \%Cr) - (21 * \%Mo) \tag{3.2}$$

Ms-temperatures for the batches used in the experimental test are listed in Table 6 below:

Table 6: Test batch chemical compositions and M_S-temperatures based on Equation 3.2.

Batch	%C	%Mn	%Ni	%Cr	%Mo	Ms (°C)
1 (d=10mm)	0,18	1,2	0,09	-	-	434.55
2 (d=20mm)	0,21	0,57	-	-	-	452.13
3 (d=32mm)	0,2	0,58	-	-	-	447.06

The inspection certificates do not give the composition of all the elements used in the formula. The value of M_s-temperature is strongly connected to the carbon composition of steel. Both temperature values see a rapid fall when the carbon composition of the austenite increases. (Verhoeven 2007, p. 30-31). The graph shown in Figure 9 below illustrates the phenomena. According to the graph, the M_f-temperature for rebar steel with 0,2%C is somewhere between 110°C to 230°C.

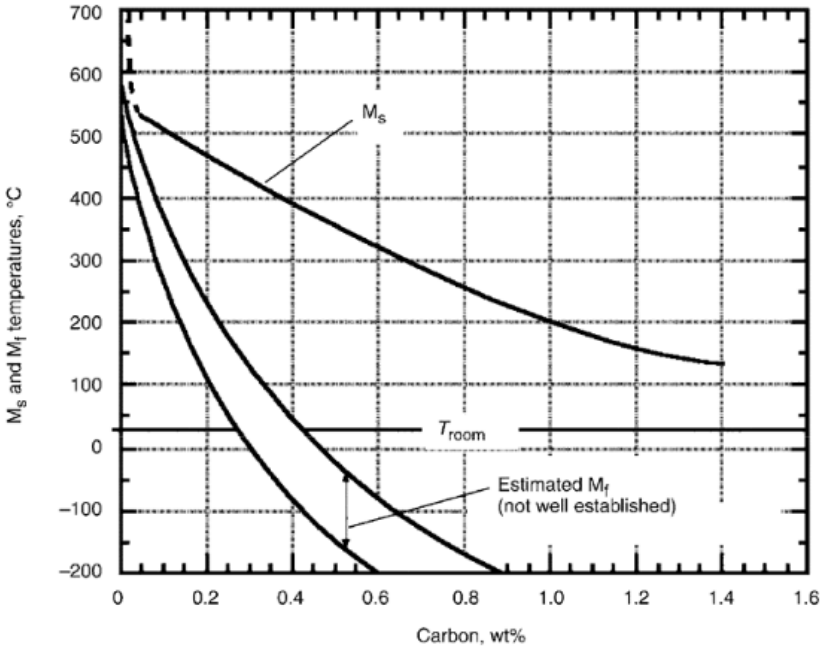

Figure 9: Martensite transformation temperatures compared to the amount of carbon (Verhoeven 2007, p. 31).

When the cooling rate is not fast enough, pearlite will form in the old austenite grain boundaries. When the temperature drops below the M_s-temperature, the excess austenite transforms martensite + retained martensite. For lath martensite, the amount of retained austenite is relatively small. The structure where both pearlite and martensite can be seen is shown in Figure 10 (right side). In the picture, the dark areas present the pearlite nodules on the grain boundaries surrounded by martensite + retained austenite.

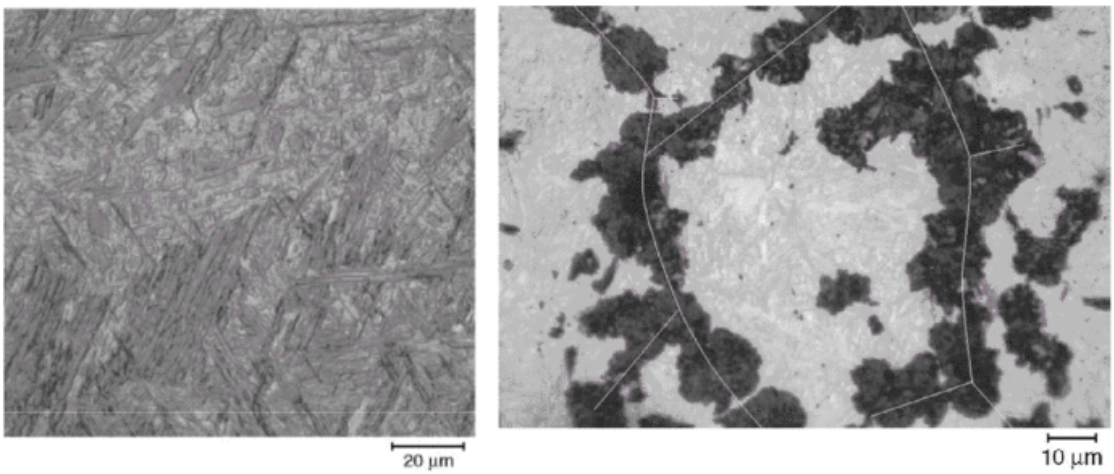

Figure 10: Fully lath-martensite structure (left) and martensite structure with pearlite nodules due to little too slow cooling (right) (Verhoeven 2007, p. 29, 32).

3.3.2 Formation of bainite

Bainite is formed when the cooling rate is too slow to form martensite and fast enough to form pearlite. Like pearlite, bainite is a mixture of ferrite and Cementite, but the difference compared to pearlite is that Cementite is in the form of filaments or small particles inside the ferrite matrix instead of being in organized layers. (Campbell 2012, p. 165.)

In steels, two forms of bainite can be seen, known as upper- and lower-bainite. Microstructures of these forms are shown in Figure 11 below. Upper bainite is formed just below the temperatures in which pearlite is formed, being around 550−400°C, whereas lower bainite is formed at temperatures around 400 to 250 °C. The main difference between upper- and lower-bainite is that the Cementite is much more closely packed and finer in lower-bainite than in upper-bainite. Bainite starts forming the same way as pearlite from the grain boundaries of the austenite, which sometimes results in a mixed structure of bainite and pearlite as some of the grain boundaries form pearlite and some bainite. Lower bainite has higher strength- and hardness properties than upper bainite. (Verhoeven 2007, p. 34-35.)

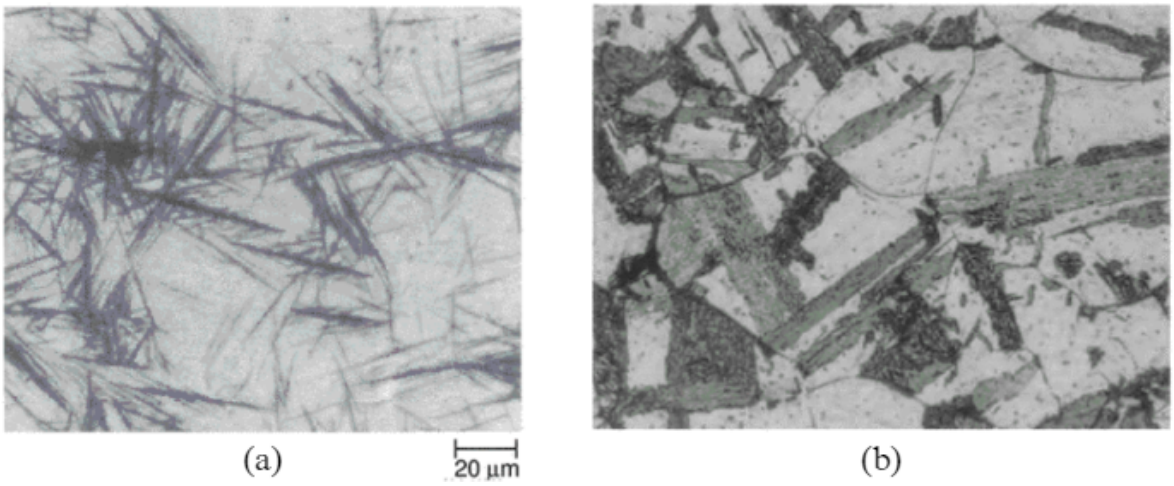

Figure 11: Light micrograph of lower bainite (a) and upper bainite (b) (Krauss 2015, p. 104, 106).

3.3.3 TTT and CCT-diagrams

Transformation diagrams are plots used to illustrate the phase transformations of specific materials as a function of time and temperature. Transformation diagrams can be used to optimize the heat-treating process so that the desired microstructure and mechanical properties are achieved during the heating- or cooling process. The two most used transformation diagrams are Continuous Cooling Transformation diagram (CCT-diagram) and Time Temperature Transformation diagram (TTT-diagram). (Dossett 2020, p. 55.)

TTT-diagrams are used to define phase transformations as a function of time at constant temperatures. From the TTT-diagram, it is possible to read the time required for a phase transformation to occur at a given temperature and the resulting microstructure when step-wise cooling is used. The curves on the diagram represent the conditions where a specific transformation occurs. In Figure 12, a schematic TTT-diagram for hypoeutectoid steel is introduced. (Dossett 2020, p. 55.) As can be seen, the TTT-diagram for hypoeutectoid steel has an extra curve showing the area for proeutectoid ferrite formation.

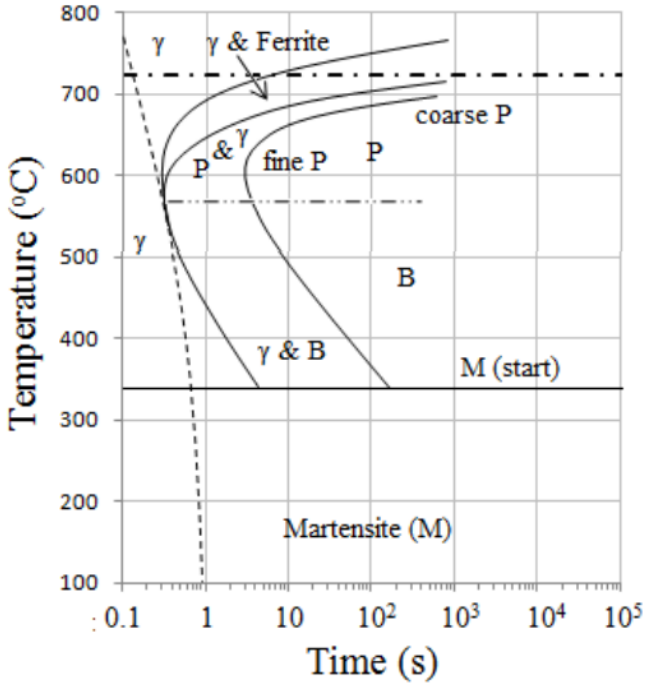

Figure 12: Schematic TTT-diagram for hypoeutectoid steel (Maraveas 2014, p. 3).

CCT-diagrams represent the transformation from austenite on cooling with different cooling rates when the temperature is continuously decreasing. In commercial practices, most heat treatments are done with continuous cooling, making CCT-diagrams more practical than TTT-diagrams. From CCT-curves, it is possible to see the temperatures in which a phase transformation occurs, the amount of different crystal structures obtained at different cooling rates and times, and the cooling rates needed to obtain wanted microstructure. (Totten, Shah, and Forester 2019, p. 979.)

Diagram shown in Figure 13 is a CCT-diagram made for B500B-grade rebar steel. The chemical composition of the rebar is close to the same as the rebars tested in this thesis, which makes it a valuable source of information. The diagram is modified with colors to make it easier to understand in what areas different phases occur. (Hameed S et al. 2021)

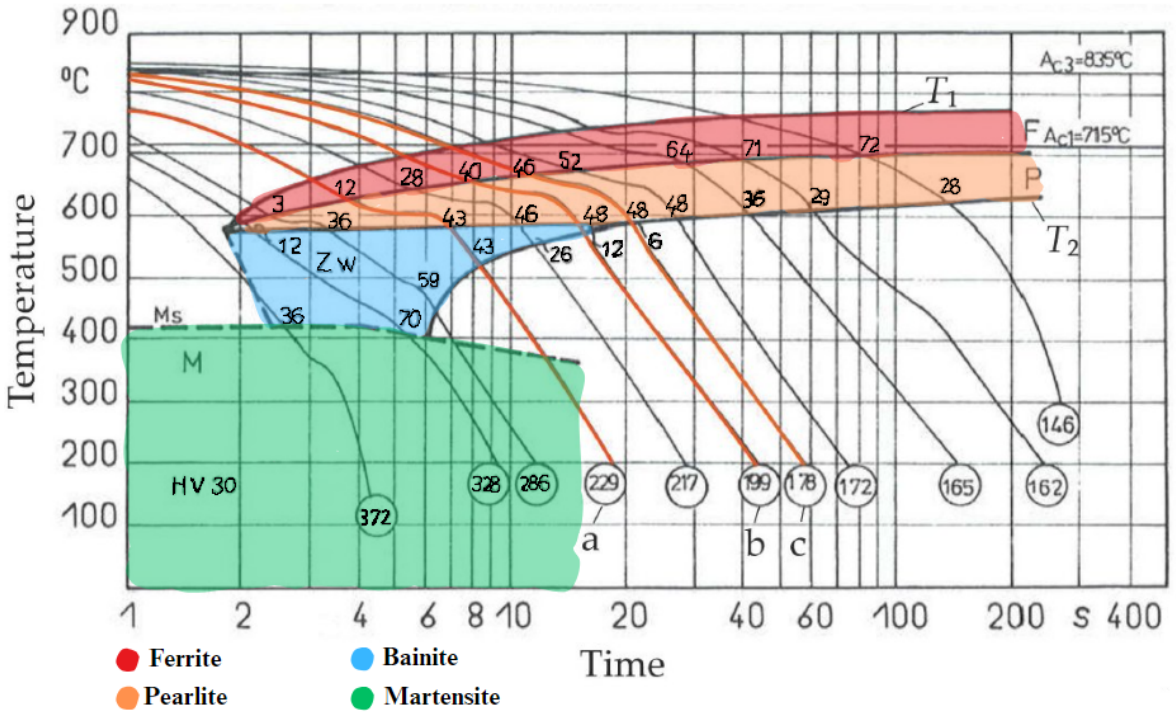

Figure 13: CCT-Diagram for B500B class rebar steel, modified (SteelData 2022).

3.3.4 Hardenability and hardness of steels

Hardenability is a material property used to measure how deep the material hardens during quenching, e.g., formats martensite. Steels with high hardenability form a deep martensite layer, while low-hardenability steel forms only a shallow layer. The material's chemical composition and grain size are the two most important factors affecting the material's hardenability. (Dossett 2020, p. 79.)

Hardness is a material property describing the material's ability to resist deformations and scratching. The harder the material is, the better the resistance against localized deformations. Hardness is highly dependent on the carbon content of the steel and the cooling rate of the heat treatment process. The material's ability to form martensite while quenching depends on the material's hardenability. The hardenability can be increased or decreased with other alloying elements. Manganese, chromium, copper, molybdenum, and boron are common alloying elements used to enhance the hardenability of the material. (p. 80, 88.)

Many different testing methods have been developed to measure materials' hardness. This study uses a common indentation hardness testing method known as the Vickers hardness test to check the hardness of differently heat-treated and forged rebars. A diamond-shaped indenter is pressed into the material's surface with a specific load in the test. The indenter will make an indentation to the surface, and by measuring its diagonal lengths, a Vickers hardness number (HV) is achieved. The load value used to make the indentation can vary, but gener-

ally, it does not affect the hardness value obtained. Vickers values are generally independent of the used load. In these tests, a load of 5 kg is used to make the indent. Vickers test needs better material preparation than other indentation test methods such as Rockwell or Brinell hardness test, but the results are more accurate. (Metsuco 2020) Vickers is a good hardness test for this work, as the metallographic samples work well as test pieces to be utilized for the Vickers test. Schematics of the Vickers test are shown in Figure 14 below.

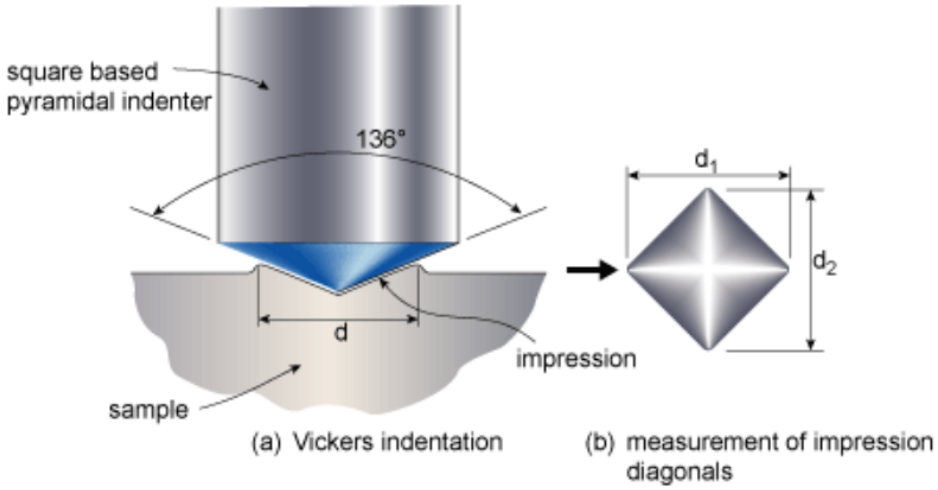

Figure 14: Schematic of Vickers hardness test (Gene, n.d.).

The CCT-diagram in Figure 13 had Vickers hardness values measured for B500B rebar steel with different microstructures. The table below lists Vickers values depending on the carbon concentration and martensite content. (Dossett 2020, p. 50.) These hardness values can be utilized later on when analyzing the obtained microstructures.

Table 7: Effect of carbon and martensite percentage to the hardness of steel, Listed in HV-values (Dossett 2020, p. 50).

Carbon content	99% martensite	95% martensite	90% martensite	80% martensite	50% martensite
0.18	406	376	342	311	285
0.20	438	388	361	332	303
0.22	448	393	376	342	311

4 HOT WORKING OF REBAR STEEL

Hot working is a widely used deformation process of materials, where the workpiece is plastically deformed above its recrystallization temperature to a predetermined shape. Recrystallization temperature is the temperature at which the formation of new grains occurs, resulting in increased ductility and a decrease in hardness and strength, making the workpiece easier to mold. (Dossett 2020, p. 39.) The process can be divided into three stages. The first part is to heat the material above the recrystallization temperature, then apply a compressive force on the material to gain the desired geometry, and lastly, cool down the material at a desired rate to achieve the desired microstructure. With heat treatment, the mechanical properties of the workpiece can be adjusted according to application.

In this study, the heating of the workpiece is done with induction heating, and the deforming is done by upset forging machinery. The forged bars are heat-treated by quenching and tempering with water as a quenchant.

As stated in the introduction chapter, this work aims to study the heating and heat treatment processes and their effect on the mechanical properties of the headed rebars and find suitable production parameters according to theory, simulations, and practical tests.

4.1 Upset forging

Upset forging is a forging process where the cross-sectional area of the workpiece is increased by compressing its length. In upset forging, the workpiece is held between grooved dies while an axial pressure is applied to the head of the workpiece, reshaping the geometry and cross-sectional area to the predetermined shape. Both hot- and cold upset forging are possible with the difference in the temperature in which the billet is forged.(Davis 2015, p. 852.)

The deformation process is often progressive depending on the workpiece's shape and size. This means that the forging is done in multiple strokes of the ram. Figure 15 illustrates the upset forging process.

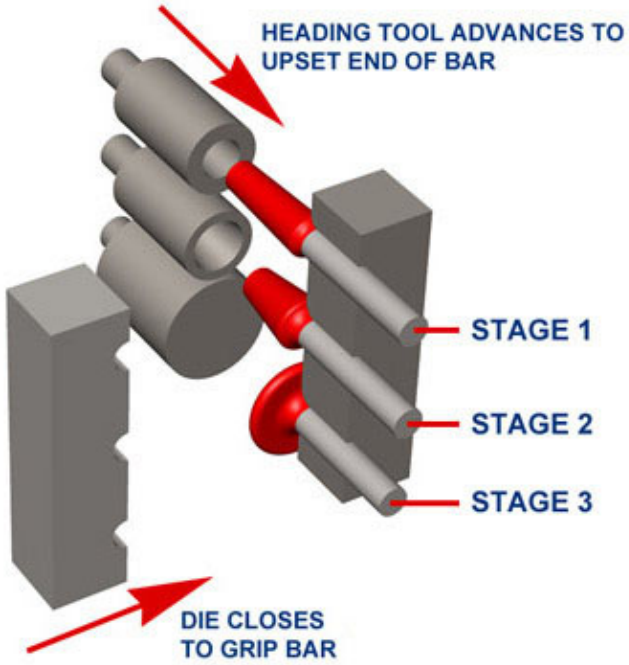

Figure 15: Upset forging with multiple stages (Chisen 2021).

Different input parameters that affect the forging process are listed in the fishbone diagram shown in Figure 16 below.

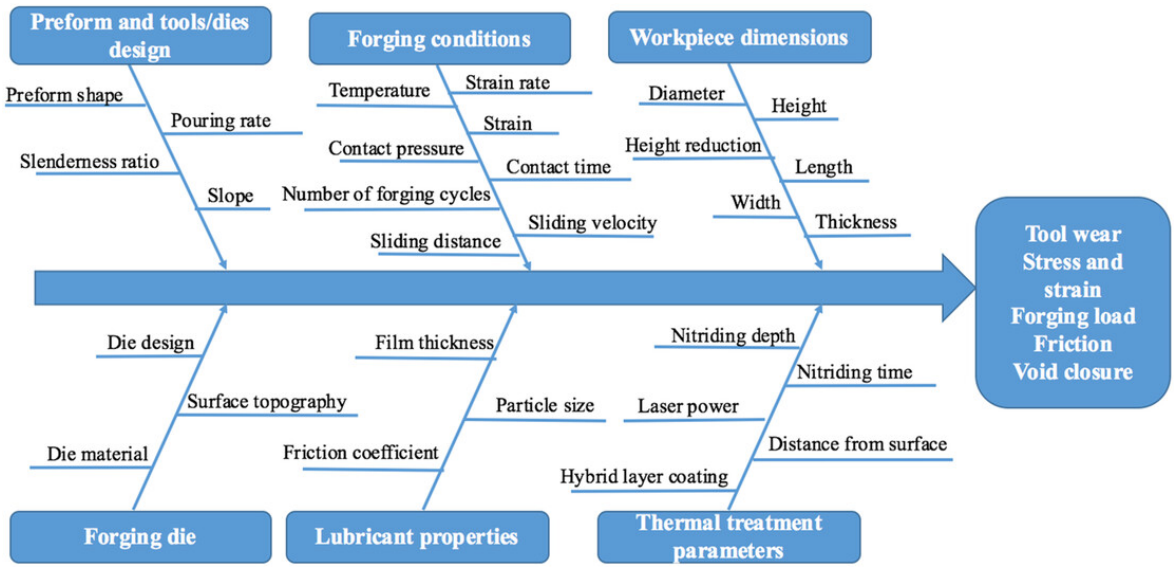

Figure 16: Parameters affecting the forging process (Sharma, Sharma, Gupta, and Singh 2023, p. 4).

It is important to consider these factors listed in the diagram to achieve good-quality products. The diagram is generally made for the forging process, so some parameters are not always

needed. For example, the need for thermal treatment of the dies and lubrication is not widely used in upsetting. (Davis 2015, p. 853.) The parameters and factors affecting the forging itself are analyzed by the company commissioning this work.

4.2 Thermal material properties

When analyzing heating and heat treatment, there are material properties that affect both processes.

Specific heat c (J/kg°C) represents the energy needed to heat the material. The higher the value of c is, the more energy is required to heat the material to the wanted temperature. Thermal conductivity of the material k (W/m·K) describes the material's ability to conduct heat. The higher the value of k is, the better the material is at conducting heat. Materials with good thermal conductivity are easier to heat uniformly and cool down, as the heat conducts inside and outside of the material faster. Metals have good thermal conductivity because of the crystal structure and the existence of free electrons that carry the heat. For metals, thermal conductivity generally decreases as the temperature rises. (Rudnev 2017, p. 90-91.)

The temperature, chemical composition, grain size, and many other factors affect both specific heat and thermal conductivity. For metals, thermal conductivity generally decreases, and specific heat rises as the temperature increases. In Figure 17, temperature-dependent values of specific heat capacity and thermal conductivity for reinforced steel are shown. (Gribniak, Bacinskas, and Kaklauskas 2006, p. 6.)

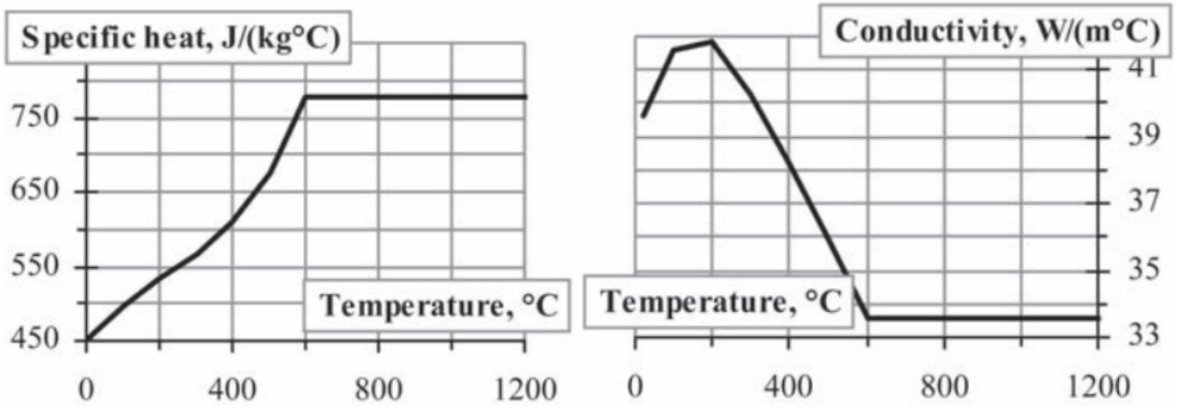

Figure 17: Temperature-dependent specific heat capacity and thermal conductivity of reinforcement steel (Gribniak et al. 2006, p. 6).

Density ρ (kg/m^3) affects the material's transformation kinetics and thermal properties. According to research papers, the density of reinforcing bars does not change significantly with temperature, so a constant value of 7855 kg/m^3 is used in this study.

4.3 Heat transfer modes

To fully understand the hot working process, knowing how the produced heat transfers in and out from the workpiece and how the rate of these transfers can be predicted is needed. Heat can be transferred by conduction, convection, or radiation. These three heat-transfer modes are the basis of heat treatment and are present in induction heating and heat treatment.

Conduction heat transfer

Conduction heat transfer occurs when energy transfers through a material or between materials in contact due to a temperature gradient where the heat transfers from higher to lower temperatures. Heat flux ϕ represents the amount of heat flowing through a unit area per unit of time and is often expressed as watts per square meter (W/m^2). Heat flux during conduction can be determined with Fourier's law,

$$q = -k \cdot \frac{dT}{dx} \tag{4.1}$$

Where k is the material's thermal conductivity (W/m·k), T is the temperature (K), and x is the direction of the heat flow. dT/dx is the temperature gradient that describes in which direction and at what rate the temperature changes. (Kreith and Black 1980, p. 1.) According to the law, the rate of heat transferred is proportional to the thermal conductivity of the material and temperature gradient; the better heat conductor the material is (high value of k) and the larger the temperature difference, the more intense heat transfer by conduction occurs. (Rudnev 2017, p. 92-93.)

Convection heat transfer

If the solid surface comes into contact with fluid or gas and there is a temperature difference, the heat will transfer from higher to lower temperature through convection. In convection, the heat is transferred by the movement of fluid or gas that carries energy. Convention heat transfer can be explained by using Newton's law,

$$q = \alpha \cdot (T_s - T_a) \tag{4.2}$$

Where α is the convection heat-transfer coefficient (W/m$^2\cdot$ K), T_s is the surface temperature of the material, and T_a is the ambient temperature, for example, the temperature of the fluid or gas that surrounds the material. According to the law, the heat transfer rate is directly proportional to the difference in surface and ambient area temperatures. (Rudnev 2017, p.93-94.) Heat transfer coefficient varies with temperature, so the temperature-dependent coefficient gives more accurate results. α is often measured experimentally by quenching the material and measuring the temperature change with thermocouples as a function of time. (Hasan, Peet, Jalil, and Bhadeshia 2011, p. 315.)

Convection can be divided into forced- and natural convection. In forced convection, the movement of the fluid or gas is generated in an external source, for example, in a pump or fan. In natural convection, the fluid or gas starts to flow as the temperature change causes density differences inside the material, which causes body forces like gravity to move the fluid or gas. Heat losses (convection rate) are often higher when forced convection occurs.

Radiation heat transfer

In radiation heat transfer, energy is transferred as electromagnetic radiation, meaning there is no need for interaction or movement of matter. Every material with a temperature above absolute zero emits thermal radiation. Stefan-Boltzmann law of thermal radiation can be used to describe the intensity of thermal radiation:

$$q = \sigma_s \cdot \epsilon \cdot T^4 \tag{4.3}$$

Where σ_s is the Stefan-Boltzmann constant with a value of $5.67{\cdot}10^{-}8$ W/m^{2}K^4, ϵ is the emissivity coefficient of the metal, and T is the temperature of the material. ϵ describes the material's ability to emit infrared energy and can have a value from 0 to 1. The higher the ϵ is, the more infrared energy the material emits. According to the law, warmer material emits more heat than colder material. (Rudnev 2017, p. 94.) For mild steel with a rough surface finish, the emissivity coefficient is around 0.6 to 0.9 (Fluke 2007).

4.4 Induction heating

The hot upset forging process starts with austenitizing the steel, which means that the rebar is heated onto the austenite temperature range. In this thesis, the austenitizing is done with Induction Heating (IH). Induction heating, which aims to heat the workpiece to temperatures suitable for hot forming, is called induction mass heating.

IH systems consist of a power supply, converters, a cooling system, and an induction coil. During the IH process, Alternating current (AC) is applied to the induction coil, producing an alternating magnetic field inside the coil. When electrically conductive material such as metal is placed inside the coil, two physical phenomena, eddy currents and magnetic hysteresis, heat the material. No contact is required between the coil and the workpiece. A basic induction heating system with main components named is presented in Figure 18.

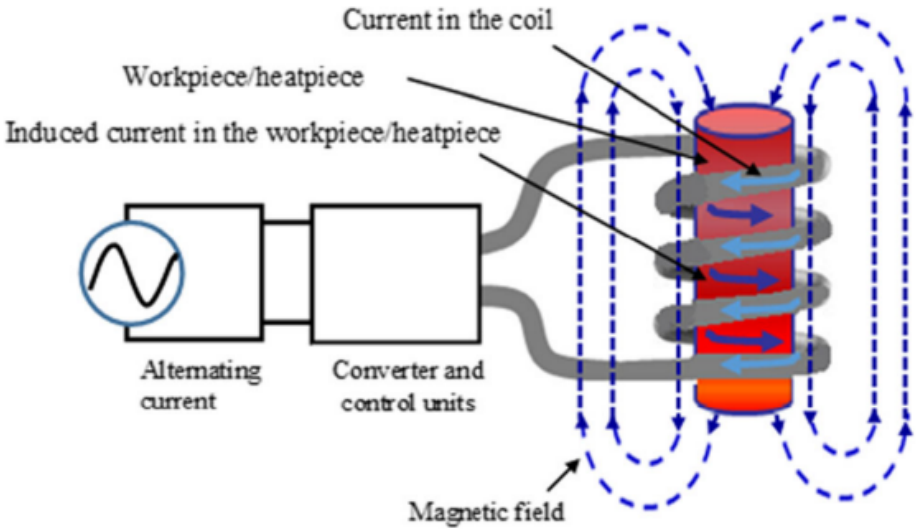

Figure 18: Induction heating system (El-Mashad and Pan 2017, p. 83).

Eddy currents are formed due to the changing magnetic field inside the coil. The passage of this circulating current through a conductive material produces heat. The formed eddy currents are the primary heat source during induction heating, but in ferromagnetic materials like steels, some heat is generated by magnetic hysteresis. Hysteresis is caused by the oscillation of the magnetic dipoles of the material when the altering magnetic field changes its polar orientation, producing heat due to internal friction. In steels, magnetic hysteresis occurs only until the curie temperature, when the material loses its magnetic properties. For pure iron, the curie temperature is 770 °C, and for steels, the curie point depends on the material type and purity. (Lucia, Maussion, Dede, and Burdio 2014; El-Mashad and Pan 2017) The Curie temperature of the steels processed in this work is in the same range as that of pure iron. It is estimated that hysteresis produces 6-8 % of the heat below the curie temperature in steels (Haimbaugh 2015, p. 12.)

Induction heating offers high power density, fast heating rate, and controllability compared to other heating techniques used in industrial applications such as flame- or resistance heating (Lucia et al. 2014, p. 2510.). On the other hand, induction heating comes with many phenomena causing uneven distribution of heat that can cause bad forging quality if not fully

understood or considered in production. These different phenomena are discussed in the next subsections. (Rudnev 2017, p. 51.)

4.4.1 Electromagnetic properties of materials

Electromagnetic properties of materials are a broad expression referring to many material properties. This study will only concentrate on the most important parameters that affect the induction heating process.

Electrical resistivity ρ_e (Ω*m) and electrical conductivity σ (S/m) describes the material's property to conduct electric current. Metallic materials are considered good electrical conductors, but the electrical resistivity differs between metals. Factors influencing the resistivity are, for example, temperature, chemical composition, and microstructure. Steel is considered a metal that has high electrical resistivity. (p.53-54.) When the metal has high electrical resistivity, substantial heat is produced when an electric current passes through the metal. During heating, the electrical resistivity tends to rise with temperature, meaning that both ρ and σ are temperature-dependent variables.(Haimbaugh 2015, p. 10.)

Magnetic permeability μ_r is a value used to indicate the material's ability to conduct magnetic flux and is an important parameter for the magnetic hysteresis to occur during induction heating. Materials with high μ_r respond more to the changing magnetic field during induction heating, resulting in better heat generation. When heating steels and other iron alloys, the value of μ_r starts to decrease when the temperature rises approximately above 550 °C. After curie temperature, which was around 770 °C, the workpiece becomes non-magnetic, resulting in a significant drop in the value of μ_r.

4.4.2 Skin effect

Skin effect describes the uneven current distribution that occurs in induction heating. The maximum current density value is always on the surface of the workpiece, and the value will decrease when moving closer to the center. This phenomenon causes the eddy currents, the primary heat production source during induction heating, to concentrate on the surface of the workpiece, heating the surface faster than the core. (Rudnev 2017, p. 61.) Figure 19 illustrates the current density distribution when the cylindrical billet is heated.

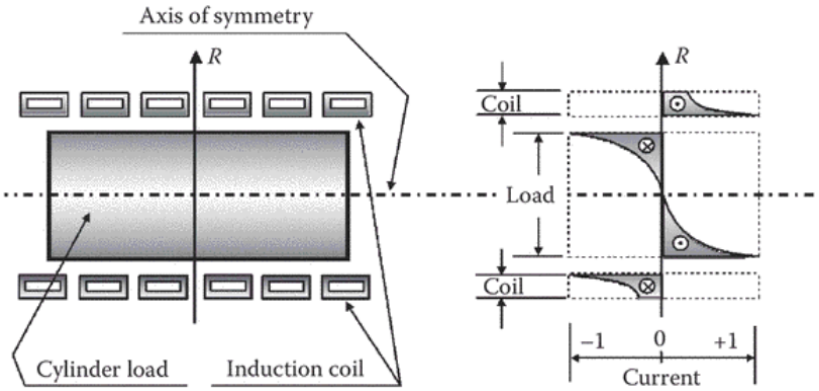

Figure 19: Current density distribution during induction heating (Rudnev 2017, p. 61).

Penetration depth δ [m] is used to analyze the magnitude of the skin effect in different circumstances. It describes the depth to which 86 % of the power used concentrates measured from the surface of the workpiece towards the center. The following equation can be used to calculate δ.

$$\delta = 503 \cdot \sqrt{\frac{\rho_e}{\mu_r \cdot F}} \tag{4.4}$$

Where F is the frequency (Hz), ρ_e is the electrical resistivity of the workpiece, and μ_r is the relative magnetic permeability. (Rudnev 2017, p. 62.). Penetration depth decreases with higher frequency and increases when the temperature rises as the value of ρ increases with temperature, and the value of μ_r gets lower.

Taking skin effect into account is essential to gain a uniform heating pattern. When the surface of the workpiece reaches the target temperature, the temperature in the center might not be near the target temperature. Because of this, the temperature needs to conduct from the surface to the core. If too high input power is used to achieve target temperature faster in the core, it will often result in melting the surface (Ghoshdastidar 2012, p. 76.)

4.4.3 Electrical end and edge effect

In addition to the skin effect, nonuniform heating in IH is caused by the changes in the electromagnetic field in the induction coil's end region and at the workpiece's edge, which is known as the electromagnetic end-and-edge effect.

The end effect is caused when the magnetic field changes near the part end, and if not taken into consideration, it can cause under- or overheating of the hot end of the workpiece. The hot end refers to the end of the bar that is intentionally heated. The following parameters need to be considered to define the effect of the end effect: (Rudnev 2017, p. 78.)

- Ratio of coil inner radius and workpiece radius (R_i/R)
- Coil overhang σ_c (mm)
- Power density
- Frequency
- Electromagnetic properties of the workpiece

Typically, Increased frequency and extended coil overhang result in excess power concentrated at the end of the heated bar, leading to noticeable overheating. Lower frequencies and larger radial gaps between the coil and the bar reduce electromagnetic coupling, causing the head to be under-heated. (Indutrial Heating 2008)

Coil overhang refers to the length of the induction coil that extends the heated part. The effect of coil overhang on the power density at the end of the workpiece is illustrated in Figure 20 below. As illustrated, with large coil overhangs, σ_6, σ_7, the power density focusing on the end is much larger compared to other parts of the billet, causing severe overheat on the hot end of the bar. With negative coil overhang, meaning that the head of the workpiece is outside the coil, only 10 % Of the power density in the middle occurs in the end. Correct coil overhang to gain uniform heating is case-specific and is affected by the factors listed above. (Rudnev 2017, p.80-83.)

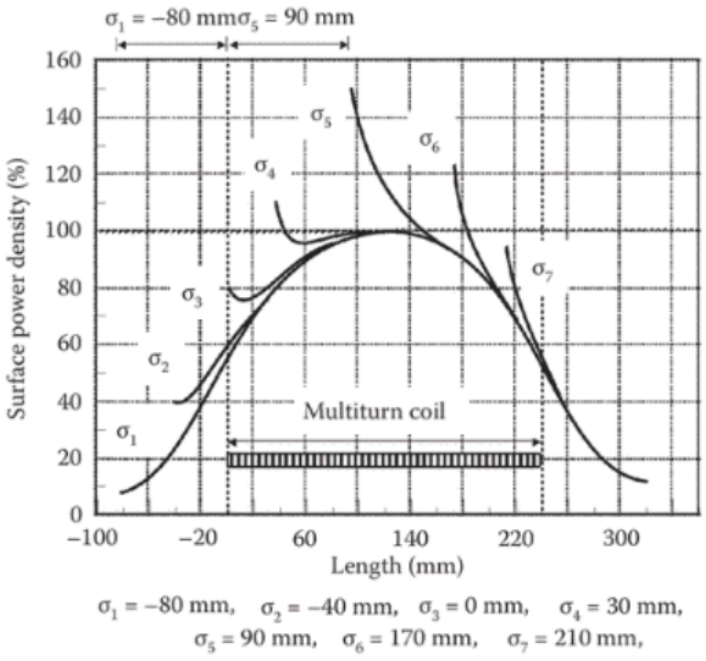

Figure 20: Effect of different coil overhang lengths to the power density distribution of cylindrical workpiece (Rudnev 2017, p. 81).

The electromagnetic field distortion in corner areas of the billet causes the edge effect. At the corners, the magnetic field creates higher current density, leading to more intense heating. With poor induction heating design and heating recipe, the combination of both end- and edge effect can easily cause too intense heating in the head of the heated bar.

4.4.4 Heating time and finishing temperature

In hot forging, the heating time t and final temperature T_f must be enough to heat the whole forging stock over the austenite region of the alloy. When using induction heating, the surface of the workpiece tends to heat faster than the core of the bar due to different phenomena, for example, the skin effect. It is important that enough time is used to heat the material to gain even temperature distribution in the whole heated area. The larger the cross-sectional area of the bar is, the longer time is needed to heat up the billet.

Inside the austenite region, the forgeability of the workpiece differs. The plasticity of steel increases as the temperature rises, resulting in improved forging processes and reduced die wear. Increasing the forging temperature too much could lead to steel overheating. If steel is overheated, it will decrease the ductility and tensile strength of the end product. If the temperature gets close to the solidus temperature, more severe phenomena, known as burning, might occur. In burning, irreversible and permanent damage occurs due to internal oxidation and local melting in grain boundaries due to low-melting point elements such as copper penetrating, weakening the grain boundaries, and causing embrittlement. Copper, Phosphorus, and sulfur significantly affect steel overheating; all of these elements are found in rebar steels. Heat treatment cannot be used to restore properties in burned steel. (Rudnev 2017, p. 502-506.)

During forging more heat is generated as deformational and frictional heat. If the billet is heated close to the region where overheating might occur, the overheating might occur during the forging process instead of during the heating phase. The temperatures in which overheating occurs depend on the steel composition and time exposed at high temperatures. For low-alloy steel, overheating occurs in temperatures over 1200°C, and burning in temperatures over 1400°C. If overheating or burning happens during the forging process, the forged workpiece will often break after cooling or heat treatment. (Campbell 2012, p. 603.)

The temperature at which the forging process is done should be well above the transformation temperature to gain better forgeability and ensure the whole structure is austenitic. On the contrary, too high temperatures need to be prevented to prevent excessive grain growth and overheating. For rebar steels, a temperature of 1150°C is suitable for the forging process. For a carbon steel with a carbon content of 0.2% the maximum forging temperature is 1275°C.(Davis 2015, p. 863.)

4.4.5 Heating length

In upset forging, the diameter of the workpiece increases while the length of the workpiece shortens. During upsetting, a specific bar length must be compressed to fill the die sufficiently. The die fills completely when the bar is compressed from a distance so that the volume of the compressed bar is the same as the volume of the die.

When hot upsetting, the whole length of the deformed bar must be heated into the approximate forging temperature as uniformly as possible. This way, incomplete deformation, cracking, dimensional inaccuracy, unwanted microstructural changes, and tool wear can be minimized. On the other hand, by heating only the needed amount of the bar, no extra energy is consumed by heating unnecessary material. It is easy to set a specific heating length when utilizing induction heating. To define the needed heating length L_b [mm], the following formula is utilized:

$$L_b = \frac{V_h}{\pi \cdot R} + 20 \tag{4.5}$$

where V_h is the volume of the forged head, and R is the radius of the reinforced bar. 20 mm is added as a safe factor to ensure enough material is heated. The equation is based on basic geometry calculations assuming that the volume of the heated bar and the volume of the forged head must be the same. Head volumes are collected from 3d models to get accurate values.

4.4.6 Heating power

Required heating power P_w (W) to heat the material to the required temperature can be roughly estimated with the following formula:

$$P_w = m_w \cdot c \cdot \frac{T_f - T_{in}}{t} \tag{4.6}$$

Where m_w is the mass of the heated area (kg), c is the material's specific heat, T_f is the finishing, and T_f is the starting temperature of the workpiece. P_w represents the power that needs to be induced from the coil to the workpiece to achieve the desired temperature in a given time. This does not take into account the power losses happening during the process. during the process, energy is lost in thermal losses, coil turns, heating undesirable materials in the surrounding area, energy conversion, and by cooling the coils and heating machinery. (Rudnev 2017, p. 98.)

In this study, a constant system efficiency of 51 % is used, which is a typical system efficiency for solid-state power supply induction heating systems (Haimbaugh 2015, p.21). More precise, case-specific system efficiency could be calculated, but there is no need for it as the power is only used as ballpark estimation at the start of the simulation, and the power is then adjusted. For example, suppose 15 kW of power is needed to heat a workpiece to the forging temperature in a given timescale. In that case, 29.4 kW must be taken from the power supply to consider all the energy losses during the process.

4.5 Quenching and tempering

In quenching, steels with a temperature above the austenite region are rapidly cooled down to harden the workpiece. Typically, quenching aims to achieve as much untempered martensite as possible, but other phases of steel (bainite, pearlite, ferrite, and cementite) might be formed depending on the quenching time and cooling rate. For most applications, untempered martensite obtained during the quenching is too brittle, so another heat-treating method called tempering is needed to achieve tempered martensite. In tempering, the quenched steel is reheated to a specific temperature for a specific time to reduce the brittleness and increase the toughness of the steel while losing some of the hardness obtained in quenching. In Figure 21 below, the generic structure of the quenching and tempering process is shown in the time-temperature diagram.

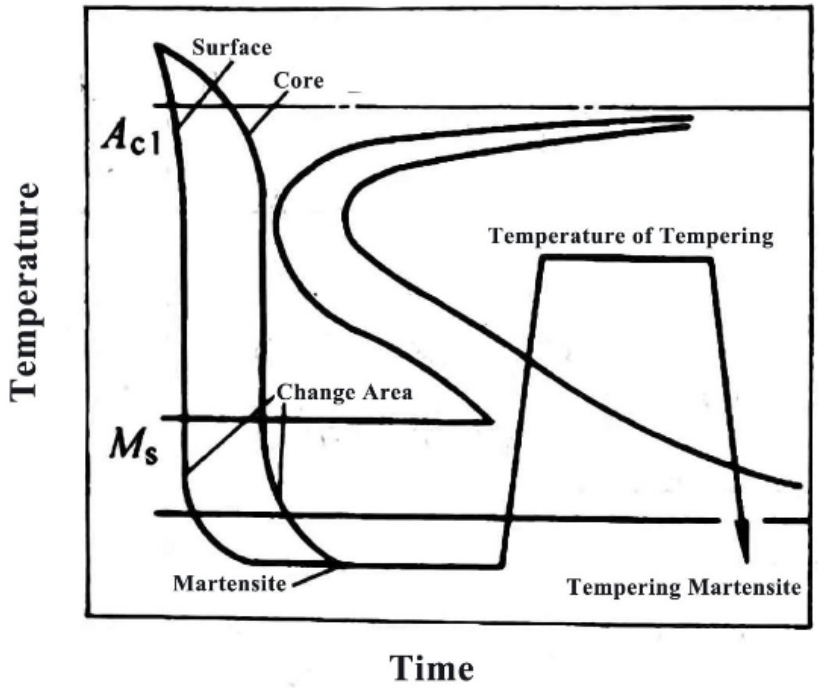

Figure 21: Schematic temperature curve of quenching and tempering including TTT-diagram to reflect the structure changes during the process (RMC 2021).

Quenching and tempering (Q&T) is a common combined heat treatment process and can be utilized for forged rebars to tailor the mechanical properties according to the use case. Statistically, approximately 80 % of problems related to heat treatment happen during cooling processes, while 20 % occur during heating, which is why understanding the quenching and tempering process is essential. (Canale, L.C.F, Mesquita, R.A, and Totten, G.E 2008, p. 255.)

4.6 Quenching and self-tempering

In quenching and self-tempering (QST), instead of cooling the whole workpiece and afterward heating the workpiece to a specific temperature to temper it, the residual heat is utilized. In the process, the workpiece in the austenite region is quenched, causing the surface and outer layers of the workpiece to cool rapidly, forming martensite while the core remains hot. As the quenching is stopped before the core gets cold, the residual heat from the core tempers the outer, hardened layer.

Quenching and self-tempering is widely used in steel mills as the method offers many advantages compared to the traditional Q&T process. Self-tempering saves energy, as the energy used for tempering is obtained from the core. Also, no additional capital investments are needed for additional tempering furnaces, thus simplifying the production process and reducing the floor space needed. Also, fewer micro-alloying elements are needed to produce needed mechanical properties. (Kanaev, Bogomolov, Kanaev, and Reshotkina 2018)

Tempcore, a trademark of the CRM group, was developed in the 1970s to manufacture high-strength weldable rebars with good ductility from mild steel billets. In the Tempcore process, after rolling the hot steel billet to the desired shape and size, controlled cooling, typically water spraying, is applied to the billet to achieve martensite on the surface while the core temperature stays high. When the quenching is stopped, self-tempering at the surface layers occurs as the temperature gradient between the core and surface increases the surface temperature. After slowly cooling on air, the end structure of the bar is a combination of a tempered martensite surface layer with a core that consists of bainite, ferrite, and pearlite. The schematic structure of the process is shown in Figure 22 below. (Satyendra 2020)

Utilizing QST as a heat treatment method for headed rebars is an interest of this thesis. Important aspects that need to be taken into account when analyzing if QST is applicable are the following: (Rudnev 2017, p. 347.)

1. Suitability of the headed rebar geometry for self-tempering. Self-tempering is easier to handle when dealing with simple geometries.

2. Possibility to use self-tempering for small-sized headed rebars. Achieving enough residential heat in workpieces with low mass might be problematic.

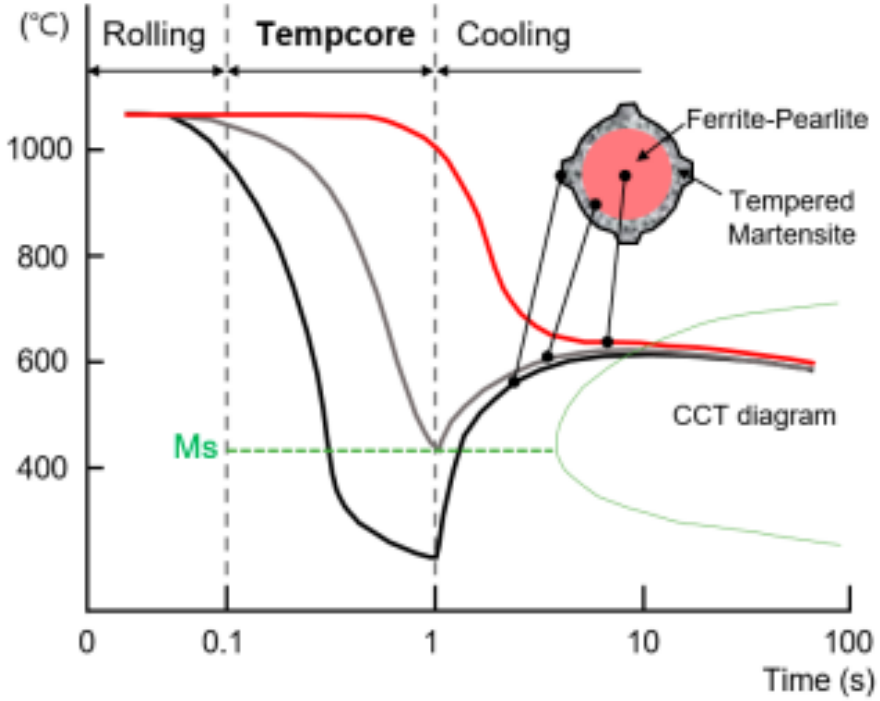

Figure 22: Schematic time-temperature chart of tempcore treated rebar (Park, Yi, Kim, Han, Lee, and Moon 2019).

During quenching, both inadequate and excessive cooling can cause problems. The better the heat-extracting potential is, the faster the rebar cools down, and more untempered martensite is achieved. However, using quenchants with too high cooling power can cause problems such as increased distortion and cracking. The goal is to have a quenching process that provides cooling high enough to achieve the required microstructure with as low a cooling rate as possible to prevent unwanted distortions. (Dossett 2020, p. 69.)

4.6.1 Quenching in water by immersion

The quenching medium can be liquid, solid, or gas if it extracts heat from the part with the wanted rate. In this case, water without any additives is used as a quenchant. When liquid media is used, the process of quenching can be split into three different stages illustrated in Figure 23: the vapor blanket stage (a), the boiling stage (b), and the convection stage (c). (Mackenzie and Lambert 2003, p. 2.)

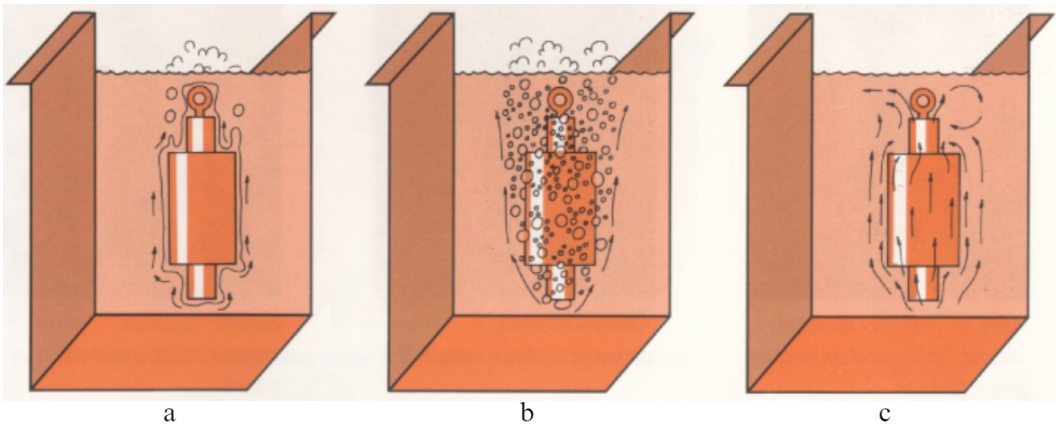

Figure 23: Cooling stages during quenching (Mackenzie and Lambert 2003).

The vapor blanket stage occurs when the hot workpiece first comes in contact with the liquid quenchant. In this stage, the heat transfer between the workpiece and quenchant is slow as a thin vapor pocket produced by the vaporization of the quenchant insulates the workpiece, causing weak convection between the materials. The thickness of vapor pockets differs between quenchants.

The boiling stage occurs when the insulating vapor pocket collapses, and the quenchant is in contact with the hot workpiece, forming boiling bubbles. In this stage, heat extraction is at its highest as the hot liquid at the surface of the workpiece mixes well with the colder liquid. This stage stops when the workpiece surface temperature reaches temperatures under the boiling point of the liquid. After this, the cooling process moves to the convection stage, causing the heat transfer rate to drop.

4.6.2 Effect of water temperature

When the temperature of water used as a quenchant rises, the energy required to start the vaporization lowers. This decreases heat flux and cooling rate as the vapor film formed at the start thickens. As stated in subsection 4.6.1, the vapor film prevents direct contact between the workpiece and quenchant, resulting in a lower heat transfer rate. During the boiling stage, the cooling rate also depends on the temperature difference between the quenching liquid and the workpiece. Figure 24 below presents the effect of water temperature on the cooling rate for a 60mm Inconel 600 probe with a 12.5mm diameter. (Totten, Howes, and Inoue 2002, p. 270.)

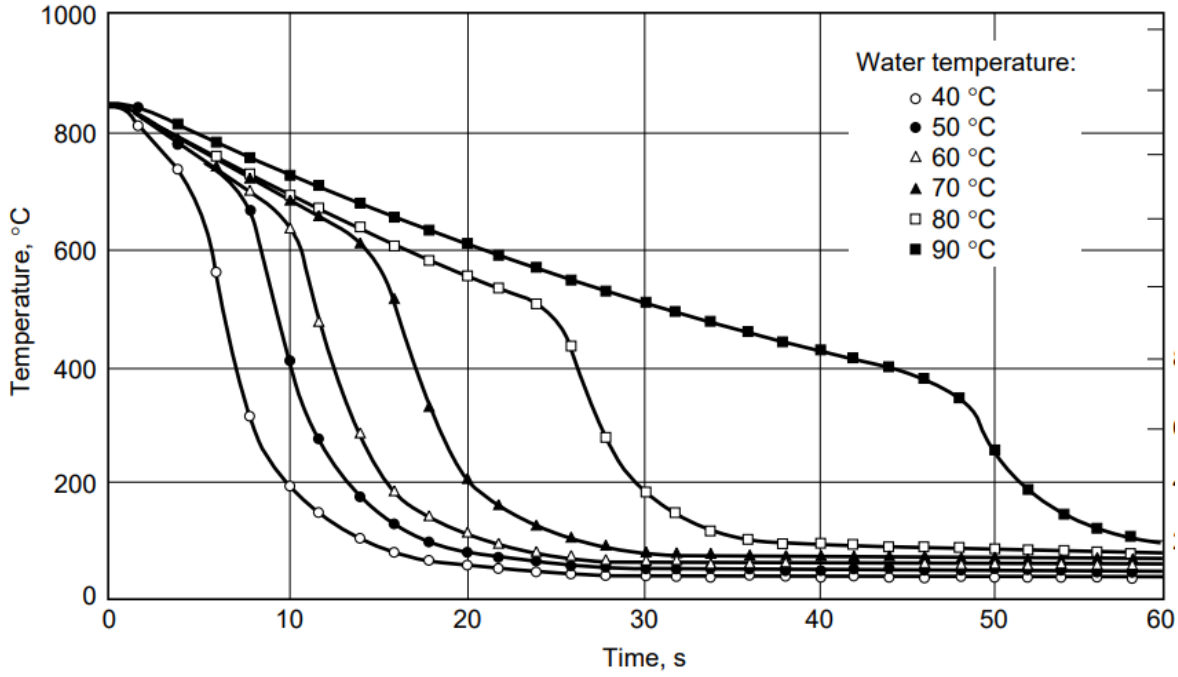

Figure 24: Affect of water temperature to the cooling rate (G. Totten et al. 2002, p. 270).

This study uses a constant water temperature of 35 °C. In production, the quenching water tends to warm, which is why a cooling system to keep the water temperature constant is essential to achieve uniform quality.

4.6.3 Heat transfer rate

During quenching, most heat transfer happens through convection heat transfer between the quenching medium and the workpiece quenched. Some heat is also transferred through radiation heat transfer. Heat is also transferred between the surface and core through conduction. The heat flux for the convection heat transfer can be calculated when the heat transfer coefficient and the temperature difference between the workpiece surface and quenchant are known.

Temperature-dependent heat transfer coefficient k can be calculated with the following equation: (Hasan et al. 2011, p. 3.)

$$k = \frac{\rho \cdot V \cdot C_p \cdot T}{A \cdot (T_s - T_a)} \tag{4.7}$$

Where ρ is the material density (kg/m^3), V is the workpiece volume (m^3), and C_p is the specific heat capacity (J/kg°C). T is the cooling rate (°C/s), A is the workpiece area (m^2), T_s is the workpiece surface temperature, and T_a is the quenchant temperature. All values except

the cooling rate T can be found in the literature, but the cooling rate is case-specific and needs to be measured experimentally.

The temperature-dependent value for the cooling rate was achieved through experimental tests. The general structure of the test is shown in Figure 25. First, the rebar was heated to around 1150 °C. After this, the bar was immersed into a water tank with a water temperature between 30-40°C, and the surface temperature was measured every second with a thermocouple attached to the surface of the bar. Three measurements were done for each rebar diameter, and the average cooling rate at different temperatures was used in calculations. The data was processed in Excel to obtain the data used in simulations.

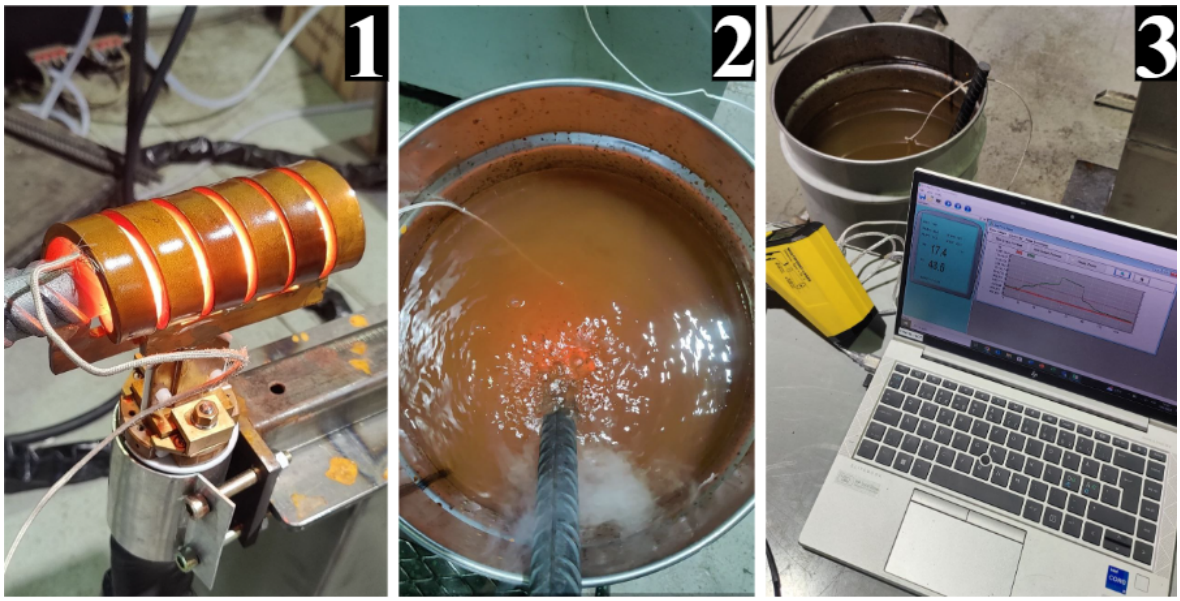

Figure 25: Cooling rate measurement method utilized for all rebar diameters. 1. Heating the rebar billet from the needed length to 1150 °C. 2. Immersing the heated billet into water. 3. measuring the cooling rate during the process.

In Figure 26, the cooling rate achieved through the test for 32mm rebar is shown on the left side, and the conduction heat transfer coefficient (HTC) calculated with Equation 4.7 on the right side. To calculate the HTC, the volume V and surface area A were achieved from the 3D model of the headed rebars.

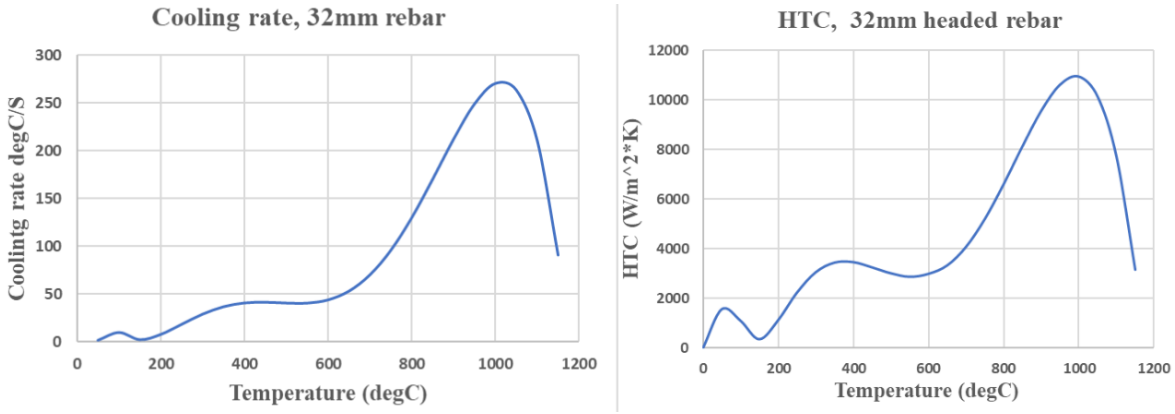

Figure 26: Cooling rate and Heat-transfer coefficient for 32mm headed rebar.

4.6.4 Quenching time

The end temperature after quenching is directly proportional to the heat transfer rate between the workpiece and quenchant and the time that the workpiece is kept in the quenchant. As the tempering is done with the residual heat from the core, the tempering time needs to be adjusted so that there is still enough heat in the core to achieve the necessary tempering temperatures.

According to subsection 3.3.1. The amount of martensite achieved during quenching depends on the materials M_s- and M_f-temperatures. To achieve martensite, the temperature needs to go below M_s-temperature, and the martensite volume fraction depends on how close to the M_f-temperature the material is quenched. According to subsection 3.3.1 the M_s-temperature for rebar steel is around 430 °C and M_f-between 230-150 °C.

Therefore, the needed quenching time is affected by the desired temperature, cooling rate during the quenching, workpiece size, and geometry. Specific quenching times for headed rebars are achieved through simulation later in this study.

4.6.5 Tempering temperature

Typically, tempering is done in temperatures from 150 °C to 650 °C. Higher Tempering temperature (TT) results in better ductility and toughness while losing strength and hardness. Defining precise TT depends on the mechanical properties required by the end product and is affected by the material, geometry, and size.

The self-tempering process differs from the traditional tempering process in that instead of having a constant tempering temperature, where the material is kept for a specific time, the tempering temperature changes continuously. Self-tempering is typically more complex to control than traditional tempering and does not work for all geometries and sizes.

This study defines a suitable Self-tempering temperature (STT) using simulations and experimental tests. First, simulation determines quenching time that leaves enough residual heat to achieve STT of around 400 °C. 400 °C is the average temperature between min. and max tempering temperatures that are typically used. By increasing or decreasing the quenching time, the STT changes in the opposite direction, and thus, the correct value providing the best tensile properties can be defined with tensile tests. By making a tensile test with quenching time obtained through simulation and with time above and below the simulation time, the correct tempering temperature can be defined for each headed bar.

4.6.6 Temper embrittlement

Ductility describes the material's ability to have plastic deform before a fracture. Materials with good ductility are called ductile materials, and materials with low ductility, on the other hand, are brittle materials. In tensile tests, the material's ductility can be estimated with the value of total elongation at maximum stress, A_{gt}.

Previous tensile test reports made by the company for headed steel bars suggest that headed bars with short quenching time or without quenching after forging are prone to have bad total elongation in tensile tests without much difference in yield strength if compared to test samples with longer quenching time. The headed bars with short and longer quenching times tend to have the same yield strength but significantly different total elongation.

Bad total elongation in tensile tests might result from temper embrittlement. It is an inherent phenomenon occurring primarily in alloyed steel if tempered or slowly cooled inside specific heat areas. Two different versions of embrittlement can occur. first is called upper-temperature embrittlement in temperature areas of 400 °C to 600, and the other is lower temperature embrittlement from 300 °C to 400 °C. Upper-temperature embrittlement is reversible by heating the material above 600 °C and then cooling the material quickly. Low-temperature embrittlement, on the other hand, is irreversible. (Total materia 2003)

Temper embrittlement is greatly dependent on the chemical composition of the material. Temper embrittlement is caused by the segregation of specific alloying elements and impurities at grain boundaries during the slow cooling, causing intergranular cohesion. Material is prone to embrittlement if it contains Manganese (Mn), Nickel (Ni), and/or Chromium (Cr), which are often used as alloying elements in steels. The presence of impurities antimony (Sb), phosphorus (P), tin (Sn), or arsenic (As) can lead to co-segregation of alloy- and impurity elements on the grain boundary. A low percentage of molybdenum (Mo) can be added to prevent embrittlement. (Dossett 2020, p. 193.)

Temper embrittlement has not been proven to happen in reinforced steel bars. Still, the chemical composition of reinforced steel contains many of the alloying elements and impurities

that cause temper embrittlement. This is why considering it as a reason for weak elongation in short quenching time is essential. When the quenching time is short, or the material is entirely cooled in air, the material slowly cools over both embrittlement areas. In Figure 27 below, the Chemical composition for B500B reinforced steel obtained for one production batch is shown. Alloys and impurities causing embrittlement are highlighted with red, and the material preventing it with green.

C	Mn	Si	P	S	Cr	Ni	Mo	Cu	Sn	As
0,18	0,87	0,19	0,026	0,037	0,19	0,11	0,02	0,18	0,019	0,008
Al	Ti	V	Nb	B	N	Ca				
0,001	0,001	0,002	0,003	0,0002	0,011					

Figure 27: Chemical composition of B500B rebar steel, values are from inspection document for rebar used in production.

5 RESULTS

In this chapter, parameters for induction heating, quenching, and self-tempering will be defined. With a combination of simulations and practical measurements, directional parameters are defined that are used to make test samples. The test samples are experimentally tested by making tensile tests, metallographic analysis, and Vickers hardness measurements. By combining the achieved information, heating- and heat-treatment parameters to be used in production are defined if possible. The goal is to define the needed parameters for both processes so, that the results can be supported by the theory, simulations, and with real-life experiments.

Finding the correct production parameters for each rebar size is done with a combination of simulations and real-life tests. The reasoning for this is to utilize the strength of both methods. With simulation, it is possible to obtain directional values to be used in real-life experiments fast and with a low cost, but making real-life experiments offers a ground truth, which can be used to verify the validity of the simulations. If it seems that the results obtained through simulations produce realistic data, it is easy to predict the temperature distribution in different areas of the heated billet using simulations for both processes. Measuring accurate temperature change in real-life experiments would require expensive measurement devices and a lot of time to obtain data for all bar sizes. Another benefit that 3D simulation provides is the easy way to visualize how the heat distributes and transfers during the process, giving a better understanding of the process.

To achieve accurate simulation results, some parameters need to be obtained first through real-life tests. A good example is the way the heat transfer coefficient k was obtained in subsection 4.6.3. When all the necessary parameters have been collected from the literature and through testing, directional production parameters are found with the help of simulation. Finally, the validity of the parameters obtained in the simulation is tested in reality, and the parameters are fine-tuned if needed, as differences between the obtained results may occur. When it seems that both simulation and real-life experiments produce similar results, they can be used together to find optimal process parameters.

Two different simulation software are used in this work. For induction heating, CENOS 3D-simulation software is used. With CENOS induction heating software, it is possible to design heating recipes in less time by replacing physical tests with computer simulations and gaining accurate temperature distribution data at all points of the workpiece. For the quenching and self-tempering process, Comsol multiphysics is used, as it enables the simultaneous

analysis of different heat transfer modes, giving accurate and realistic time-dependent temperature data. Also, with Comsol, the possibility of analyzing the temperature distribution more precisely all over the workpiece is an important aspect of finding suitable quenching properties.

5.1 Induction heating simulation

For induction heating, the proper heating parameters for each rebar diameter to be used in production are obtained through real-life experiments and measurements. Before starting to do experimental testing, the heating processes for the batches analyzed in this study are modeled in CENOS induction heating software. In simulation, it is fast and easy to adjust the heating parameters and accurately measure the temperature at different points of the heated billet. Achieved 3D models and time-temperature charts give an understanding of what affects the heating process and how the best possible results can be achieved in reality.

With CENOS, the modeling of the heating process and finding a suitable heating recipe for each bar diameter is straightforward. The process starts with importing or creating a geometry for the workpiece and inductor. In this work, the geometry for both parts is created in the software, as ready-made 3D geometries were not available. When using the built-in geometry-making tool, instead of using the geometry of reinforced steel bar, where the bar surface has ribs on the surface, in these simulations, cylindrical billet with the material properties of reinforced steel is used.

After the geometry is done, following material properties were needed to complete the simulation: Thermal conductivity k (W/m·K), Heat capacity c (J/kg°C), Density ρ (kg/m^3), Electric conductivity σ (S/m), magnetic permeability μ_r materials curie temperature (°C). Inductors operating frequency f (kHz), heating time (t) and used power (kW)

Material-specific properties k, c, ρ, σ, μ_r, and curie temperature are taken from the theory part of this work. The frequency used in simulations is the same that the inductor uses in practice. The frequency range of the heater is reported to fluctuate between 10-25 kHz, but while conducting experimental testing, it was found that the frequency tends to fluctuate between 17-19 kHz during the process without depending on the used coil or heated billet diameter, so constant 18 kHz frequency was used in the simulations. The simulation is thus adjusted with two parameters: heating time and used power.

As found out in previous chapters, the goal during the heating is to achieve a temperature between 1100-1200 °C in as short time as possible, but so that the heat is evenly distributed across the whole needed heating length. With the simulation software, this was achieved by adjusting the induction power and heating time.

5.1.1 Heating power and time

Figure 28 below shows simulation results obtained for 32 mm bar. A similar type of data was also obtained for 10- and 20-mm bars. From the 2D photo on the upper left, the temperature distribution across the cross-sectional area can be easily analyzed. The temperature change of the bar during heating is measured with four different temperature probes. Probes are tools used in simulations to gather data during the simulation process. In these induction heating simulations, probes are used to check the temperature change of specific points once per second. Based on the theory, these probes are placed on the areas of the heated part of the workpiece that tend to have the highest and lowest current density during the induction heating. The placement of these temperature probes can be seen in the figure below. The probe data is plotted in a time-temperature diagram, where the temperature differences between the probes can be more accurately examined. The 3D photo placed on the right side in Figure 28 is used to analyze how the temperature distributes during the heating process.

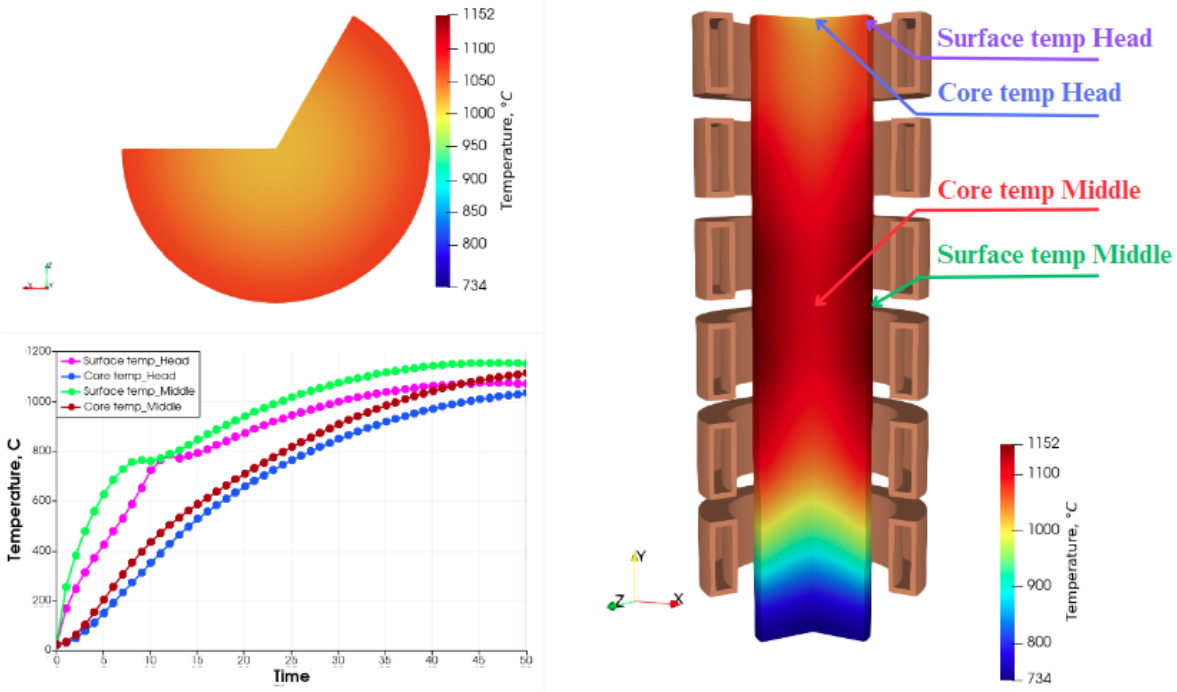

Figure 28: Induction heating simulation results obtained for 32mm bar.

The overall structure of the heating recipe made with the simulation software is as follows:

1. At the start, high power is used to heat the material fast to high temperatures (1050-1200°C). The used power and time depend on the bar diameter. The bigger the heated billet, the more power can be used for a longer time.

2. When the surface temperature gets to the desired temperature, the core of the bar has not yet reached the same temperature as the surface. Therefore, more heating is needed to gain an even temperature distribution. If the same power is used as in part 1, the surface temperature rises too high and starts to melt. Therefore, the used power needs to be adjusted so that the surface temperature does not rise too fast or stays the same while the core temperature rises.

Using this kind of recipe is important for bigger bars to reduce the heating time. For smaller diameters, constant heating power can be utilized, as 1150 °C across the whole heating length is achieved fast enough for heating not to be the production bottleneck.

5.1.2 Affect of coil-to-workpiece gap

The smaller the gap between the heated workpiece and coil is, the less energy is lost during heating, making the process more energy efficient. If the gap is increased, the needed heating power and time need to be increased so that the energy losses are taken into account. Because of this, the heating recipe is coil-dependent and, therefore, needs to be adjusted if the coil geometry changes.

5.1.3 Affect of coil overhang

Coil overhang refers to the length of the induction coil that extends the heated part. As explained in subsection 4.4.3, electrical end and edge effects can cause over or under-heating on the head of the workpiece, causing uneven temperature distribution. One of the affecting parameters for these phenomena to occur is the coil overhang σ. Figure 29 below illustrates the effect of bar placement inside the coil on the heat distribution with similar heating parameters used.

In the simulation on the left, where the σ is 0, The hottest area of the bar is at the surface in the center of the coil. When moving from the center coil towards the ends, some drop in the temperature is seen. In the simulations at the middle and right side of the Figure 29 where the head of the workpiece is moved toward the center, and the coil overhang grows, more severe temperature distribution in the workpiece is noticed. In practice, using a setup similar to the last simulation could result in the melting of the head.

If needed heating length is shorter than the coil length, the billet head can be relocated more to the middle of the coil. If this is done, the used heating power needs to be lowered, but at the same time, the needed heating time needs to be longer to achieve enough energy to achieve the desired temperature.

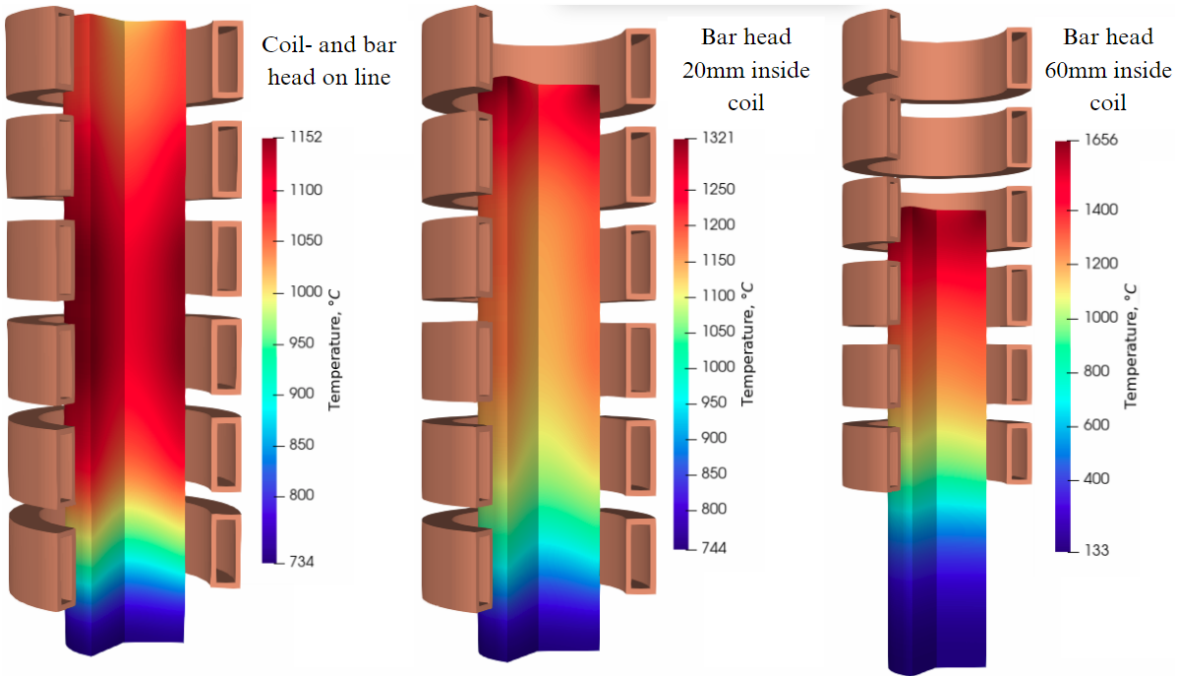

Figure 29: Affect of bar placement to the heat distribution for 32mm bar.

5.2 Experimental heat-treatment tests

Experimental testing for Induction heating was done with parameters achieved through the simulations. In these tests, both the core temperature during the heating and the surface temperature after the heating were measured. To obtain core temperature data, a small hole was drilled into the mid-point of the cross-sectional area of the bar, and a k-type thermometer was inserted into the hole as shown on the left side of Figure 30. A time-temperature graph illustrating the heat change during the process is shown on the right side of the figure.

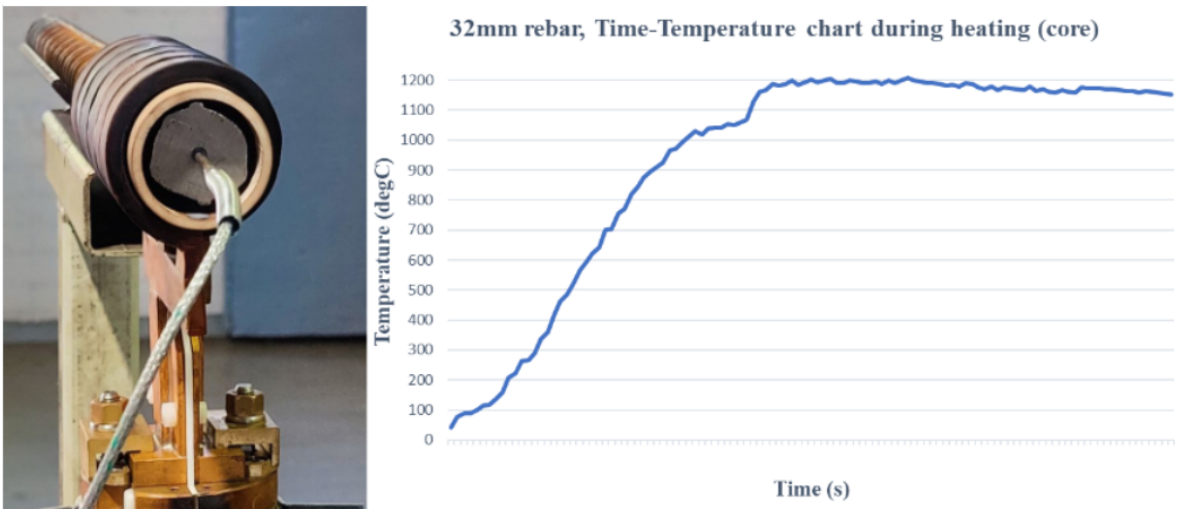

Figure 30: Measurement method used to achieve core temperature data for rebars.

Accurate surface temperature at the end of the induction heating is achieved with a thermocouple. The thermocouple is attached to the surface of the heated rebar. The primary purpose of the thermocouple was to measure the cooling rate of the rebar when quenched in water to achieve the heat-transfer coefficient k for quenching and self-tempering simulations. Although the thermocouple was connected to the object's surface during induction heating, it did not give reliable temperature results until the induction heating recipe stopped. During heating, the thermocouple mounted on the surface was probably in contact with the coil, so it interfered with the thermocouple. Therefore, accurate surface temperature data during the induction heating was not achieved through real-life experiments. The thermocouple attachment and data achieved with it are shown in Figure 31 below.

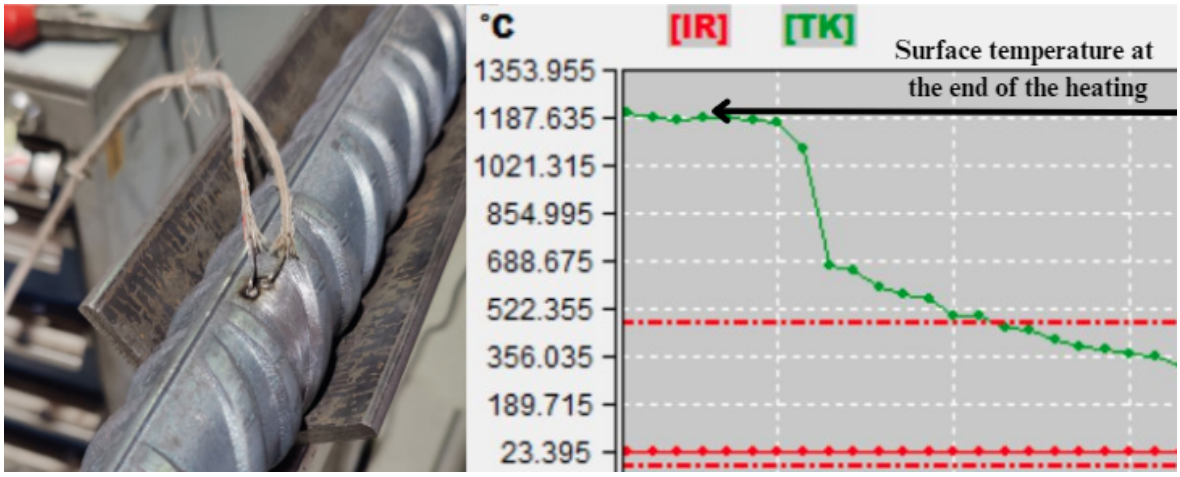

Figure 31: Measurement method used to achieve surface temperature data at the end of the heating recipe.

A graph that combines the measured temperature data during induction heating and quenching for 10, 25, and 32mm rebars can be seen Figure 32 below. This graph combines the values measured with a k-type thermometer from the bar's core during induction heating and the measurements done with the thermocouple attached to the bar's surface while quenching. In this graph, the sample is immersed in water until it achieves the ambient water temperature across its whole cross-dimensional area, being around 30 to 40 °C.

Solid line reflects the heating phenomena and dotted line quenching. 25mm diameter is presented in the chart instead of 20mm rebar, as 20 mm rebar was not measured with a k-type thermometer due to a device failure in the heat measuring device. If 20 mm rebar is added to the graph, it would settle between the 10 and 25mm bars. As the graph illustrates, the smaller the size of the rebar steel is, the more sensitive it is to the changing temperature during heating and cooling.

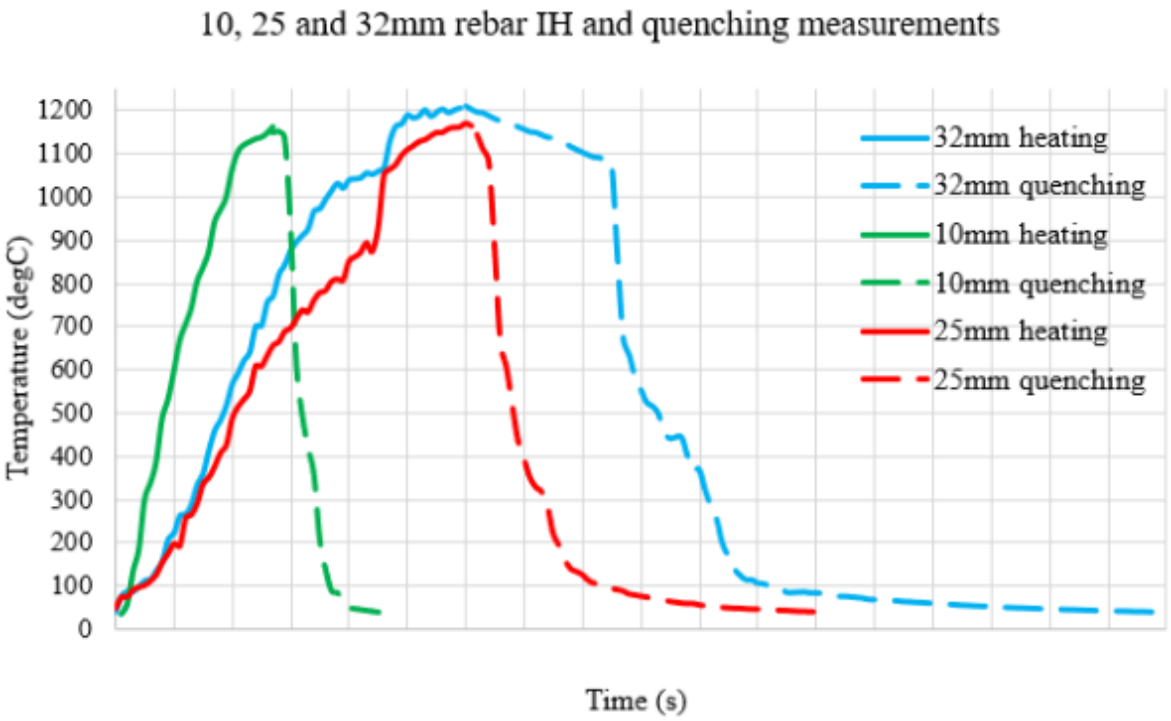

Figure 32: Time-temperature graph combining the heating and cooling measurements obtained through experimental tests for 10, 25, and 32mm rebars.

When the results obtained for 10, 20, and 32mm rebars are compared in a graph where the x-axis is the rebar surface area, and the y-axis is the energy used during the induction heating, a straight trend line can be drawn between the values. Using this trend line, it is possible to define indicative heating values for other rebar sizes. The graph can be seen in Figure 33 below.

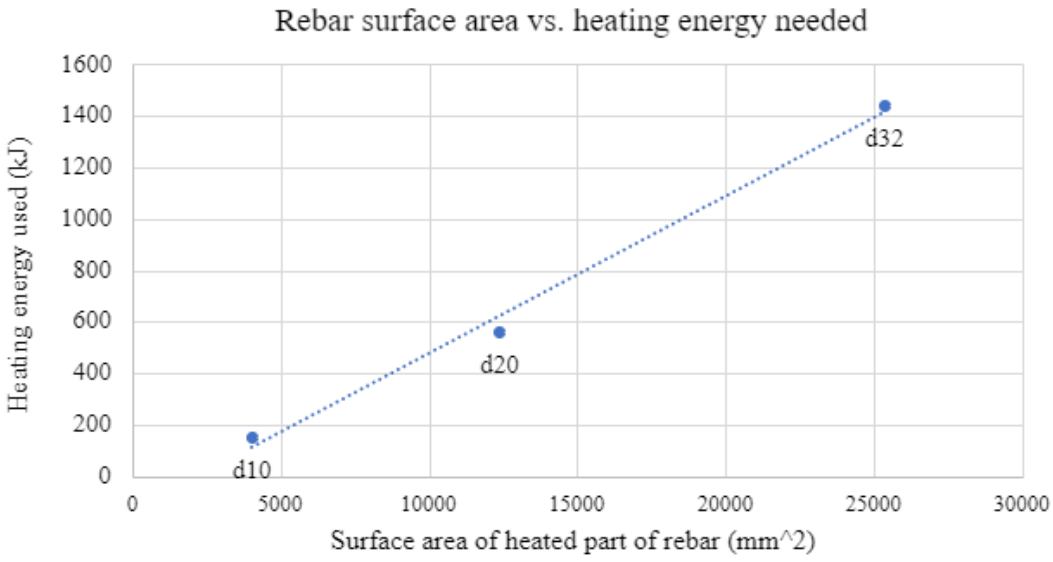

Figure 33: Rebar surface area vs. needed heating energy.

All of the three rebar sizes that were simulated and experimentally measured in this study had approximately the same gap between the coil and workpiece. If the gap is different when defining the heating recipe for other dimensions, the value obtained from Figure 33 above needs to be adjusted. If the gap grows, more energy is needed, and if the gap is smaller, less energy is needed.

5.3 Quenching and self-tempering simulation

Comsol multiphysics simulation software with a heat transfer module was used for quenching and tempering simulations. With Comsol, the temperature distribution across the bar's radius after quenching and the tempering was achieved. With simulation, it is easy to define the needed quenching time to get under Ms-temperature at the surface but still keep enough residential heat for self-tempering.

As stated in subsection 4.6.5, the goal of the heat treatment simulation is not to achieve specific quenching parameters to be used in production. Instead, it is used to gain directional heat-treatment parameters for the forged bars to be tested in tensile tests and to understand better how the heat distributes during the process.

The simulated component's geometry resembles the headed bars forged in real life. The component material is low carbon steel 1020, with material properties important regarding the process adjusted. For example, Specific heat c, Density ρ, thermal conductivity k, and emissivity coefficient ϵ were adjusted according to the values obtained in section 4.2.

The quenching and self-tempering are modeled with two boundary heat sources available in Comsol: heat flux and surface-to-ambient radiation. Heat flux boundary heat source is used to simulate the convection heat transfer between the workpiece and the quenchant during quenching, and surface-to-ambient radiation is used to simulate the heat transfer between the workpiece and the ambient area. In Comsol, both the heat flux and surface-to-ambient radiation use the same equations as shown in 4.3 to calculate the values. Both radiation- and convective heat transfer are time- and temperature-dependent, and the temperature change is measured every 0.5 seconds.

Equation 4.7 used to define convective heat transfer coefficient in chapter 4.6.3 is used in the simulations. Volume V and surface area A needed in the equation are achieved straight from the 3D model that is also being used as the geometry in these simulations. The heat flux simulating the quenching phenomena affects the workpiece for a set time, whereas the radiation heat transfer affects the workpiece for the whole simulation. For example, if the quenching time simulated is 10 seconds, the heat flux boundary is set to affect from 10 seconds to 20

seconds in the simulation. This is done as in real life it can take around 5 to 15 seconds before the forged rebar is immersed into the quenchant after forging.

Five virtual temperature probes are placed into the geometry before computing the study. These virtual probes measure the temperature during the simulation. The placement of the probes is shown in Figure 34 below. The probes are placed on the head to describe the temperature distribution and changes at the head as versatilely as possible. Initially, more sensors were used in the simulation, but the chart became hard to read because of the many overlapping lines.

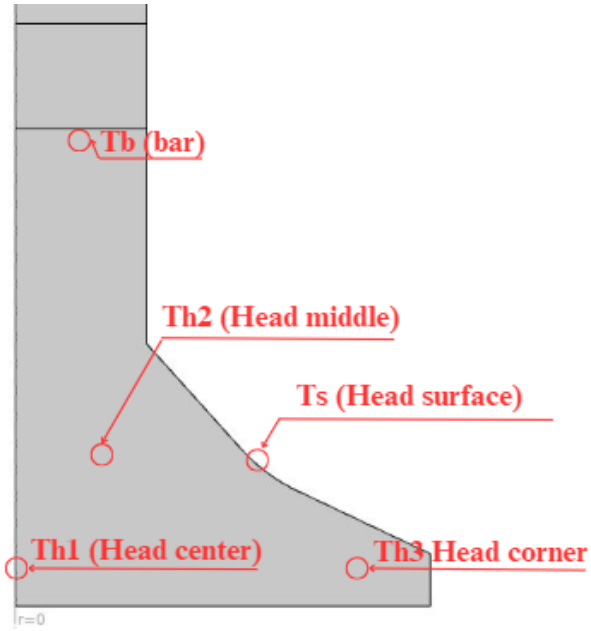

Figure 34: Temperature probes used to measure temperature change during the simulation.

The time-temperature graph shows the temperature change of the five virtual temperature probes in the simulation model. In Figure 35 below, a graph obtained for 32mm forged rebar using 15 second quenching time is shown. The STT shown in the graph below is the point used to choose the quenching times for experimental tests.

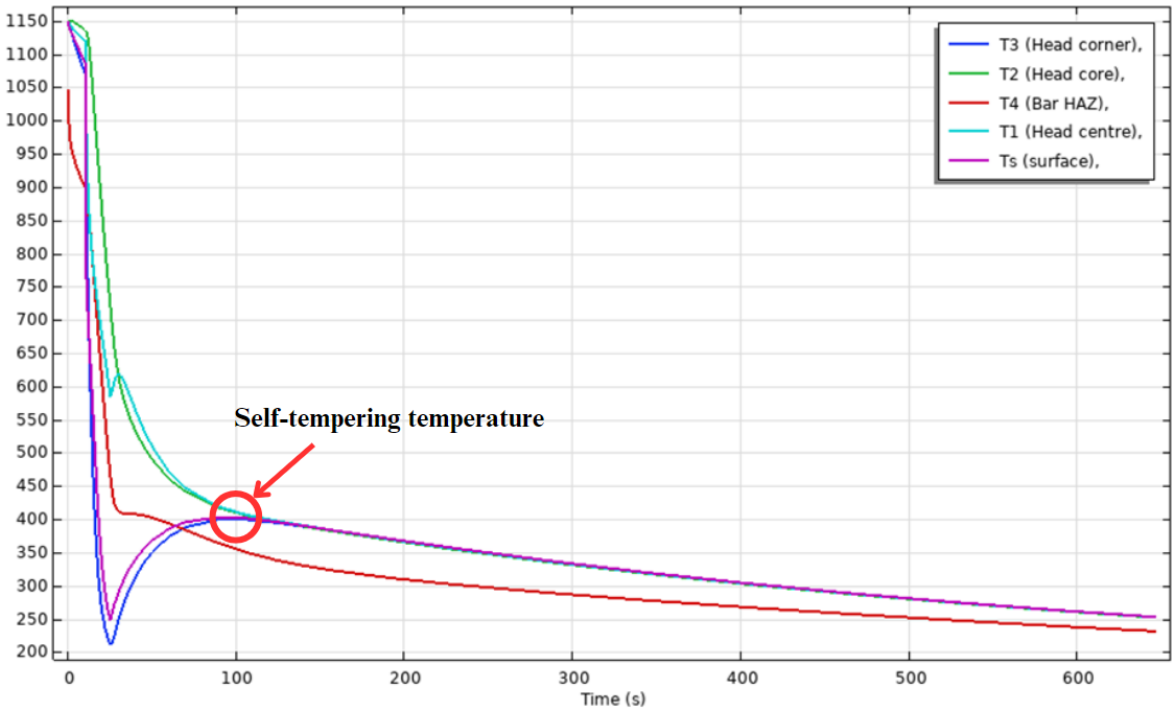

Figure 35: Time-temperature curve obtained for 32mm headed rebar. The STT point used later in the experimental test is marked on the graph.

The reliability and accuracy of the simulation can be verified by comparing the simulation results to the temperature measurements done with the thermocouple as done in Figure 36 below. The curves in the graph are taken from a situation in which the hot workpiece is immersed in water until it achieves a water temperature. The graph shows that the temperature changes until 250 °C follows each other. After this point, the cooling rate achieved through simulation is smaller than the real-life experiences proved. Differences in the cooling rates can be partly explained by the fact that in the simulations, the surface temperature of the forged head is measured, and with the thermocouple, the surface temperature of plain rebar is measured. The differences in the part geometry can cause differences in the graphs obtained. A similar verification was also made for 10mm and 20mm rebars to check the simulation reliability.

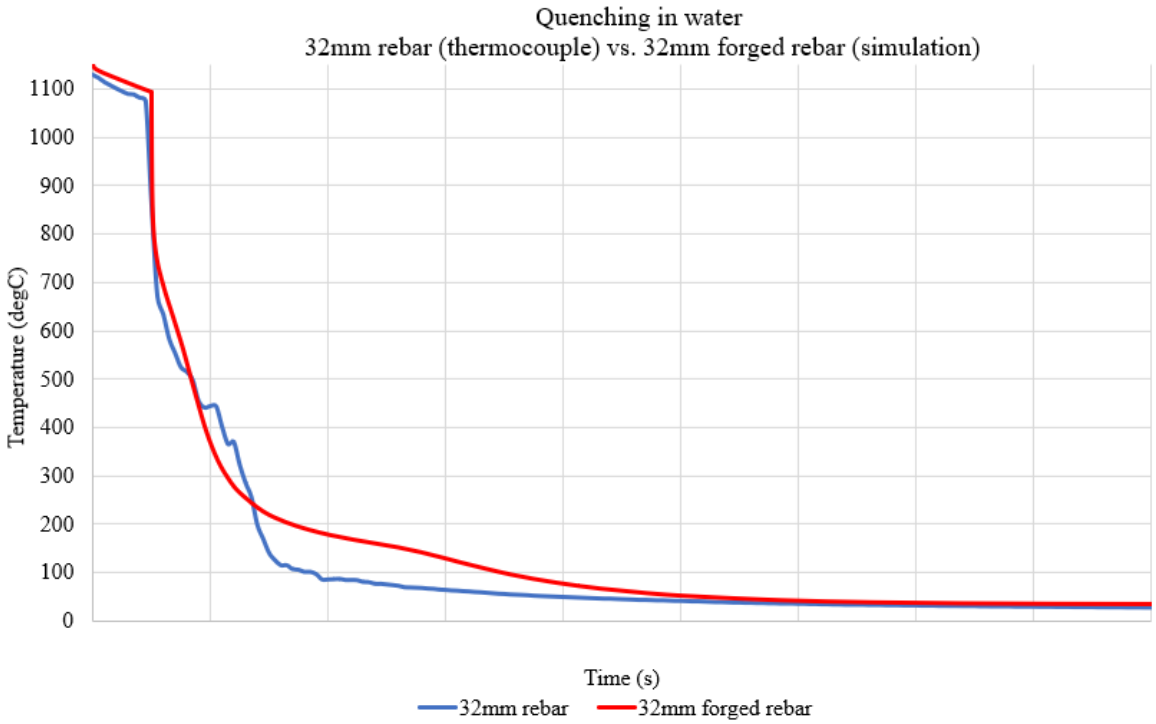

Figure 36: Comparison of the cooling rate at the surface of the bar between simulation data and the experimental measurements done with the thermocouple.

In addition to the time-temperature graphs, 3D thermal models that illustrate the temperature distribution at a specific time during the simulation are plotted. These 3D plots visually illustrate how well the forged workpiece quenches during the process and how the temperature distributes during the quenching. For example, the shape and size of the hot spot that causes the self-tempering can be analyzed using these 3D plots. Figure 37 shows the 3D thermal model obtained for 32 mm headed rebar in different points during the simulation.

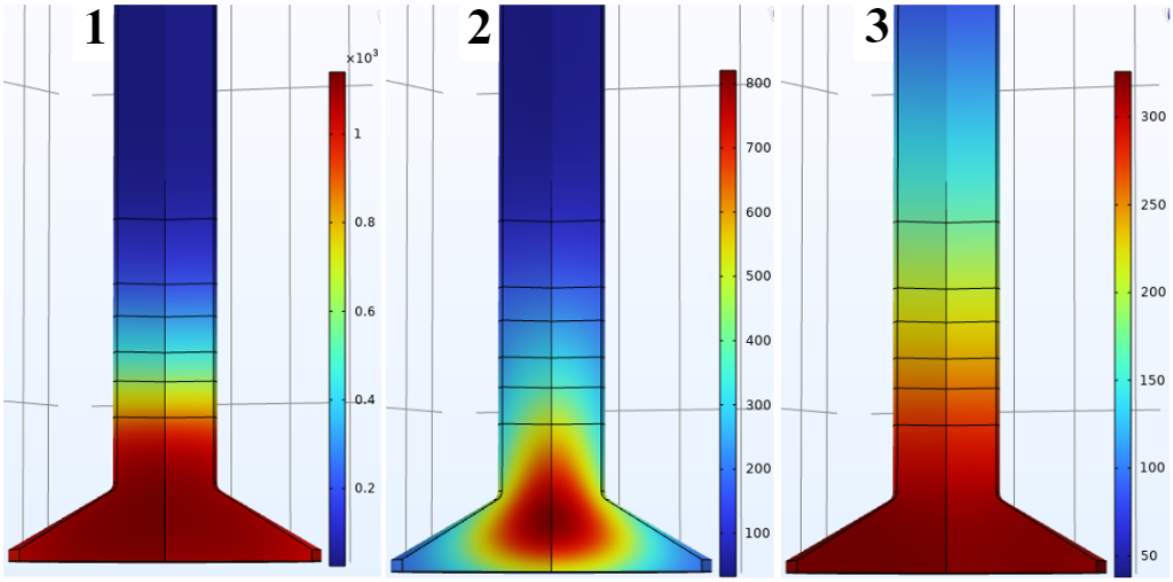

Figure 37: 3D-thermal model for 32mm headed rebar. 1) before quenching 2) Straight after 15 seconds of immersion quenching in water 3) after 5 minutes of cooling in the ambient area after quenching.

Based on the 3D model, after quenching, a hot spot remains in the core of the head, providing enough residual heat to temper the surface. The coldest part of the head is the corners, where the temperature drops around the M_f temperature. In addition to the surface and the head corners, faster cooling also happens in the bar's heat-affected zone, where the heat tends to conduct and convect to the bar part that is not heated and to the ambient area. All surface areas of the head, except the surface near the bar-end at the head, reach temperatures under M_s during quenching. Longer quenching time could also form martensite in these areas, but the hot spot at the core would not have enough heat for self-tempering.

Comparing the 3D thermal model of 32 mm to 10 mm rebar shown below in Figure 38, the most significant difference between the obtained results is the needed quenching time to achieve M_f temperature and how the temperature distributes during the heat treatment. The quenching in a 10mm forged rebar tends to result in a more even temperature distribution across the whole head area. This might be problematic because the goal is to achieve a hard martensite surface and a soft but ductile ferrite-pearlite core. When the core and surface temperature are closer, obtaining different phases at the surface and in the core is harder.

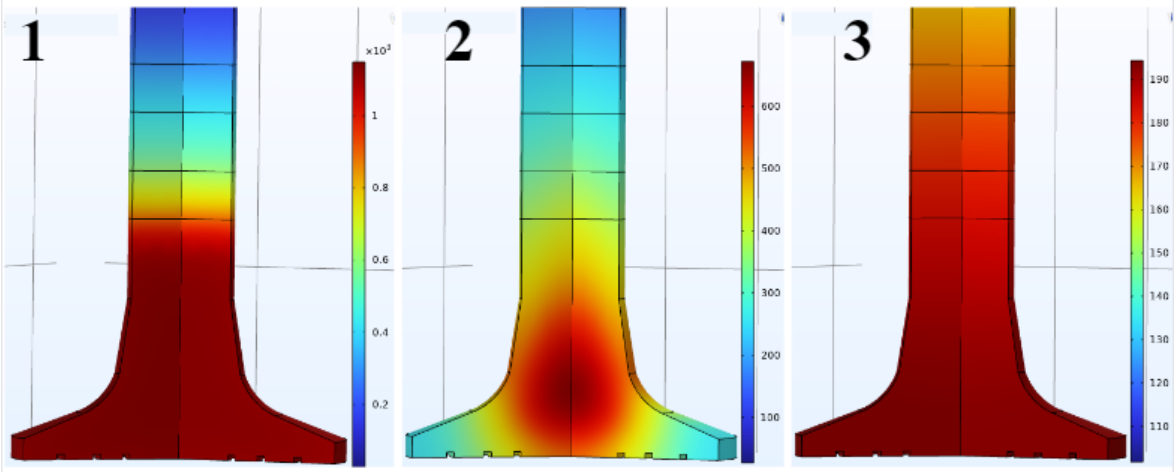

Figure 38: 3D-thermal model for 10mm headed rebar. 1) before quenching 2) Straight after 3 seconds of immersion quenching in water 3) after 5 minutes of cooling in the ambient area after quenching.

The goal of the simulation is to obtain quenching time long enough to get at least below M_s and as close to M_f-temperature as possible, still having enough residential heat to temper the workpiece. According to subsection 3.3.1, the M_s rebar temperature for rebar steel is around 430°C and M_f-temperature 230 - 150 °C. As said in subsection 4.6.5, the simulations' goal is to find quenching parameters that provide a self-tempering temperature of 400 °C from where the workpiece is let to cool down in ambient temperature slowly. When the obtained quenching times are plotted in the same diagram as done in Figure 39 below, a linear trendline can be drawn between the obtained values. This trendline can be utilized to define indicative quenching times that provide 400 °C self-tempering temperature for other rebar sizes also when the head surface area is known.

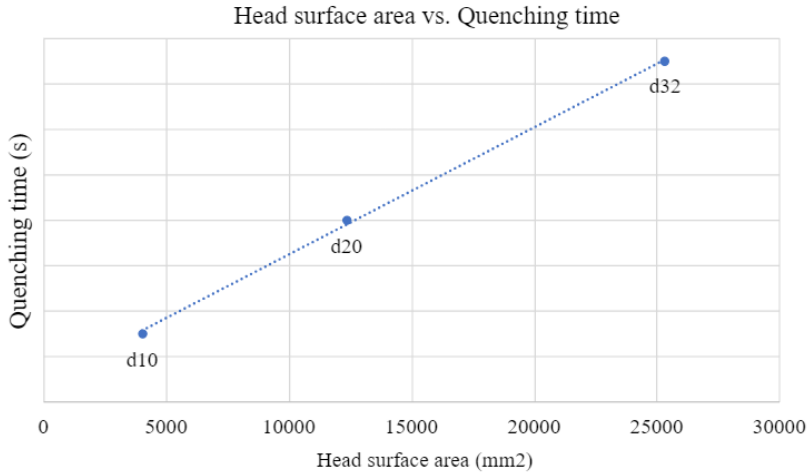

Figure 39: Rebar surface area vs. quenching time according to simulation results.

5.4 Experimental testing

Experimental tests are done for 10mm and 20mm rebars to find out how the quenching and self-tempering works as a heat-treatment method for the headed rebars in practice and to find parameters that could be used in production. The test samples are heated according to parameters defined in section 5.2, upset forged with the target company's methods, and then quenched and self-tempered with different quenching times in water and then let to self-temper in air. The quenching time is the only variable parameter in these tests. The quenching time directly affects the workpiece temperature after quenching and the self-tempering temperature.

The quenching times used in the tests are based on the quenching simulations done in section 5.3. The times are chosen so that a wide range of different quenching and tempering temperatures between 100 °C to 700 °C are achieved. Air quenching is analyzed in both processes to see how it could work as a heat treatment method for the bars analyzed.

Three different experimental procedures are conducted for each sample tested: Tensile test, metallographic analysis, and hardness test. Overall, four test samples are made for each quenching time. Three of these samples will be tensile tested, and the fourth will be used to make the metallographic sample. The metallographic sample can be used in the hardness test after the metallographic analysis.

5.4.1 Tensile test

All quenching times are tensile tested to see how they fulfill the tensile strength requirements. The requirements in which the achieved results are compared are the mechanical properties of the base material and the minimum mechanical characteristics given in European Assestment Document (EAD) 160003 annex D.3. EAD 160003 is a technical specification developed by European Organisation of Technical Assestment (EOTA) for double-headed rebars. The part of the technical specification that specifies the minimum values is attached as Appendix A at the end of this work. Both the base material's mechanical properties and the properties based on the EAD are added to the comparison tables later on. In addition, the tensile test gives information about the quenching time that gives the best mechanical properties. Offset yield strength $R_{p0,2}$, Tensile strength R_m, and total elongation A_gt are achieved through the tensile test. As stated in section 2.2, these values are also used to define the minimum mechanical properties of rebar steels in most standards.

During the tensile test, a controlled tension is applied to the rebar, and the strain of the tested bar is measured with an extensometer. An extensometer is a measuring device that measures the changes in length during the test. In these tests, a contact extensometer, which is attached

to the surface of the rebar at the beginning of the test, is used. These tests are performed with universal tensile testing machinery equipped with a special clamping system designed for headed rebars. The clamping system supports the head so that when the controlled tension is applied, the test piece stays in place. In Figure 40, the tensile testing machinery and the clamping system used are shown.

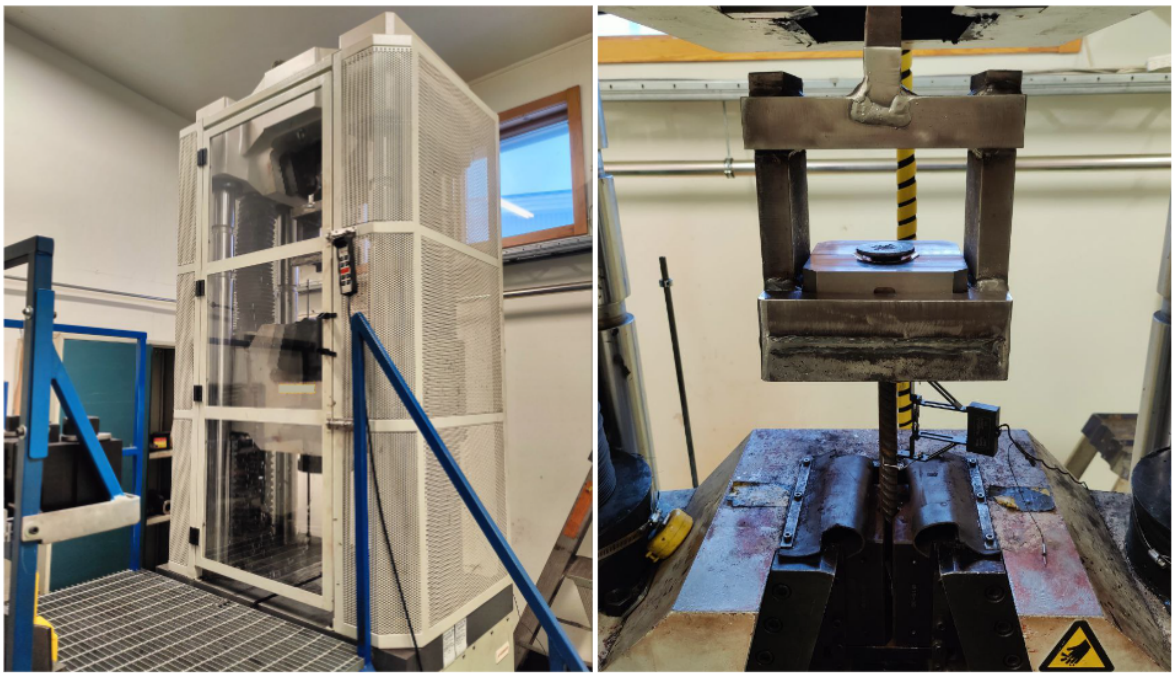

Figure 40: Tensile test machinery used on the left and clamping system on the right.

An example Stress-strain curve obtained from the tensile test is shown in Figure 41. The program automatically calculates the maximum values for $R_{p0,2}$, R_m, and A_{gt}, but these values can also be checked and verified from the graph manually, as illustrated in the figure below.

Test Number	Heat	Date of test	d0	Rp 0,2 [N/mm2]	Rm [N/mm2]	Agt [%]	Location of fracture	
		22.11.2023	d20	558,8	671,3	17	Rebar	

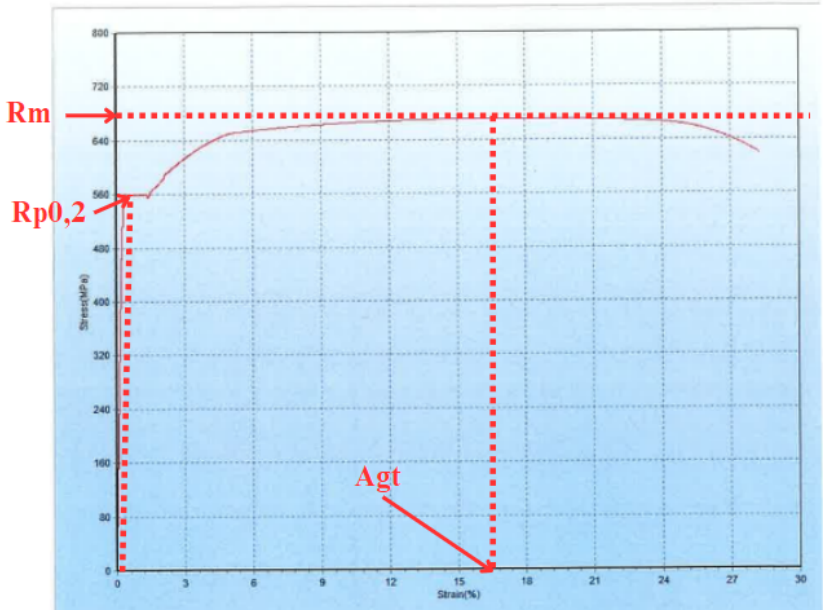

Figure 41: Shematic stress-strain curve obtained from the tensile test.

5.4.2 Sample preparation for metallography and hardness measurement

To make the Metallography and the Vickers hardness tests, the samples analyzed need to be prepared carefully. First, a sample piece shown in Figure 42 below is milled from the headed rebar. Milling is utilized to make the samples as the surface of the workpiece does not heat up so much that it would affect the microstructure of the analyzed workpiece.

Figure 42: Milled testpieces for metallography and hardness measurements. 20mm rebar on the left and 10mm rebar on the right.

In Figure 43 below, the preparation process of the metallographic samples is shown. The machined test samples are coarse- and fine-grinded to remove the depths of deformation (a). To achieve a cleaner surface, the surface is polished. The result after polishing can be seen in Figure B. The polished workpiece is then etched in nitric acid called Nital to reveal the microstructure of the steel (C). After etching, the sample can be analyzed with macro and microscopy (D).

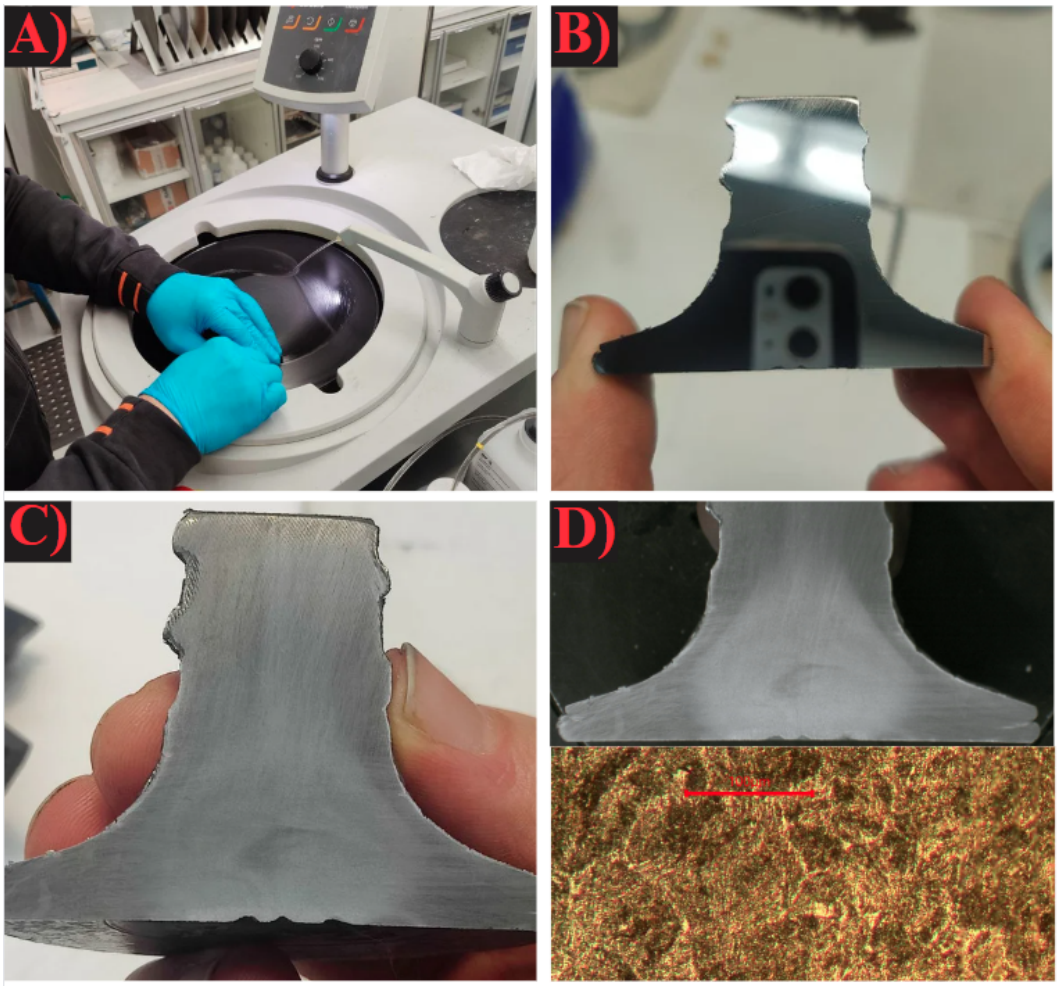

Figure 43: Sample preparation process for metallography and hardness measurements.

5.4.3 Metallography

Metallography is the study of the micro- and macro-structures of metals. Metallography can be used to represent the chemical and atomic structure of metals. In this study, micrographic- and macrographic examinations are made to understand more precisely the phase transformations happening during the hot working process and to fully understand how different heat-treatment parameters change the crystalline structure of the workpiece. (Colpaert 2018, p. 25-30.)

The macrographic examination is used to analyze the gross structure of the metal with a maximum magnification of 10 times. From the macrostructure, observing the homogeneity of the analyzed sample through the cross-section and evaluating the dimensions of possible cracks and pores is possible. It can be utilized, for example, to analyze the presence, depth, and homogeneity of thermomechanical heat treatment. (Colpaert 2018, 39–42.)

For iron-carbon alloys like the one analyzed in this study, it is possible to obtain information about the crystal structure achieved by the heat-treatment process by making micrographic examinations. As stated in chapter 3, the metallurgy of steel highly affects the material's physical properties, such as strength and toughness. Analyzing the microstructure might give more information regarding the quenching time that provides the best possible physical properties based on theory. A micrographic examination is taken from 5 different points of the structure. The location and naming structure of these points can be seen in Figure 44 below.

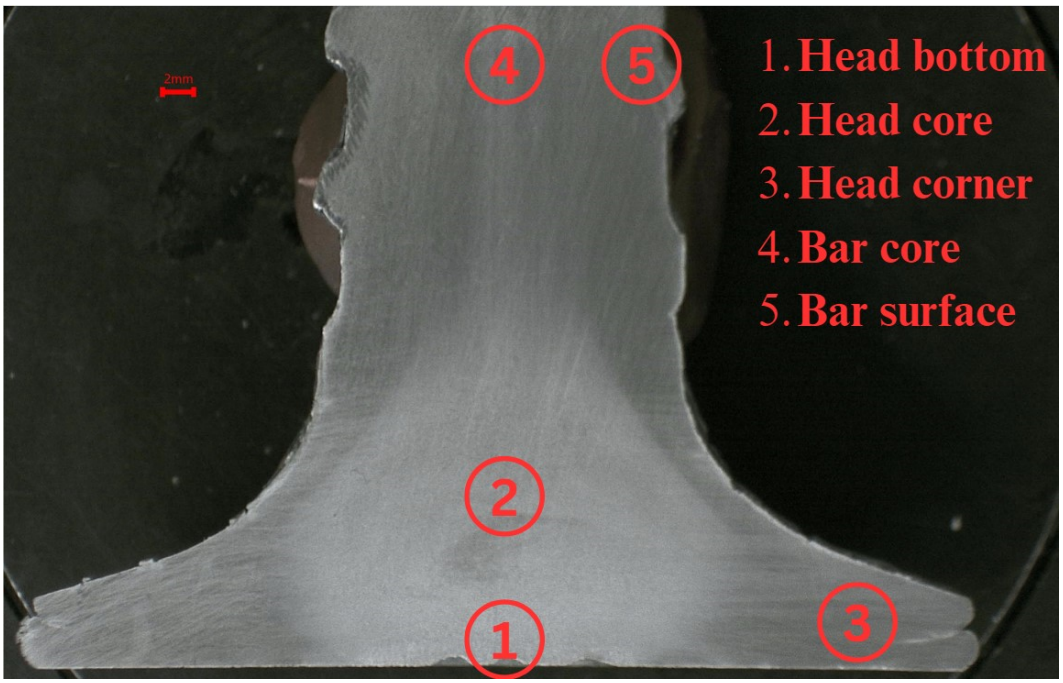

Figure 44: Location and naming structure of points where micrographic examinations are taken.

5.4.4 Vickers hardness test

The Vickers hardness measurements are taken from the forged head and from the rebar close to the head. Both 10 and 20-mm rebars are analyzed the same way. Analyzed hardness points and the numbering style are shown in Figure 45 below. Overall, 15 hardness measurements are taken from the forged head, and 6 measurements are taken from the bar. The numbering

always starts from the core, so in hardness measurements, number 1 is the core, and 15 is the head corner. At the bar area, number 1 is also the core, and number 6 is the surface. A more precise introduction to Vickers hardness was made in subsection 3.3.4.

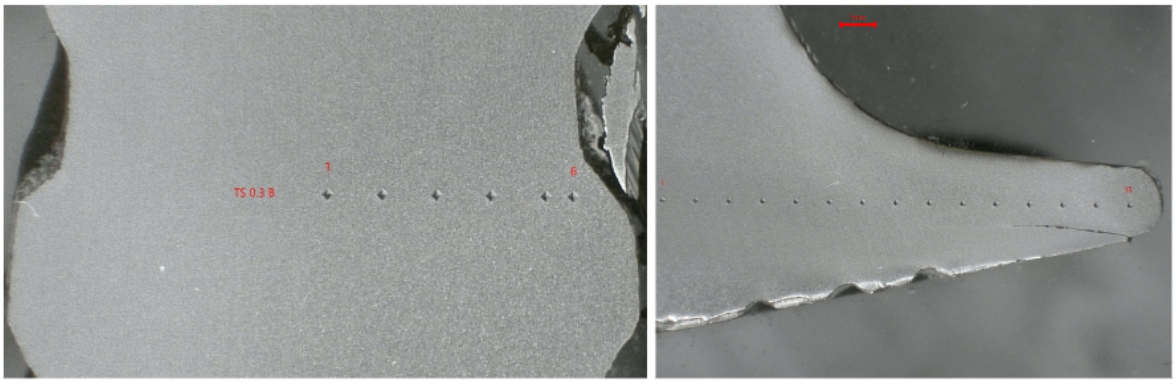

Figure 45: Analyzed hardness points and their position, right picture is 10mm rebar, and left picture is 20mm rebar head.

5.5 Experimental test results

This section introduces the results of the experimental tests made for the 10mm and 20mm rebars. The results of both sizes are shown and analyzed in their own subsections below. The results combine the tensile tests, metallography, and Vickers hardness measurements done for the test samples.

Instead of giving the specific quenching times that were used in these experimental tests, the STT achieved with different quenching times is used. STT-values for each rebar dimension and quenching time were achieved from the simulations made. The method of how the values were defined from the simulations was introduced in Figure 35 in section 5.3. By using the STT instead of quenching time, comparing the results obtained between different-sized rebars is easier than by using quenching times that had a lot of variation between 10 and 20mm rebars. Some differences in the STT-values used in the tests for 10 and 20mm can be seen as a result of using even seconds in the tests. For example, obtaining 400 °C STT for 10mm rebar would need to use quenching time with an accuracy of tenths of a second, which is not viable when making the quenching in water by hand.

5.5.1 10mm forged rebar results

Tensile test results obtained for 10mm rebar are listed in Table 8 below. The values listed in the table are the average values of the three tensile tests made for each quenching time. Overall, the results obtained are promising, as every rebar tested filled all the requirements

listed in the EAD technical specification. In every test piece for every quenching time, the failure location was in the rebar. This area where the failure occurred during the test was not heat treated or hot worked during the hot working process. It explains why the obtained mechanical properties for each quenching time are close to the mechanical properties informed in the material certificate from the steel mill. This means that the base material is the determining factor regarding the tensile properties of the workpiece instead of the heat-treated and forged part. Thus, it is really hard to analyze the mechanical differences between differently quenched bars based on the results obtained.

Table 8: Tensile test results for 10mm headed rebars.

STT [°C]	R_{p02} **[MPa]**	R_m/R_{p02}	A_{gt}**[%]**	**Location of failure**
Cooling in air	522	1.16	8.3	Rebar
600	530	1.13	7.2	Rebar
500	521	1.15	9.3	Rebar
375	526	1.14	8.8	Rebar
250	526	1.15	8.2	Rebar
175	524	1.14	8	Rebar
Batch (Material certificate)	536	1.15	7.5	
Minimum requirements (EAD 160003)	ReH> 500 [MPa]	Rm/Rp02 >1,05	2.5 [%]	

Figure 46 below shows the base materials macro- and microstructure. It is taken directly without any treatment or fabrication procedures from the same batch as the rebar steels from which the test samples are made.

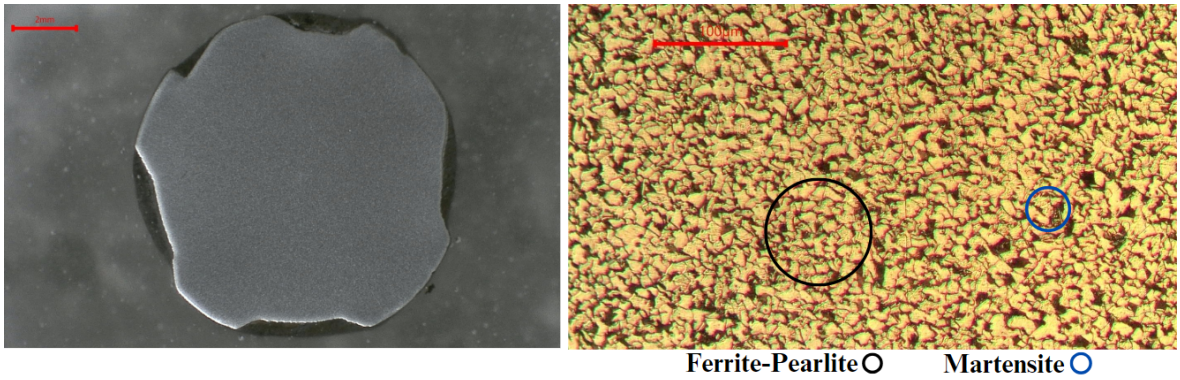

Figure 46: Left: Macrostructure of 10mm rebar steel. Right: Microstructure of 10mm rebar steel.

The microstructure is a combination of ferrite-pearlite with some features of martensite. The black spot in the structure is pearlite, and most white grains are ferrite. The white grains having a sharper appearance are martensite, but only a tiny amount of these features are seen in the base material. The hardness values obtained for the sample are 183 HV from the core and 207 HV from the surface. The hardness is higher the closer to the surface it was taken. The microstructure is homogenous across the whole cross-section of the material, the only difference being the amount of martensite features on the surface. Based on the hardness and microstructure obtained, it might be possible that the 10mm rebar was let to cool in the air in steel mills.

Analysis regarding the effect of the quenching time on the microstructure of the forged head is started with a comparison between three different microstructures and their hardness values taken from the core of the head. The analysis is made for air-cooled, and samples with STT of 500 °C and 175 °C. In Figure 47 below, the microstructures are shown.

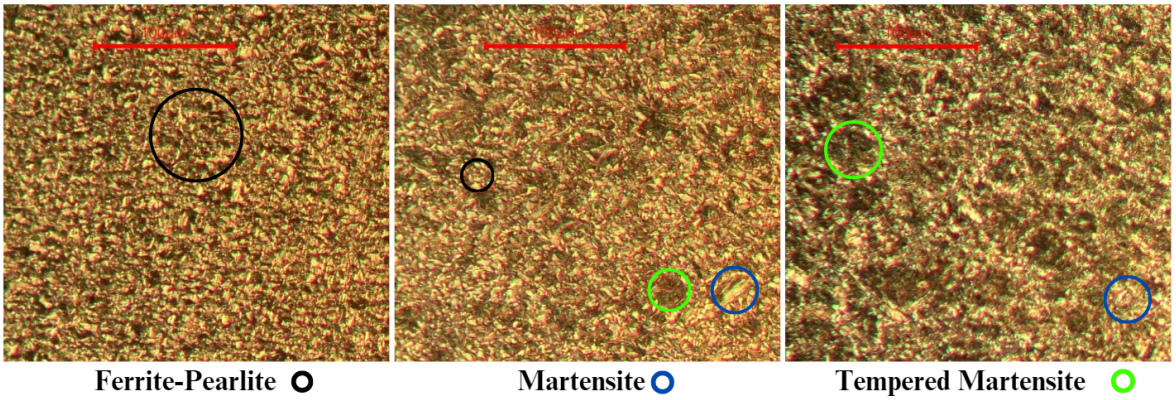

Figure 47: Microstructures of 10mm forged rebar taken from the head core. Left: Air cooled. Middle: STT 500°C. Right: STT 175°C.

With air cooling, the bar's core has a microstructure similar to the base material's, but the grain size is smaller. Smaller grain size is often a result of a faster cooling rate, which means that the bar core cools faster in the forged head than in the base material heat-treated in a steel mill. Even though the grain size is smaller, which often results in harder material, the Vickers test showed results between 178 and 190 in the core area, around the same value achieved for the base material.

When the rebar is quenched in water, some of the ferrite-pearlite microstructure at the core seen in air cooling is replaced by martensite and untempered martensite. Martensite is seen in the microstructure as white grains with a sharp look, and tempered martensite forms the more dark-looking sharp areas. With a 175°C STT, more martensite and tempered martensite are formed. The hardness in the core area with 500°C STT is 270 Vickers and with 175°C STT, 318 Vickers.

Differences in microstructure at the surface of the head are evaluated between the same test samples: air-cooled, 500, and 175°C STT. The microstures shown in Figure 48 below are taken from the ”head-bottom” -point.

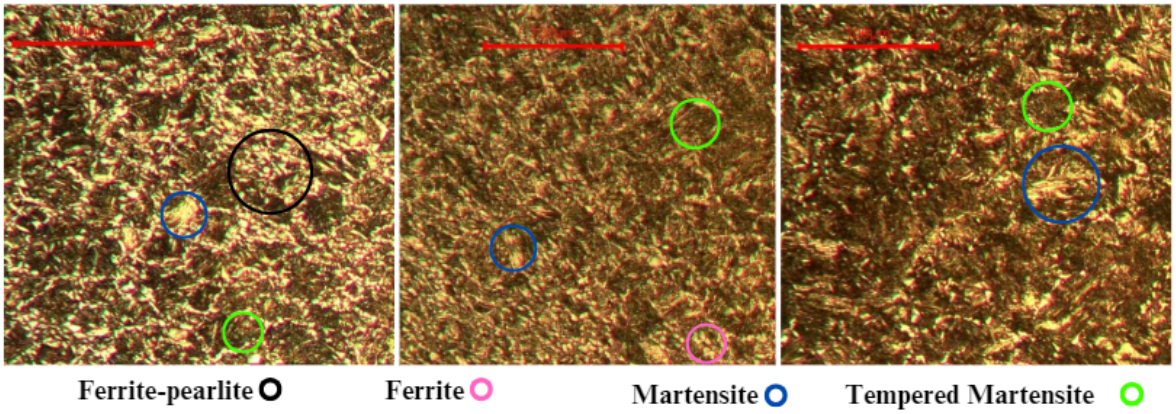

Figure 48: Microstructures of 10mm forged rebar taken from the head bottom. Left: Air-cooled. Middle: STT 500°C. Right: STT 175°C.

The microstructure of the air-cooled sample is a combination of ferrite-pearlite, with some features of martensite and tempered martensite. When comparing the obtained microstructure of the air-cooled head to the bar with 175°C STT, the amount of ferrite-pearlite microstructure decreases and is replaced with features of martensite and tempered martensite. An interesting finding in these microstructures is the high amount of ferrite features. A theory that might explain ferrite formation at the bar's surface with water quenching could be a lower surface temperature than expected before the water quenching proceeded. Based on the iron-carbon equilibrium diagram introduced in section 3.2, if the temperature of the steel with similar $wt\%C$ is between 800 to 875 °C before the quenching occurs, already some of the iron is in

the form of ferrite instead of being 100 % austenite. This results in some ferrite features in the end product, even though the cooling rate should be fast enough to obtain martensite.

This phenomenon partly explains the hardness results obtained for the analyzed 10mm forged rebars. Based on the hardness results taken from the core of the bar to the head-corner area, the hardness is partly higher in the core area of the bar compared to the near-surface area at the corner. As the temperature at the surface is lower because of the conduction heat transfer between the cold forging tooling and the hot workpiece, the hot spot at the bar core stays in temperatures in which the microstructure is 100% austenite before quenching. When quenched, the potential to obtain a harder microstructure at the bar's core is higher than at the surface because no ferrite is formed at the core before the quenching. As the 10 mm-headed bar has a relatively small volume, the bar core achieves cooling rates fast enough to form martensite. Based on the hardness measurements, the hardness of the rebar close to the head is the same for both water-quenched bars with STT of 175 °C and 500 °C. Also, the hardness values are relatively close between the core and the surface. A summary of the Vickers hardness test results for 10 mm rebars tested can be seen in Figure 49 below.

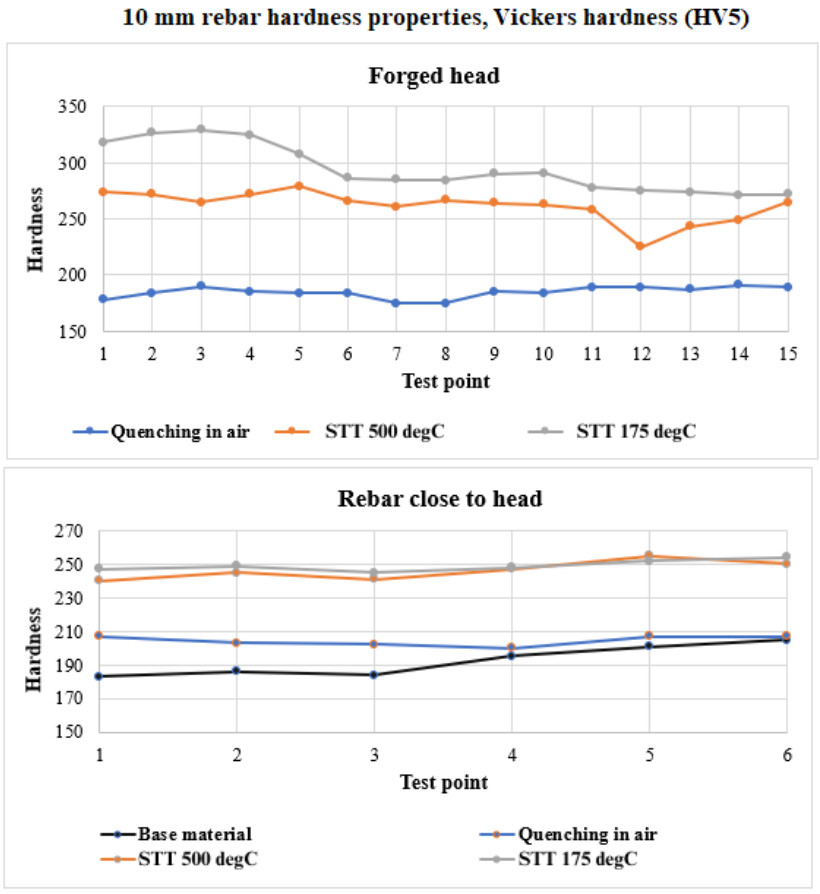

Figure 49: Summary of the Vickers hardness tests made for 10mm test samples.

Based on the microstructures obtained, as well as the Vickers hardness values obtained at different points, it can be said that obtaining a heterogenous microstructure that is a combination of a uniform martensite layer at the surface of the bar and a ferrite-pearlite core seems to be hard for small size headed rebars like 10mm. Also, the controllability of the heat-treatment procedure is difficult. This is due mainly to the relatively small volume of the head. The head reacts quickly to changes from the outside environment, such as cold tooling during forging. Also, because of the small volume, the core reacts to the conduction heat transfer so fast that obtaining different microstructures is problematic when utilizing water quenching.

5.5.2 20mm forged rebar results

The tensile test results for the 20mm rebar steel are listed below in Table 9. The table structure is similar to the one previously made for 10mm rebar.

Table 9: Tensile test results obtained for 20mm headed rebars.

STT [°C]	R_{p02} **[MPa]**	R_m/R_{p02}	A_{gt}**[%]**	**Location of failure**
Cooling in air	557	1.09	3	Head
650	552	1.18	8.5	Head OR rebar close to head
550	560	1.20	14.2	Rebar close to head OR base material
425	548	1.21	17	Rebar
350	554	1.20	17	Rebar
250	549	1.20	17.2	Rebar
150	554	1.20	16.8	Rebar
Batch (Material certificate)	576	1.18	10.7	
Minimum requirements (EAD 160003)	ReH> 500 [MPa]	Rm/Rp02 >1,05	2.5 [%]	

The tensile test results for the 20 mm rebar contain more variation than the results achieved for the 10 mm rebar. All the tensile tests for the 20 mm bar fulfilled the minimum requirements. The tensile strength of differently quenched bars is roughly the same. In shorter quenching times, where the obtained STT is higher, and for air-cooled rebars, the ultimate

strength was slightly less than with higher quenching times. The most significant difference between the quenching times can be seen in the value of total elongation, A_{gt}. As stated in subsection 4.6.6, ductility is the material property that measures the material's ability to deform before fracture. According to the tensile test results obtained, the elastic deformation of air-cooled and water-quenched rebars was pretty much the same. Differences in the stress-strain curves were seen in the area where plastic deformation occurred after reaching the offset yield strength: The rebars with short quenching time or cooling in air tended to have a small amount of plastic deformation, and the fracture location was in the heat-treated area.

The quenching time, after which the amount of plastic deformation before breaking was no longer reflected negatively in the results of tensile tests, was after reaching STT-values under 425 °C. Figure 50 below shows a stress-strain curve obtained for air-cooled rebar and rebar with a STT-value of 350 °C.

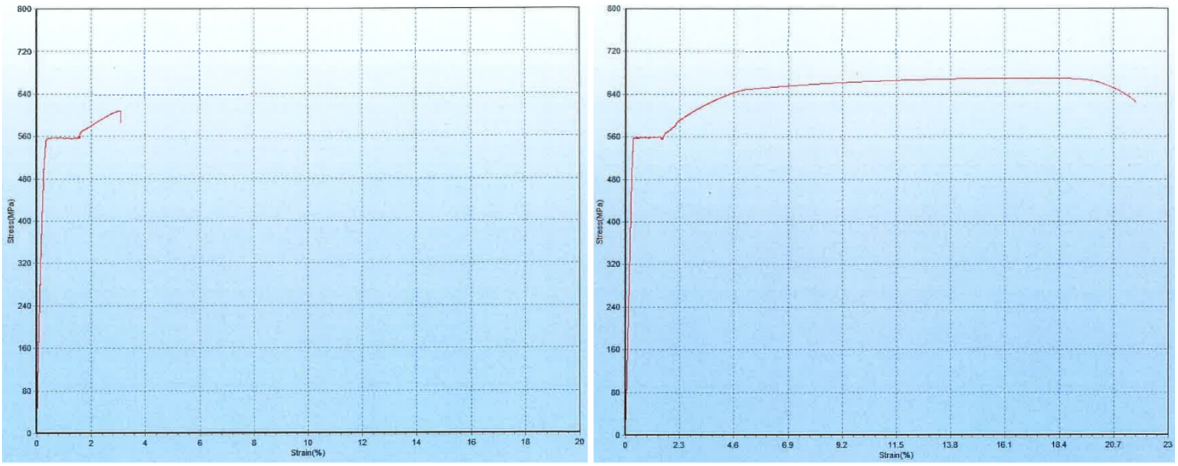

Figure 50: Stress strain curve of 20mm forged bar cooled in air (left) and with 350 °C STT (right).

Based on the results, the best tensile properties are achieved when the STT is between 425 to 150 °C. Using a higher tempering temperature than 425 °C causes loss in plastic elongation and the location of failure to move into the hot worked area of the bar. Based on the tensile test, a more precise analysis regarding the best quenching time between this timeframe is challenging, as the fracture location moves to the base material, causing the tensile results to look the same.

The macro and microstructure of the 20mm rebar before any working or treatment is done can be seen in Figure 51 below. In the macrostructure, uniform layers of different structures can be seen. Based on the macrostructure of the base material, it can be assessed that the

heat-treatment method used in steel mills varies between 10mm and 20mm reinforced steel. The hardness at the core of the rebar is 191 HV, and at the surface, it is 270 HV. The harder surface layer tells that the cooling rate at the surface have been faster compared to the core of the bar. Based on microanalysis, the bar core is a combination of ferrite-pearlite with some features of martensite, reminding the microstructure of the 10mm base material. The surface of the rebar is a combination of martensite and tempered martensite.

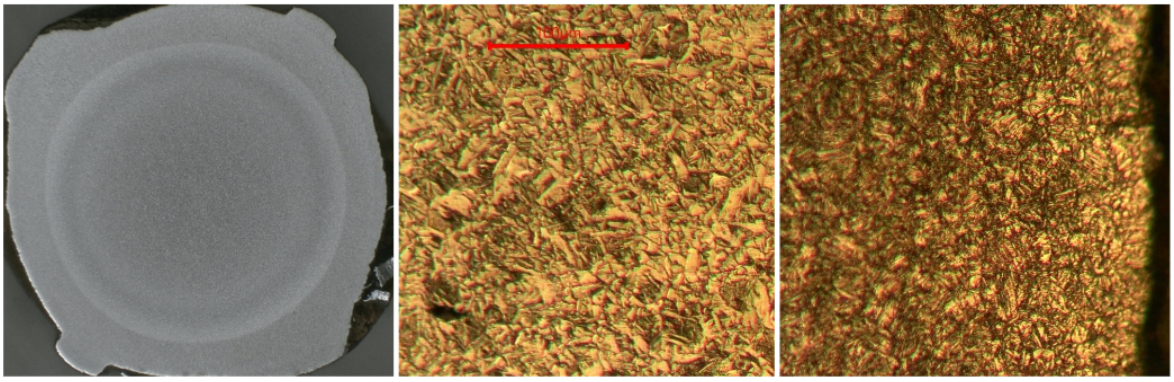

Figure 51: Left: macrostructure of 20mm rebar steel. Middle: Microstructure of the core. Right: Microstructure of the surface.

The effect of the quenching time on the microstructure of the 20mm bar is done by comparing bars that achieved STT-values of 650, 425, and 250°C. In Figure 52 below, the micrographic images taken from the core of the bar for these samples can be seen.

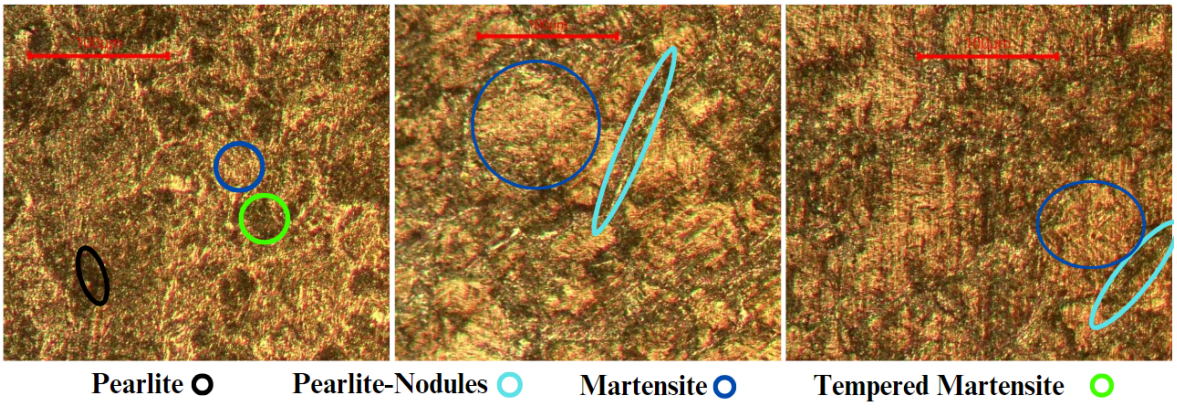

Figure 52: Microstructures of 20mm forged rebar taken from the head core. Left: 650 °C STT Middle: 425°C STT. Right: 250°C STT.

The microstructure of the heat-treated rebar that achieved 650°C STT is a mixed structure of pearlite with martensite and tempered martensite features. With STT-values of 425 and 250 °C, The pearlite is located as nodules at the prior-austenite grain boundaries, and the martensite can be seen in the interstices between these grain boundaries. As stated in subsection 3.3.1, when a phase transformation occurs during cooling, the new phase always forms from the old austenite grain boundaries. When pearlite is formed in the prior austenite grain boundaries, it means that the cooling has been too slow to avoid the formation of pearlite. When the temperature drops below the Ms-temperature, the surrounding austenite forms martensite. When the quenching time is increased, fewer dark pearlite nodules can be seen, and more martensite is formed, resulting in higher hardness values. This means that the core achieved the M_s-temperature faster the longer the used quenching time was, resulting in less pearlite formation.

The effect of the quenching time on the microstructure at the surface of the head is analyzed at the same STT values. The point where these micrographs are taken is the head bottom. The microstructure of the bar with 650 °C STT is a mixture of martensite and tempered martensite, which tells that the cooling rate with short quenching times is enough to form martensite. When analyzing the microstructure obtained for 250°C STT bar at the surface area of the head, the quenching time is fast enough that martensite is formed at the prior austenite grain boundaries. The longer the quenching time is, the bigger the martensite nodules formed at the grain boundaries are, as seen when comparing the microstructure of 425°C STT and 250°C STT samples shown in Figure 53.

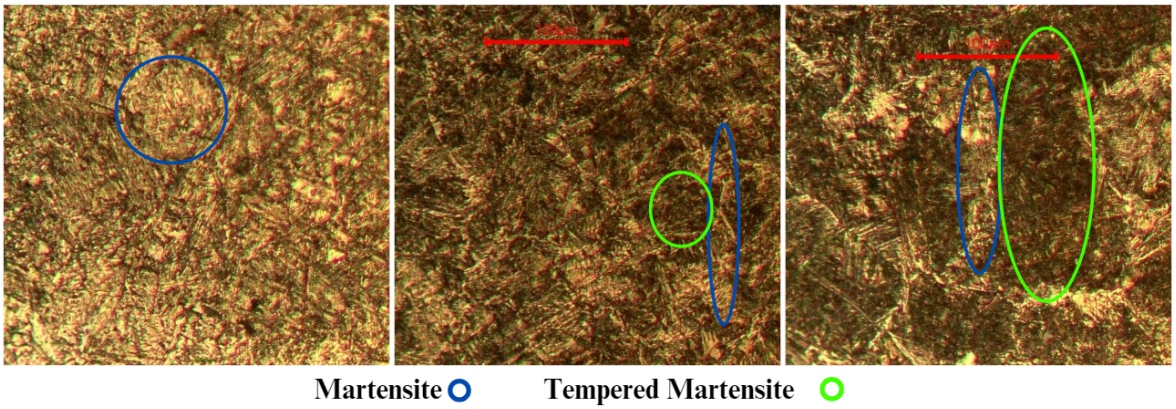

Figure 53: Microstructures of 20mm forged rebar taken from the head bottom. Left: 650 °C STT Middle: 425°C STT. Right: 250°C STT.

The hardness values obtained for 20 mm test samples are compared in Figure 54 below. As the results show, the hardness values obtained for 20mm bar differ from those obtained for 10mm rebar in both values and structure of the hardness distribution. These values are

measured with the same structure and methodology used for 10mm rebars introduced in subsection 5.4.4.

The hardness values obtained for differently heat-treated 20mm reinforced bars follow the same pattern. The hardness is lowest at the core of the head, and the closer the measurement point gets to the surface, the higher the hardness value is. The shorter the used quenching time is, and the higher the achieved STT is, the lower the obtained hardness value. If comparing the hardness near the surface, it can be seen that the hardness values at the last measurement point are close to the same for bars with 425 and 250 °C, around 450 HV. The longer the quenching time is, the closer to the core the formed hard layer gets.

The rebar close to the head has pretty much the same hardness values for all the samples measured. Also, the values between the core and surface do not differ from each other, meaning that the rebar above the head reaches room temperature during the quenching, with shorter quenching times.

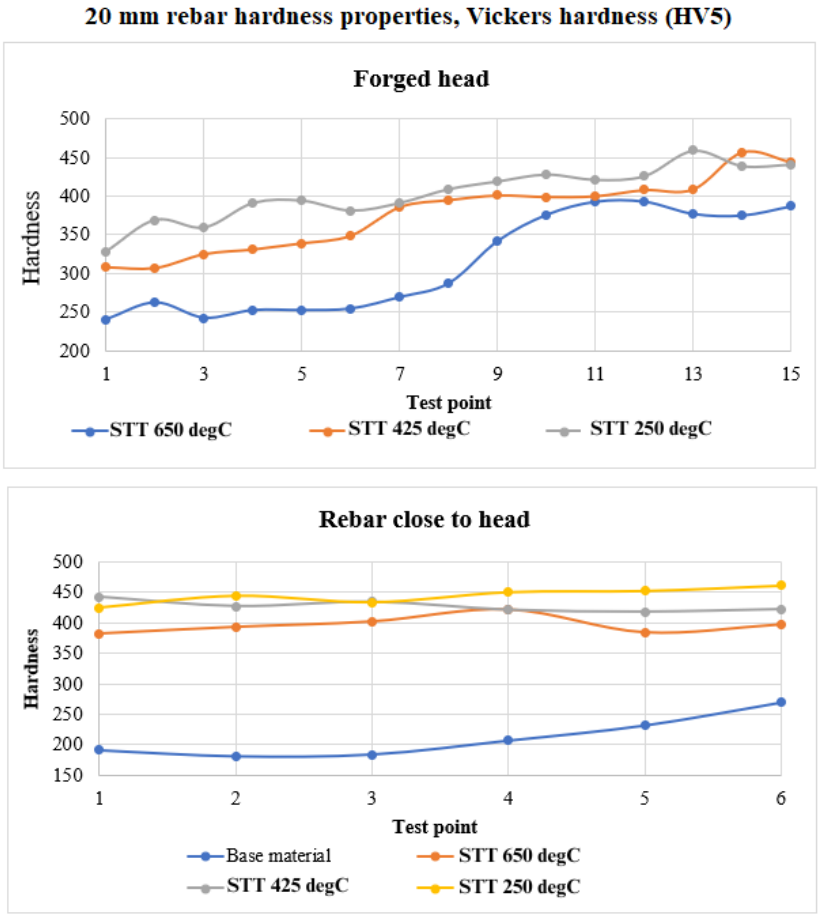

Figure 54: Summary of the Vickers hardness tests made for 20mm test samples.

Overall, the hardness values obtained for 20mm rebar are much higher than those obtained for 10mm rebars. As stated in subsection 5.5.1, the hardness of 10mm rebar is highly affected because the quenching is done when the material is already in the form of austenite and ferrite. All the ferrite formed before the quenching happens is out of the possibilities to form harder phases such as martensite. In 20mm rebars, the microstructures and the hardness values obtained tell that in this size, the headed bar is fully austenitic before the workpiece is immersed in water.

6 DISCUSSION

Heating parameters such as correct temperature before quenching, heating time, directional heating power, and needed heating length were achieved through theory. Induction heating simulations made with CENOS simulation software provided directional input parameters for practical induction heating, and by fine-tuning these values while doing practical measurements with the induction heating machinery, correct input parameters such as input power and heating time were found for the three dimensions analyzed in this work. When a trendline is drawn between the values obtained, the values are on the same linear line as shown in Figure 33 in section 5.2. This means that based on the results obtained for induction heating, directional heating parameters can be determined for other rebar sizes.

The quenching and self-tempering simulations made with Comsol multiphysics gave a better understanding of how the heat distributes at the workpiece during the heat-treatment process. The results obtained through simulations quite well represented the practical tests made for 20mm rebar, but the simulations made for 10mm rebar didn't. To better understand the reason why the simulation did not provide accurate data, it is important to compare the ratio of the surface area (mm^2) and head volume (mm^3) of the rebar sizes analyzed in this work. The ratios for 10, 20, and 32mm forged heads are provided in Table 10 below.

Table 10: Ratio of surface area and volume of head for different size rebars.

Rebar diameter [mm]	**Ratio of surface area and volume of head**
10	1.7
20	3.4
32	4.6

As stated in the theory part of this study, the heat transfer during the whole hot working happens with all of the three common heat transfer phenomena: Conduction between the surface and core, convection between the quenchant and the surface of the head, and radiation between ambient area and the surface of the head. When the ratio of the surface area and volume is small, a large amount of the total volume of the head is on the surface. This means that the heat transfer happening between the workpiece and ambient area is more intense in smaller rebars. In heating, this means faster response to heat, and in quenching and self-tempering, faster response to the cold. When defining the induction heating parameters, it

was found that the larger the diameter of the rebar steel is, the longer the rebar steel has to be heated to achieve uniform heat distribution across the whole workpiece. This same happens when quenching and self-tempering: The smaller the quenched rebar steel, the less quenching time is needed to obtain uniform temperature distribution across the cross-section.

This is the reason why the heat-treatment simulations made for 10mm rebar did not correspond to the practical forging and heat-treatment process. In the simulations, some simplifications were made, such as the effect of the forging tooling on the temperature of the headed bar. At 10mm, this drastically lowered the temperature of the hot worked rebar, which caused the simulation results to be inaccurate. In 20mm, these simplifications did not affect the results as much anymore because the size makes it less sensitive to the heat transfers that were not taken into account because of the simplifications. Even though the simulation results are not as accurate for 10mm as for 20mm, they still give insight into how the heat is distributed at the head during the heat-treatment procedure. For example, the simulation provided information that the temperature difference between the surface of the bar is smaller in smaller sizes compared to larger rebars.

The hardness tests and metallographic examinations made for the 10 and 20-mm test samples confirmed the difficulty of utilizing the QST process to heat-treat small-size rebars. In 20mm rebars, significant differences in the microstructure and hardness values between the core and surface were seen, but in 10mm, the core and surface had more similarities in the microstructure as well as in the hardness values. Basically, when martensite was formed at the surface area in the 10mm rebar, the core of the bar also had more martensite features compared to a 20mm bar with a martensite surface.

All the test samples made for 10 and 20-mm rebars passed the minimum technical requirements defined in EAD-160003 during the tensile test. This is a positive thing, as it means that there is room to work with the parameters, and therefore, the manufacturing process can have more tolerance without fear of loss in mechanical properties. A good rule of thumb when defining the process parameters would be to adjust the quenching to happen with a tolerance of +-1 second from the defined parameter. Based on the experimental test made for 10 and 20-mm reinforced bars, no exact quenching time that provides the best mechanical properties was achieved. However, the test gave an overall guideline regarding the heat treatment. For tests made for 20mm rebar, test samples in which the self-tempering temperature stayed under 425 °C had better elongation than samples having higher tempering temperatures.

6.1 Topics for further research

Analyzing the effect of the heating and heat-treatment parameters on the mechanical properties of larger rebars could bring important information and data for this study. As seen

when analyzing the 10 and 20mm rebars in this work, the analysis and experimental tests made for 20mm rebars had a lot more variation than 10mm rebars. By analyzing, for example, the 32mm rebar experimentally, more variation between the test samples might be seen, and therefore, more accurate parameters that produce the best mechanical properties might be achieved. In the future, making experimental analysis for 32mm rebar is easy and straightforward as the directional parameters are simulated and defined in this work, and the test procedures are already defined.

Future tests for smaller sizes in which the temperature of the workpiece during the induction heating is raised might help to achieve 100% austenite phase before the quenching occurs, resulting in a better microstructure. Raising the temperature from the current 1150 °C might cause problems that were discussed in subsection 4.4.4. If the bar is heated near the solidification temperatures, internal oxidation and local melting of alloy elements with low melting points might occur, causing a decrease in the ductility and strength of the material. One thing to consider in production could also be analyzing the potential to preheat the forging dies and ram before the process to prevent the effect of the cold tooling on the temperature of the forged piece.

The metallography made for the test samples was done by utilizing optical microscopy. Based on the images obtained, the quality and magnification limited how precise microstructural analysis could be made according to the photos obtained. In future analysis, utilizing a scanning electron microscope to make the metallography would give photos that would give the possibility to make a more precise analysis of the structure.

Both induction heating and quenching and self-tempering simulations made in this work can be used to define indicative parameters for real-life use. With some further refinement, both of these simulations could be viable methods to define production parameters without the need for practical testing. The induction heating simulations in this work did not have accurate coil- and workpiece geometries defined, so some adjustment between the parameters obtained as simulation results and in practice was needed. By using the exact rebar geometry and by modeling the coils used in reality, the results obtained might be more accurate. The quenching and self-tempering simulations could result in more realistic data if the effect of the forging tooling on the temperature of the workpiece is taken into account more precisely. Basically, this could be achieved by making more precise practical measurements in reality.

7 CONCLUSIONS

In this thesis, the effect of heating and heat-treatment parameters on the mechanical properties of hot-upset forged rebar steels was analyzed. In this chapter, the conclusions made as a result of the information obtained as a combination of literature review, simulations, practical measurements, and experimental tests are made.

Heating is an important part of the hot working process. When the heating parameters are specified correctly, incomplete deformation, cracking, dimensional inaccuracy, unwanted microstructural changes, and forging tool wear can be minimized. According to theory, the forging process should be processed at a temperature around 1150 °C to have good forgeability while still being in safe temperatures to prevent overheating or even burning the steel. In this study, the forged rebars are heated with Induction heating. Induction heating offers high power density, fast heating rate, and good controllability. Understanding different electromagnetic phenomena such as skin effect and electrical end and edge effects are important in order to achieve even temperature distribution during the heating process. Correct heating parameters that provide an even temperature distribution across the whole forged workpiece were successfully defined in this thesis.

Quenching and self-tempering is a widely used heat-treatment method utilized in steel mills when manufacturing rebars. Utilizing it as a heat-treatment method for the headed rebars after forging was analyzed in this study. Based on the simulations made with Comsol multiphysics, the geometry of the head makes it possible to achieve a hot spot at the core of the head that leaves enough residential heat to self-temper the quenched surface. The size of the heat-treated rebar affects how well QST works as a heat-treatment method. The bigger the heat-treated workpiece is, the easier it is to control the process. Based on the metallography and hardness measurements made for 10 and 20mm heat-treated rebars, a conclusion can be made that in smaller sizes, the process tends to form a more homogenous microstructure than in larger sizes.

The tensile test made for the 10 and 20mm test samples gave good results, and with the hot-working process currently utilized, it is possible to manufacture headed rebars that meet the given minimum requirements. Based on the experimental test made in this work, no clear best quenching time to be used in production was obtained, but a lot of new information on how the parameters of heating and heat treatment need to be adjusted to achieve good quality headed rebars was obtained.

REFERENCES

American Welding Society (AWS). 2015. “Chemical compostion (CE).” In *Welding Inspection Handbook (4th Edition),* 37–43. American Welding Society (AWS). ISBN: 978-0-87171-855-6. https://app.knovel.com/hotlink/pdf/id:kt00UBX7G3/welding-inspection-handbook/causes-delayed-cracking.

Bhadeshia, Harshad, and Robert Honeycombe. 2017. “3.1 Iron-Carbon Equilibrium Phase Diagram.” In *Steels - Microstructure and Properties (4th Edition),* 62. Elsevier. ISBN: 978-0-08-100270-4. https://app.knovel.com/hotlink/pdf/id:kt011G66P8/steels-microstructure/iron-carbo-carbon-equilibrium.

Bustillo Revuelta, Manuel. 2021. “Cement.” In *Construction Materials: Geology, Production and Applications,* edited by Manuel Bustillo Revuelta, 117–119. Springer Textbooks in Earth Sciences, Geography and Environment. Cham: Springer International Publishing. ISBN: 978-3-030-65207-4, accessed May 19, 2023. https://doi.org/10.1007/978-3-030-65207-4_6. https://doi.org/10.1007/978-3-030-65207-4_6.

Campbell, F.C. 2008. “10.5 Bainite.” In *Elements of Metallurgy and Engineering Alloys,* 2008:166. ASM International. ISBN: 978-0-87170-867-0. https://app.knovel.com/hotlink/pdf/id:kt00URLQ93/elements-metallurgy-engineering/bainite.

———. 2012. “A.7.2.1 Compressive Residual Stress.” In *Fatigue and Fracture - Understanding the Basics,* 2012:603. ASM International. ISBN: 978-1-61503-976-0. https://app.knovel.com/hotlink/pdf/id:kt00AW5M1B/fatigue-fracture-understanding/compressive-residual.

Canale, L.C.F, Mesquita, R.A, and Totten, G.E. 2008. “9. Steel Heat Treatment Failures due to Quenching - Knovel.” Accessed October 2, 2023. https://app-knovel-com.ezproxy.cc.lut.fi/web/view/khtml/show.v/rcid:kpFAHTSC09/cid:kt008G4WXS/viewerType:khtml//root_slug:9-steel-heat-treatment-failures-due-to-quenching/url_slug:steel-heat-treatment?b-q=heat%20treating%20failure&b-toc-cid=kpFAHTSC09&b-toc-title=Failure%20Analysis%20of%20Heat%20Treated%20Steel%20Components&b-toc-url-slug=steel-heat-treatment&include_synonyms=no&view=collapsed&zoom=1&page=1&q=heat%20treating%20failure.

Capar, Yasin. 2023. “Engineering Stress/Strain vs True Stress/Strain – Yasin ÇAPAR.” Accessed November 8, 2023. https://yasincapar.com/engineering-stress-strain-vs-true-stress-strain/.

Chemistry LibreTexts. 2013. “12.2: The Arrangement of Atoms in Crystalline Solids.” Chemistry LibreTexts, November 24, 2013. Accessed May 22, 2023. https://chem.libretexts.org/Bookshelves/General_Chemistry/Book%3A_General_Chemistry%3A_Principles_Patterns_and_Applications_(Averill)/12%3A_Solids/12.02%3A_The_Arrangement_of_Atoms_in_Crystalline_Solids.

Chisen. 2021. “Upset Forging | CHISEN® Forging | Chinese Forging Company.” Accessed July 19, 2023. https://www.forgedproduct.com/upset-forging.html.

Colpaert, Hubertus. 2018. “Knovel - Metallography of Steels - Interpretation of Structure and the Effects of Processing.” Accessed November 30, 2023. https://app-knovel-com.ezproxy.cc.lut.fi/kn/resources/kpMSISEP03/toc?b-q=metallography.

Davis, J.R. 2015. “104.14.2 Upset Forging Equipment.” In *Metals Handbook, Desk Edition (2nd Edition),* 852. ASM International. ISBN: 978-0-87170-654-6. https://app.knovel.com/hotlink/pdf/id:kt010QUPZ3/metals-handbook-desk/upset-forging-equipment.

Djavanroodi, F., and Alaa Salman. 2017. “Variability of Mechanical Properties and Weight for Reinforcing Bar Produced in Saudi Arabia.” *IOP Conference Series: Materials Science and Engineering* 230 (September): 012002. https://doi.org/10.1088/1757-899X/230/1/012002.

Dossett, Jon L. 2020. “Knovel - Practical Heat Treating - Basic Principles (2nd Edition).” Accessed October 4, 2023. https://app-knovel-com.ezproxy.cc.lut.fi/kn/resources/kpPHTBPE05/toc?b-content-type=tsection&b-q=temper%20embrittlement&cid=kpPHTBPE05&include_synonyms=no.

EN-10080. 2005. *SFS-EN 10080: Steel for the reinforcement of concrete. Weldable reinforcing steel. General.* Accessed May 19, 2023. https://online-sfs-fi.ezproxy.cc.lut.fi/fi/index/tuotteet/SFS/CEN/ID2/1/3341.html.stx.

Gene, Mathers. n.d. “Hardness Testing Part 1.” Accessed November 29, 2023. https://www.twi-global.com/technical-knowledge/job-knowledge/hardness-testing-part-1-074.aspx.

Ghoshdastidar, P.S. 2012. “13.6 Induction Heating - Knovel.” Accessed July 13, 2023. https://app-knovel-com.ezproxy.cc.lut.fi/web/view/khtml/show.v/rcid:kpSFDPSTA1/cid:kt004FQBF5/viewerType:khtml//root_slug:steel-forgings-design/url_slug:manufacturing-induction-heating?b-q=induction%20heating%20bar&include_synonyms=no&sort_on=default&view=collapsed&zoom=1&page=4&q=induction%20heating%20bar.

Gribniak, Viktor, Darius Bacinskas, and Gintaris Kaklauskas. 2006. "Numerical Simulation Strategy of Reinforced Concrete Tunnel Bearing Members in Fire." *The Baltic Journal of Road and Bridge Engineering* 1 (March 1, 2006): 5–9.

Haimbaugh, Richard E. 2015. "Practical Induction Heat Treating (2nd Edition)." Publisher: ASM International, ISSN: 978-1-62708-089-7. https://app.knovel.com/hotlink/toc/id:kpPIHTE00B/practical-induction-heat/practical-induction-heat.

Hameed S, Zubair M, Christoph Wölfle, Tobias Robl, Thomas Obermayer, Stefan Rappl, Kai Osterminski, Christian Krempaszky, and E. Werner. 2021. "Parameter Identification for Thermo-Mechanical Constitutive Modeling to Describe Process-Induced Residual Stresses and Phase Transformations in Low-Carbon Steels." *Applied Sciences* 11 (January): 550. https://doi.org/10.3390/app11020550.

Hasan, H. S., M. J. Peet, J. M. Jalil, and H. K. D. H. Bhadeshia. 2011. "Heat transfer coefficients during quenching of steels." *Heat and Mass Transfer* 47, no. 3 (March 1, 2011): 315–321. ISSN: 1432-1181, accessed September 5, 2023. https://doi.org/10.1007/s00231-010-0721-4. https://doi.org/10.1007/s00231-010-0721-4.

Heaton Manufacturing. 2020. "Steel Reinforcement Grades - B500A, B500B, B500C | Heaton Manufacturing." Section: Steel Reinforcement, February 18, 2020. Accessed May 21, 2023. https://heatonmanufacturing.co.uk/steel-reinforcement-grades/.

Heidari Ghaleh, Milad. 2011. *Effect of cooling rate on quenched & tempered steel rebar properties.* April 7, 2011.

Herring, Daniel H. 2015. "Influence of Alloying Elements on Heat Treatment | 2015-03-11 | Industrial Heating." Accessed November 8, 2023. https://www.industrialheating.com/blogs/14-industrial-heating-experts-speak-blog/post/92131-influence-of-alloying-elements-on-heat-treatment.

Hongteng. 2023. "From Scrap Iron or Steel to High-Quality Rebar: A Guide to the Rebar Rolling Mill-Hongteng Electrical Equipment," June 5, 2023. Accessed October 5, 2023. https://www.lyhonten.com/A-Guide-to-the-Rebar-Rolling-Mill.html.

Indutrial Heating. 2008. "Innovative Induction Heating of Oil Country Tubular Goods | Industrial Heating." Industrial heating, March 2, 2008. Accessed September 29, 2023. https://www.industrialheating.com/articles/88012-innovative-induction-heating-of-oil-country-tubular-goods.

Kanaev, A. T., A. V. Bogomolov, A. A. Kanaev, and E. N. Reshotkina. 2018. “Influence of Intermittent Quenching and Self-Tempering on the Mechanical Properties of Rebar Steel.” *Steel in Translation* 48, no. 2 (February 1, 2018): 130–134. ISSN: 1935-0988, accessed July 3, 2023. https://doi.org/10.3103/S0967091218020079. https://doi.org/10.3103/S0967091218020079.

Kauppi, Timo. 2020. “Käytännön hitsausmetallurgiaa. Osa 1: Terästen faasimuutokset.” *Hitsaustekniikka. 72 (4), 15-20.,* 15–20.

Krauss, George. 2015. “4.3 Pearlite Transformation Kinetics.” In *Steels - Processing, Structure, and Performance (2nd Edition).* ASM International. ISBN: 978-1-62708-083-5. https://app.knovel.com/hotlink/pdf/id:kt00U9LQ91/steels-processing-structure/pearlite-transformation.

Kreith, F., and W.Z. Black. 1980. *Basic Heat Transfer.* January.

Leong, Huat. n.d. “Effects of Mn, P, S, Si & V on the Mechanical Properties of Steel.” Accessed October 5, 2023. https://www.leonghuat.com/articles/elements.htm.

LinkStudPSR. 2023. “LinkStudPSR™ - Hot Upset Forging - Punching Shear Reinforcement Specialists - ©2023 Linkstud PSR.” Accessed December 14, 2023. https://linkstudpsr.com/manufacturing/hot-upset-forging.

Lucia, Oscar, Pascal Maussion, Enrique J. Dede, and Jose M. Burdio. 2014. “Induction Heating Technology and Its Applications: Past Developments, Current Technology, and Future Challenges.” Publisher: IEEE, *IEEE transactions on industrial electronics (1982)* 61 (5): 2509–2520. ISSN: 0278-0046.

Mackenzie, D., and David Lambert. 2003. *Effect of Quenching Variables on Distortion and Residual Stresses.* November 24, 2003.

Maraveas, Chrysanthos. 2014. “POST-FIRE MECHANICAL PROPERTIES OF STRUCTURAL STEEL.” January.

El-Mashad, Hamed M., and Zhongli Pan. 2017. “Application of Induction Heating in Food Processing and Cooking.” *Food Engineering Reviews* 9, no. 2 (June 1, 2017): 82–90. ISSN: 1866-7929, accessed July 18, 2023. https://doi.org/10.1007/s12393-016-9156-0. https://doi.org/10.1007/s12393-016-9156-0.

Metsuco. 2020. “Brinell, Rockwell, and Vickers Hardness Tests: The Differences Explained.” Metsuco. Section: Hardness Testing, June 22, 2020. Accessed November 29, 2023. https://metsuco.com/brinell-rockwell-and-vickers-hardness-tests-the-basic-differences-explained/.

Molderings, Michael. 2020. “Steel Properties | Carbon Equivalent Fundamentals | Hitachi High-Tech.” Hitachi High Tech Analytical Science, October 26, 2020. Accessed May 19, 2023. https://hha.hitachi-hightech.com/en/blogs-events/blogs/2020/10/26/carbon-equivalent-fundamentals-for-predicting-steel-properties/.

Park, Chun Su, Hyang Jun Yi, Yong-Tae Kim, Sang Wook Han, Taekyung Lee, and Young Hoon Moon. 2019. “Tempcore Process Simulator to Analyze Microstructural Evolution of Quenched and Tempered Rebar.” *Applied Sciences* 9, no. 14 (July 23, 2019): 2938. ISSN: 2076-3417, accessed July 3, 2023. https://doi.org/10.3390/app9142938. https://www.mdpi.com/2076-3417/9/14/2938.

RMC. 2021. “Quenching and Tempering for Steel Castings - Industrial News - Steel Investment Casting Foundry | Stainless Steel Casting Company.” Accessed July 24, 2023. https://casting-foundry.com/article/quenching-and-tempering-for-steel-castings.html.

Rudnev, Valery. 2017. *Handbook of induction heating.* Second edition. Manufacturing engineering and materials processing ; 61. Publication Title: Handbook of induction heating. Boca Raton, FL: CRC Press, Taylor & Francis Group. ISBN: 1-5231-1806-7.

Satyendra. 2020. “Tempcore process for the Production of TMT Reinforcement bars – IspatGuru,” February 19, 2020. Www-page. Accessed October 3, 2023. https://www.ispatguru.com/tempcore-process-for-the-production-of-tmt-reinforcement-bars/.

Sharma, Shrutika, Mayank Sharma, Vishal Gupta, and Jaskaran Singh. 2023. “A Systematic Review of Factors Affecting the Process Parameters and Various Measurement Techniques in Forging Processes.” Publisher: John Wiley & Sons, Ltd, *steel research international* 94, no. 5 (May): 2200529. ISSN: 1611-3683, accessed July 20, 2023. https://doi.org/10.1002/srin.202200529. https://onlinelibrary.wiley.com/doi/full/10.1002/srin.202200529.

SteelData. 2022. “CCT and TTT Diagrams of Steels for the Windows, Mac, Linux computers and Android Phones and Tablets (9056 diagrams).” Http://www.steeldata.info/std/index.html. Accessed June 29, 2023. https://www.steeldata.info/std/index.html.

Total materia. 2003. “Temper Embrittlement :: Total Materia Article,” March. Accessed October 4, 2023. https://www.totalmateria.com/page.aspx?ID=CheckArticle&site=kts&NM=102.

Totten, G., M. Howes, and T. Inoue. 2002. “Handbook of Residual Stress and Deformation of Steel.” Publisher: ASM International 2002. ISSN: 978-0-87170-729-1. https://app.knovel.com/hotlink/toc/id:kpHRSDS00B/handbook-residual-stress/handbook-residual-stress.

Totten, George E., Rajesh J. Shah, and David R. Forester. 2019. “24.2.1.2 CCT Diagrams.” In *Fuels and Lubricants Handbook - Technology, Properties, Performance, and Testing (2nd Edition): (MNL 37-2nd-EB),* 979. ASTM International. ISBN: 978-0-8031-7089-6. https://app.knovel.com/hotlink/pdf/id:kt012WUS12/fuels-lubricants-handbook/cct-diagrams.

Verhoeven, John D. 2007. “1. Pure Iron.” In *Steel Metallurgy for the Non-Metallurgist,* 96, 99, 200. ASM International. ISBN: 978-0-87170-858-8. https://app.knovel.com/hotlink/pdf/id:kt00ACNHT3/steel-metallurgy-non/pure-iron.

A APPENDIX: EAD 160003 Mechanical characteristics of double-headed stud

D.3 Mechanical characteristics

D.3.1 General

The mechanical characteristics according to Table D.2 shall be determined by means of testing. Possible tolerances as specified by the manufacturer shall be considered. The tests shall be performed according to the method given in Table D.2.

Table D.2 determination of mechanical characteristics for static and quasi-static loading

No	characteristic	number of samples	test method and evaluation	requirement
1	characteristic yield strength	≥ 5 each stud size	D.3.2	f_{yk} ≥ 500 [MPa]
2	characteristic ratio tensile strength / yield strength	≥ 5 each stud size	D.3.2	$(f_t/f_y)_k$ ≥ 1,05 [-]
3	characteristic strain at maximum force	≥ 5 each stud size	D.3.2	ε_{uk} ≥ 2,5 [%]

D.3.2 Test methods

Tests according to EN ISO 6892-1 shall be performed.

In the tests the stud head shall be supported by a ring with a diameter 1.5 d_A. For the test set-up, see Figure D.1.

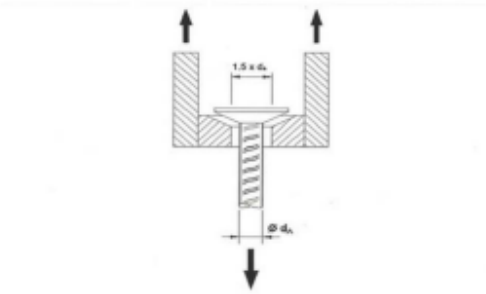

Figure D.1: test set-up for tension tests

The characteristic yield strength f_{yk} shall be determined as 5%-fractile (acc. to B.3) of the test results f_y.

The characteristic strain at maximum force ε_{uk} shall be determined as 5%-fractile (acc. to B.3) of the test results ε_u.

The characteristic ratio of tensile strength/yield strength $(f_t/f_y)_k$ shall be determined as 5%-fractile (acc. to B.3) of the ratio f_t/f_y.